



*People's Democratic and Republic of Algeria
Ministry of Higher Education and Scientific Research
Echahid Cheikh Larbi Tebessi University -Tebessa -
Faculty of Exact Sciences and Sciences of Nature and Life
Department of Mathematics and Computer Sciences
Laboratory of Mathematics, Informatics and Systems (LAMIS)*



Doctoral LMD Thesis Option: Dynamical System

Theme

On Some Fractional-Order Dynamical systems

Presented by:

Presented by Ms. Yousfi Hasna

The committee members :

President: Abdelmalek Salem	professor	<i>Echahid Cheikh Larbi Tebessi University</i>
Supervisor: Gasri Ahlem	MCA	<i>Echahid Cheikh Larbi Tebessi University</i>
Co- Supervisor: Ouannas Adel	professor	<i>Larbi Ben M'hidi University</i>
Examiner: Fareh Hannachi	MCA	<i>Echahid Cheikh Larbi Tebessi University</i>
Examiner: Rezzoug Imad	Professor	<i>Larbi Ben M'hidi University</i>
Examiner: Oussaeif Taki Eddine	MCA	<i>Larbi Ben M'hidi University</i>

Academic Year 2024-2025

CONTENTS

Table of contents	4
Liste of figures	6
Liste of tables	7
General Introduction	14
I FRACTIONAL DIFFERENCE SYSTEMS	18
1 Basics in discrete fractional calculus	19
1.1 Introduction	19
1.2 Preliminaries and notions	20
1.3 Fractional sum and difference operators	21
1.3.1 Fractional sum operator	21
1.3.2 Fractional difference operator	22
1.4 Caputo difference operator	23
1.5 Fractional h -difference operator	24
1.6 Stability of difference systems	25
1.6.1 Stability types	26
1.6.2 Stability of integer order difference systems	27

1.6.3	Stability of fractional order difference systems	30
1.7	Conclusion	32
2	Chaos in fractional order maps	33
2.1	Introduction	33
2.2	Basics of discrete dynamical systems	34
2.3	Concept of chaos theory	35
2.3.1	Mathematical definitions of chaotic attractors	35
2.3.2	Characteristics of chaotic maps	36
2.4	Examples of strange attractors	37
2.4.1	Fractional Lozi map	37
2.4.2	Fractional Rössler map	38
2.5	Lyapunov exponent	38
2.5.1	Definition of Lyapunov exponents in integer-order maps	39
2.5.2	Lyapunov exponents in fractional-order maps	41
2.6	Bifurcation diagrams	42
2.7	Routes of chaos	43
2.7.1	By period doubling	44
2.7.2	By intermittency	44
2.7.3	By quasi-periodicity	44
2.8	Conclusion	45
3	The fractional discrete Ushio system: chaos and stabilization	46
3.1	Introduction	46
3.2	The fractional Ushio system	47
3.3	Chaotic behavior of fractional-order Ushio map	47
3.3.1	Phase portrait	47
3.3.2	Bifurcation diagram and largest Lyapunov exponent	48
3.4	Chaos stabilization scheme	50
3.5	Conclusion	51

II FRACTIONAL DIFFERENTIAL SYSTEMS **53**

4 Overview of fractional-order differential operators	54
4.1 Introduction	54
4.2 Riemann-Liouville fractional integral	55
4.3 Riemann-Liouville fractional derivatives	57
4.4 Caputo's fractional derivative	58
4.5 Stability of fractional order differential systems	60
4.5.1 Stability of fractional order linear systems	61
4.5.2 Stability of fractional order nonlinear systems	62
4.6 Adomian decomposition method	64
4.6.1 Algorithm description	64
4.6.2 Algorithm example	65
4.7 Conclusion	68
5 Complexity analysis of fractional-order chaotic systems	69
5.1 Introduction	69
5.2 Fractional order continues-time dynamical systems	70
5.3 Brief overview of chaos	70
5.4 Fractional-order chaotic systems	71
5.4.1 Fractional-order Lorenz chaotic system	71
5.4.2 Fractional-order Rössler chaotic system	72
5.4.3 Fractional-order Lorenz-Stenflo chaotic system	72
5.5 Complexity measure algorithms	73
5.5.1 Spectral entropy complexity algorithm	75
5.5.2 C_0 complexity algorithm	76
5.6 Chaos synchronization	76
5.6.1 Different synchronization types	78
5.7 Application of fractional chaotic systems in image encryption	79
5.8 Conclusion	80

6 The fractional-order Halvorsen circulant system and its application on image encryption	81
6.1 Introduction	81
6.2 The Fractional-order Halvorsen circulant system	82
6.2.1 Solution of the fractional-order Halvorsen circulant system	82
6.2.2 Dynamics analysis of FOHCS	83
6.2.3 Complexity of FOHCS	84
6.2.4 Complexity with variation a and q	84
6.2.5 Chaos control	86
6.3 The technique of encryption and decryption	90
6.3.1 Chaotic sequence generator	90
6.3.2 RSA Algorithm	91
6.3.3 Encryption and decryption process	92
6.4 Simulations	93
6.4.1 Histogram	94
6.4.2 Adjacent pixel correlation	95
6.4.3 Key analysis	96
6.4.4 Entropy analysis	98
6.4.5 Different attack	99
6.4.6 Robustness analysis	101
6.4.7 Evaluation of known-plaintext and chosen-plaintext attacks	101
6.5 Conclusion	102
General Conclusion and Perspectives	103

LIST OF FIGURES

1.1	Time evolution of states of the system (1.6.12) for $\nu = 0.95$	31
1.2	Time evolution of states of the system (1.6.14) for $\nu = 0.9$	32
2.1	The Lozi attractor for $(x_0, y_0) = (0, 0)$, $\nu = 0.98$, $a = 1.7$ and $b = 0.5$	38
2.2	The Rössler attractor for $(x_0, y_0, z_0) = (0.1, 0.2, -0.5)$, $\nu = 0.903$	39
2.3	The bifurcation diagram of the logistic map.	43
3.1	Phase portrait of the FO Ushio map (3.2.2) for (a) $\gamma = 1$,(b) $\gamma = 0.95$,(c) $\gamma = 0.82$	48
3.2	Bifurcation diagram of the FO Ushio map (3.2.2) for (a) $\gamma = 1$,(b) $\gamma =$ 0.95 ,(c) $\gamma = 0.82$	49
3.3	Largest Lyapunov exponent of the FO Ushio map (3.2.2) for (a) $\gamma = 1$,(b) $\gamma = 0.95$,(c) $\gamma = 0.82$	49
3.4	Time evolution the system (3.4.2) by using the control law (3.4.1) with $\gamma = 0.95$ and $d = 1$	51
5.1	FO Lorenz chaotic attractors: (a) $x_1 - x_2$ plane, (b) $x_1 - x_3$ plane, and (c) $x_2 - x_3$ plane.	72
5.2	Attractor of the FO Rössler system (5.4.2).	73

5.3 Attractors of the FO Lorenz-Stenflo system (5.4.3): (a) $x - y$ plane, (b) $x - z$ plane, (c) $x - v$ plane, (d) $y - z$ plane, (e) $y - v$ plane and (f) $z - v$ plane.	74
6.1 dynamics of FOHCS: (a) LEs (b) bifurcation diagram, and (c) LEs with $q = 0.65$	85
6.2 FOHCS attractor with different value of q	85
6.3 Chaos diagram of FOHCS on $q-a$ plan: (a) SE complexity, (b) C_0 complexity. .	85
6.4 FOHCS complexity: (a) SE complexity with $q = 0.65$, (b) C_0 complexity with $q = 0.65$, (c) C_0 complexity with $a = 1.27$, and (d) SE complexity with $a = 1.27$	86
6.5 Time evolution of the system of the FOHCS (6.2.1) using the control law (6.2.8).	88
6.6 Error synchronization of the FOHCS (6.2.1).	90
6.7 Encryption flowchart.	93
6.8 Image Encryption and Decryption process	94
6.9 Histogram of correlation and coefficient	95
6.10 Correlation adjacent pixels in the original and encrypted images.	96
6.11 Key sensitivity analysis with using correct key	97
6.12 The impact of varying ciphertext image intensities on decrypted images. .	100
6.13 Results of encryption for every black and white image.	101

LIST OF TABLES

6.1	Key space comparison	97
6.2	Image correlation coefficient	98
6.3	<i>BACI</i> , <i>UACI</i> , and <i>NPCR</i> results for complete encryption	100

ACKNOWLEDGMENTS

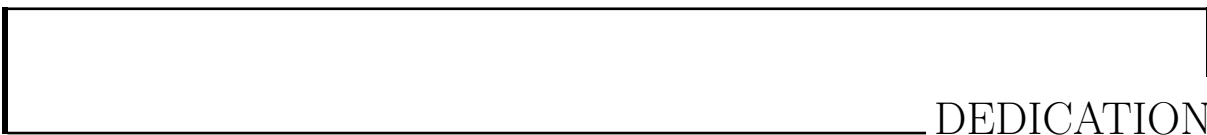
First of all, I would like to thank **ALLAH** who gave me the strength and the patience to accomplish this modest work.

The author would like to express their heartfelt appreciation to my supervisor, **Dr. Gasri Ahlem**, for providing me with essential assistance and unflinching support during the whole of this project. I am grateful to you for your excellent knowledge and commitment to my accomplishments. In addition, I would like to express my gratitude to my co-supervisor, **Prof. Adel Ouannas**, for his support, contributions of constructive ideas, and comments that were vital to the improvement of this work.

The competence of the discussion committee was essential to the successful completion of this thesis, which would not have been feasible without her. As professor at Echahid Cheikh Larbi Tebessi University, **Prof. Abdelmalek Salem** is a highly qualified individual. I am grateful to you for accepting to serve as the panel chair for my thesis. **Prof. Imad Rezzoug**, professor at Larbi Ben M'hidi University, **Prof. Taki Eddine Oussaeif**, professor at Larbi Ben M'hidi University, and **Dr. Hannachi Fareh**, assistant professor at Echahid Cheikh Larbi Tebessi University, who consented to assess my thesis, are the individuals to whom I would like to express my sincere gratitude.

In recent years, I've had the opportunity to contact several remarkable individuals, and as a result, my experience in the field of scientific research has significantly increased. In the presence of **Prof. Shaobo He** and **Prof. Chaouki Aouiti**, I had a profound sense of reverence. This was a really fun experience, and I am quite grateful that their research

methodology and quality made it possible for me to acquire a great deal of information. In addition, I would like to express my gratitude to all of the researchers for their generosity, direction, and assistance, particularly to **Yousuf Islam** and **MD Mehedi Hassan**.



DEDICATION

In loving memory of my late father, whose infinite patience and boundless love shaped me into who I am today. Though he has passed on for several years, his wise words and gentle spirit continue to guide me, like cherished quotes that accompany me through each day.

To my incredible mother. I extend my heartfelt thanks to my incredible mother for her love and unwavering support throughout my studies.

To my brothers, sisters, uncle, friends...

RÉSUMÉ

Les principaux sujets de cette étude étaient les systèmes différentiels d'ordre fractionnaire et de différence d'ordre fractionnaire. On propose initialement un contrôle linéaire pour maintenir la stabilité du système Ushio fractionnaire à temps discret, en utilisant la méthode de Lyapunov et l'opérateur de différence h de Caputo. Les conclusions de l'étude sont illustrées par des résultats numériques. Par la suite, nous fournissons une description qualitative du système Halvorsen (HCS) avec un dérivé de Caputo d'ordre fractionnaire. La stabilisation et la synchronisation de FO-HCS identiques sont également étudiées et nous proposons une solution numérique pour le système circulant Halvorsen d'ordre fractionnaire (FO-HCS) en utilisant la technique de décomposition adomienne (ADM). En outre, on a développé une méthode de chiffrement d'images en utilisant des séquences fractionnaires étendues, en exploitant les caractéristiques remarquables du système d'ordre fractionnaire. Finalement, il est performant et fiable dans le domaine des données d'images, comme le démontrent les résultats de simulation et ses résultats. **Mots clés:** Système dynamique continue, système dynamique discret, chaos, système chaotique d'ordre fractionnaire, contrôle adaptatif, synchronisation, méthode de décomposition adomienne, cryptage d'images.

ملخص

ركز هذا العمل على النظام التفاضلي للترتيب الكسري ونظام فرق الرتب الكسرية. أولاً، تم تقديم قانون تحكم خطى يعتمد على نهج Lyapunov وخصائص مؤثر Caputo h-difference ل لتحقيق الاستقرار في نظام Ushio الكسري الفوضوي في الوقت المنفصل. النتائج العددية قدمت لتوضيح النتائج. بعد ذلك، قمنا بوصف نظام هالفورسن الدائري (HCS) (HCS) بشتق Caputo ذو الرتبة الكسرية وخصائصه النوعية. تم اقتراح الحل العددي لنظام هالفورسن الدائري (FO-HCS) (FO-HCS) بالترتيب الكسري بناءً على خوارزمية (ADM)، كما أننا ندرس أيضاً استقرار ومزامنة FO-HCS المتطابقة. بالإضافة إلى ذلك، تم استخدام خصائص نظام الترتيب الكسري لتطوير تقنية تشفير الصور باستخدام التسلسلات الكسورية الموسعة. وأخيراً، ثبتت نتائج المحاكاة أنها فعالة وآمنة في بيانات الصورة.

الكلمات المفتاحية: النظام الديناميكي المستمر، النظام الديناميكي المنفصل، الفوضى، النظام الفوضوي ذو الرتبة الكسرية ، التحكم ، المزامنة، خوارزمية Adomian decomposition method ، تشفير الصور.

ABSTRACT

The fractional order differential and fractional order difference systems were the primary topics of this research. A linear control rule for stabilizing the fractional discrete-time Ushio system that is based on the Lyapunov method and Caputo h-difference operator's characteristics is first proposed. The study is accompanied by numerical results that serve to demonstrate the conclusions. A qualitative description of the Halvorsen circulant system (HCS) with a fractional-order Caputo derivative is then provided. We also study the stabilization and synchronization of identical FO-HCS and provide a numerical solution for this system using the Adomian decomposition technique (ADM). Furthermore, the approach for encrypting images using extended fractional sequences was developed by using the exceptional qualities of the fractional-order system. Lastly, it is effective and secure in picture data, as shown by the simulation results and its performance.

Keywords: Continuous dynamic system, discrete dynamic system, chaos, fractional-order chaotic system, adaptive control, synchronization, adomian decomposition method, image encryption.

GENERAL INTRODUCTION

A little over three hundred years ago, fractional calculation emerged in correspondence between L'Hospital and Leibniz. Initially addressing orders like 0.5, it later tackled arbitrary orders in differential equations. While computational difficulties and a lack of practical applications slowed progress, new computer technologies have enabled broad use in many domains, including nature, electromagnetic oscillations, system control, and material mechanics. Additionally, techniques like fractional wavelet and Fourier transforms, and fractional image processing, are gaining traction in signal processing research [23]. Fractional-order chaotic systems are derived by substituting the integer differential operator with the fractional difference operator, these systems can be classified into two main categories: continuous-time and discrete-time. In this thesis, we are interested in both chaotic systems, we referred to discrete-time chaotic systems also known as chaotic maps. Over the years, several different chaotic systems have been proposed in the literature and applied in different fields including, the Lozi system [60], the generalized Hénon map [42], the Lorenz map [58], Chen system [103], Chua system [4], Rössler system [115], etc.

Fractional-order chaotic systems have undergone thorough examination across engineering, mathematics, and physics, revealing complex dynamics capable of producing diverse chaotic behaviors [8], including strange attractors and fractal patterns. This exploration has spurred the development of novel mathematical resources tailored for examining their behavior. Various techniques, such as the active control [98] and the adaptive control method [68], have been extensively documented in the literature to further this

understanding. Since its inception, chaotic synchronization has garnered significant attention from researchers [3], leading to the proposal of various applications including chaos suppression, dynamical system monitoring, control, and communication purposes [7]. The goal of chaos synchronization is to align the variables of a slave system with those of a chaotic master system over time. Numerous methods have been developed for achieving synchronization, such as complete synchronization [62], lag synchronization [55], anti-synchronization [52], hybrid synchronization [92], projective synchronization [28], hybrid projective synchronization [102], modified projective synchronization [56]. Pecora and Carroll demonstrated the feasibility of synchronizing chaotic systems using a shared pilot signal [18]. This synchronization has found widespread applications in cryptography and secure information transmission [31], where synchronization of chaotic systems (master or transmitter and slave or receiver) is crucial for decrypting messages. Li and Deng have provided a comprehensive summary of synchronization theory and techniques [54].

The dynamical behaviors of fractional-order chaotic systems have universal significance across various disciplines, including mathematics and information security. Many image encryption techniques based on chaotic systems have emerged in recent years [104], with the permutation-diffusion mechanism being the most often used. A system with two 1D chaotic maps and a dynamic S-box was presented by Wang et al. However, these algorithms' independence from diffusion and permutation processes requires a lot of key generation repetitions, which makes them vulnerable to attacks using standard plaintext picture templates. To mitigate these vulnerabilities, Wang et al. [105] introduced a fast image algorithm based on the Logistic map, performing permutation and diffusion simultaneously. This approach reduces the iterative complexity, enhancing resistance against chosen plaintext attacks, albeit with limitations regarding key space size and scrambling effectiveness. Existing image encryption algorithms suffer from drawbacks such as reliance on low-dimensional chaotic systems (e.g., 1D and 2D), posing security risks, and poor robustness leading to decreased quality of encryption as a result of consequences of limited accuracy. Addressing these concerns, this thesis proposes an effective method to bolster image data protection, enhancing security performance while minimizing implementation costs, thereby contributing significantly to the field of image security.

This thesis is structured into two primary parts: Fractional difference equations and fractional differential equations. Let us come more specifically to a quick overview of each chapter:

Part I comprises chapters 1, 2, and 3.

- **Chapter 1:** provides an introduction to Discrete Fractional Calculus. This chapter reviews the terminology and characteristics relevant to discrete fractional calculus, followed by an introduction to fundamental functions. The chapter then explores the operators for fractional sum and fractional difference. Additionally, explore the basic ideas behind the fractional h-difference operator. Finally, the results of stability tests on linear and non-linear discrete systems of fractional and integer orders are given.
- **Chapter 2:** delves into chaos theory, focusing on its application to fractional order maps. Beginning with a brief overview of discrete dynamical systems, this chapter will go further into the mathematical theory of chaos by defining and discussing chaotic systems and their defining properties. The notion of Lyapunov Exponents for integer and fractional discrete-time systems will be covered. At long last, many paths leading from a normal dynamic system to chaos will be demonstrated.
- **Chapter 3:** This chapter presents a novel fractional-order Ushio map that is an extension of the integer-order Ushio system. First, studying the presence of chaotic behaviors in the fractional Ushio system. Then, we stabilize the chaotic fractional discrete-time Ushio system by introducing a one-dimensional linear control rule.

Part II consists of Chapters 4, 5, and 6.

- **Chapter 4:** In this chapter, the most important and often used forms of fractional integrals and derivatives are defined and discussed, along with their basic features. Furthermore, fractional-order dynamical system stability theorems are addressed. An overview of the Adomian decomposition approach is provided at the end of the chapter, along with an example to help understand how it works.
- **Chapter 5:** discusses chaos and complexity measures of fractional order chaotic systems, along with their applications.
- **Chapter 6:** This chapter explains the qualitative features of the Halvorsen circulant

system (HCS) with a fractional-order Caputo derivative. The fractional order Halvorsen circulant system (FO-HCS) is proposed to have a numerical solution based on the Adomian decomposition technique (ADM). Complexity, phase diagrams, bifurcation diagrams, and Lyapunov exponents are some of the methods used to examine dynamics thereafter. Furthermore, we study the stabilization and synchronization of identical FO-HCS, and stability theory shows that both may be achieved using adaptive feedback control. In addition, by capitalizing on the exceptional features of the fractional system, the picture encryption method is created using the extended fractional sequences. According to the improved fractional Halvorsen circulant chaotic models, the suggested solution employs a keystream generator to provide the utmost safety. When it comes to image data, the simulation's findings and performance prove that it is secure and reliable.

Part I

FRACTIONAL DIFFERENCE SYSTEMS

CHAPTER **1**

BASICS IN DISCRETE FRACTIONAL CALCULUS

1.1 Introduction

Over the last several years, the theoretical exploration of discrete fractional calculus and its practical applications has emerged as a pivotal area of research. Fractional-order derivatives are recognised for their enhanced accuracy compared to integer-order derivatives, attributed to their infinite memory. Presently, numerous definitions of fractional derivatives exist. This chapter aims to elucidate several definitions, theorems, and fundamental properties crucial for our subsequent investigations. We start by introducing basic functions and revisiting notation and properties pertinent to discrete fractional calculus. Subsequently, we outline the definitions of fractional sum and fractional difference operators. Furthermore, we delve into the fractional h -difference operator and its foundational concepts. Lastly, we offer an overview of recent stability findings concerning linear and non-linear discrete systems, encompassing both fractional and integer orders.

1.2 Preliminaries and notions

In this section, we'll introduce essential definitions and concepts in mathematical analysis crucial for our work.

Definition 1.2.1. *The gamma function, denoted by $\Gamma(z)$, is defined as follows:*

$$\Gamma(z) = \int_0^\infty e^{-s} s^{z-1} ds,$$

$\forall z \in \mathbb{C}$ and $\Re(z) > 0$ (it can be shown that the above improper integral converges for all such z).

Definition 1.2.2. *We define the falling factorial power for $n \in \mathbb{N}$ by*

$$s^{(n)} = s(s+1)(s+2)\dots(s+1-n) = \frac{\Gamma(s+1)}{\Gamma(s+1-n)}.$$

In general, for $\nu \in \mathbb{R}$ we define the generalized falling function by

$$s^{(\nu)} = \frac{\Gamma(s+1)}{\Gamma(s+1-\nu)}. \quad (1.2.1)$$

Definition 1.2.3. *The binomial coefficient $\binom{n}{k}$ is given as:*

$$\binom{n}{k} = \frac{n!}{k!(n-k)!}.$$

Remark 1.2.4. *Note that when $n \geq k \geq 0$, then the binomial coefficient can be expressed as*

$$\binom{n}{k} = \frac{n!}{k!(n-k)!} = \frac{n(n-1)(n-2)\dots(n-k+1)}{k!} = \frac{n^{(k)}}{\Gamma(k+1)}.$$

In general, for $\nu \in \mathbb{R}$ we define the generalized binomial coefficient by

$$\binom{s}{\nu} = \frac{s^{(\nu)}}{\Gamma(\nu+1)}. \quad (1.2.2)$$

Definition 1.2.5. [46] *Let $g : \mathbb{N}_a \rightarrow \mathbb{R}$, where $\mathbb{N}_a = \{a, a+1, a+2, \dots\}$ be a time scale, $a \in \mathbb{R}$. The difference operator for a function $G(t)$ is described as*

$$\Delta G(t) = G(t+1) - G(t) \quad (1.2.3)$$

The second-order difference of the function G is defined as:

$$\Delta^2 G(t) = \Delta(\Delta G(t)) = G(t+2) - 2G(t+1) + G(t). \quad (1.2.4)$$

In general, the n -th integer difference operator is written by the following mathematical formula:

$$\Delta^n G(t) = \Delta(\Delta^{n-1} G(t)) = \sum_{k=0}^n \binom{n}{k} (-1)^{n-k} G(t+k), \quad t \in \mathbb{N}_a. \quad (1.2.5)$$

1.3 Fractional sum and difference operators

This section introduces the ν -th fractional sum operator and the ν -th fractional difference operator, fundamental in discrete calculus. We'll provide essential tools and properties associated with them.

1.3.1 Fractional sum operator

Definition 1.3.1. [65] The ν -th discrete fractional sum for a function $g : \mathbb{N}_a \rightarrow \mathbb{R}$ is given as

$$\Delta_a^{-\nu} g(t) = \frac{1}{\Gamma(\nu)} \sum_{s=a}^{t-\nu} (t-s-1)^{(\nu-1)} g(s).$$

With $t \in \mathbb{N}_{a+\nu}$ and $0 < \nu < 1$. Note that the domain of $\Delta_a^{-\nu} g$ is $D\{\Delta_a^{-\nu} g\} = \mathbb{N}_{a+\nu}$.

The fractional sum stated in Definition 1.3.1 can be generalized as the binomial formula, which is shown by the following proposition:

Proposition 1.3.2. [43] Let $g : \mathbb{N}_a \rightarrow \mathbb{R}$, and $\nu > 0$ be given with $n-1 < \nu < n$. For each $t \in \mathbb{N}_{a+\nu}$, the ν -th discrete fractional sum is expressed by

$$\Delta_a^{-\nu} g(t) = \frac{1}{\Gamma(\nu)} \sum_{k=0}^{t-\nu-a} (-1)^k \binom{-\nu}{k} g(t-\nu-k).$$

Theorem 1.3.3. [9] Assume $\alpha \in \mathbb{R} \setminus \{-1, -2, \dots\}$ and $\nu > 0$. Then

$$\Delta_{a+\alpha}^{-\nu} (t-a)^{(\alpha)} = \frac{\Gamma(\alpha+1)}{\Gamma(\alpha+\nu+1)} (t-a)^{(\alpha+\nu)}, \quad t \in \mathbb{N}_{a+\alpha+\nu}$$

Example 1.3.4. Using the theorem 1.3.3, we derive the following sum:

$$\Delta_0^{-\frac{1}{2}} 1 = \Delta_0^{-\frac{1}{2}} t^{(0)} = \frac{\Gamma(1)}{\Gamma(\frac{3}{2})} t^{(\frac{1}{2})} = \frac{2}{\sqrt{\pi}} t^{(\frac{1}{2})}.$$

1.3.2 Fractional difference operator

Using the $\nu - th$ fractional sum, the $\nu - th$ fractional difference operator is introduced as follows:

Definition 1.3.5. [65] Let $g : \mathbb{N}_a \rightarrow \mathbb{R}$, and $\nu > 0$ be given with $n - 1 < \nu < n$ where $n \in \mathbb{R}$, the $\nu - th$ fractional difference operator is called also the $\nu - th$ Riemann-Liouville difference operator is given as

$$\Delta_a^\nu g(t) = \Delta^n \Delta_a^{-(n-\nu)} g(t), \quad t \in \mathbb{N}_{a+n-\nu}. \quad (1.3.1)$$

Remark 1.3.6. Using the fractional sum operator, the domain of the fractional difference may be calculated as

$$D\{\Delta_a^\nu g\} = D\{\Delta^n \Delta_a^{-(n-\nu)} g\} = D\{\Delta_a^{-(n-\nu)} g\} = \mathbb{N}_{a+n-\nu}.$$

Example 1.3.7.

$$\Delta_0^{\frac{1}{2}} 1 = \Delta \Delta_0^{-(1-\frac{1}{2})} 1 = \Delta \Delta_0^{-\frac{1}{2}} 1 = \Delta_0 \left(\frac{2}{\sqrt{\pi}} t^{(\frac{1}{2})} \right) = \frac{1}{\sqrt{\pi}} t^{(-\frac{1}{2})}.$$

Theorem 1.3.8. [65] $\forall \nu > 0, g \in \mathbb{N}_a$, then:

$$\Delta_a^\nu \Delta_{a+\nu}^{-\nu} g(t) = g(t),$$

where $n = \lceil \nu \rceil + 1$.

Remark 1.3.9. We see that $\Delta_a^{-\nu}$ is the right invers of the operateur $\Delta_{a+\nu}^\nu$.

Theorem 1.3.10. [65] $\forall \nu > 0, g \in \mathbb{N}_a$, then:

$$\Delta_{a+\nu}^{-\nu} \Delta_a^\nu g(t) = g(t) - \sum_{r=0}^{n-1} \frac{(t-a)^{(\nu-n+r)}}{\Gamma(\nu-n+r+1)} \Delta_a^{r-(n-\nu)} g(a), \quad \forall t \in \mathbb{N}_{a+n}.$$

Where $n = \lceil \nu \rceil + 1$.

Remark 1.3.11. We see that generally

$$\Delta_{a+\nu}^{-\nu} \Delta_a^\nu g(t) \neq g(t)$$

1.4 Caputo difference operator

Definition 1.4.1. [1] Let $\nu > 0$, $\nu \in \mathbb{N}$. Then ν -th order Caputo fractional difference of a function g defined by:

$${}^C\Delta_a^\nu g(t) = \Delta_a^{-(n-\nu)} \Delta^n g(t) = \frac{1}{\Gamma(n-\nu)} \sum_{s=a}^{t-(n-\nu)} (t-s-1)^{(n-1-\nu)} \Delta^n g(s), \quad t \in \mathbb{N}_{a+n-\nu}, \quad (1.4.1)$$

where $n = \lceil \nu \rceil + 1$.

The following theorem presents a rule for composing the Caputo fractional difference operators with the fractional sum.

Theorem 1.4.2. [1] For $n-1 < \nu \leq n$, we have:

$$\Delta_{a+(n-\nu)}^{-\nu} {}^C\Delta_a^\nu g(t) = g(t) - \sum_{r=0}^{n-1} \frac{(t-a)^{(r)}}{r!} \Delta^r g(a), \quad t \in \mathbb{N}_a, \quad (1.4.2)$$

where $n = \lceil \nu \rceil + 1$.

In particular, if $0 < \nu \leq 1$ then

$$\Delta_{a+(n-\nu)}^{-\nu} {}^C\Delta_a^\nu g(t) = g(t) - g(a), \quad t \in \mathbb{N}_{a+n-\nu}. \quad (1.4.3)$$

In the following theorem, we introduce the relation between the Caputo and the Riemann-Liouville difference operators.

Theorem 1.4.3. [1] Let $g : \mathbb{N}_a \rightarrow \mathbb{R}$, $\nu > 0$. For $n-1 < \nu \leq n$, we have

$${}^C\Delta_a^\nu g(t) = \Delta_a^\nu g(t) - \sum_{r=0}^{n-1} \frac{(t-a)^{(r-\nu)}}{\Gamma(r-\nu+1)} \Delta^r g(a), \quad t \in \mathbb{N}_{a+n-\nu}, \quad (1.4.4)$$

where $n = \lceil \nu \rceil + 1$.

In particular, when $0 < \nu \leq 1$, we have:

$${}^C\Delta_a^\nu g(t) = \Delta_a^\nu g(t) - \frac{(t-a)^{(-\nu)}}{\Gamma(1-\nu)} g(a), \quad t \in \mathbb{N}_{a+n-\nu}. \quad (1.4.5)$$

Now, we shall give the following theorem that allows us to construct the numerical formula for the Caputo fractional difference system.

Theorem 1.4.4. [20] Consider the discrete fractional initial value problem:

$$\begin{cases} {}^C\Delta_a^\nu X(t) = g(t + \nu - 1, X(t + \nu - 1)) \\ \Delta^k X(t) = X_k, \quad n = \lceil \nu \rceil + 1, \quad k = 0, 1, \dots, n - 1. \end{cases} \quad (1.4.6)$$

The equivalent discrete fractional equation for discrete fractional problem (1.4.6) is given by:

$$X(t) = X_0(t) + \frac{1}{\Gamma(\nu)} \sum_{s=a+n-\nu}^{t-\nu} (t-s+1)^{(\nu-1)} g(s+\nu-1, X(s+\nu-1)), \quad t \in \mathbb{N}_{a+n}. \quad (1.4.7)$$

where

$$X_0(t) = \sum_{k=0}^{n-1} \frac{(t-a)^{(k)}}{\Gamma(k+1)} \Delta^k X(k).$$

The numerical formula for (1.4.7) can be designed as follows:

$$X(t) = X_0(t) + \frac{1}{\Gamma(\nu)} \sum_{j=0}^{t-1} \frac{\Gamma(t+\nu-1-j)}{\Gamma(t+\nu-j)} g(j, X(j)), \quad 0 < \nu \leq 1. \quad (1.4.8)$$

1.5 Fractional h -difference operator

Definition 1.5.1. Let $h > 0$ and $(h\mathbb{N})_a = \{a + h, a + 2h, \dots\}$. The difference operator Δ_h is defined by

$$\Delta_h X(t) = \frac{X(t+h) - X(t)}{h}.$$

Definition 1.5.2. [12] For arbitrary $t, \nu \in \mathbb{R}$ the h -factorial function is defined by

$$t_h^{(\nu)} = h^\nu \frac{\Gamma(\frac{t}{h} + 1)}{\Gamma(\frac{t}{h} - \nu + 1)}.$$

$t_h^{(\nu)}$ read $\frac{t}{h}$ to the ν factorial.

Remark 1.5.3. [34] For $t \geq 0$ and $\nu \in \mathbb{R}$, $\lim_{h \rightarrow 0} t_h^{(\nu)} = t^{(\nu)}$.

Definition 1.5.4. [12] Let $g : (h\mathbb{N})_a \rightarrow (h\mathbb{N})_{a+\nu h}$ the fractional h -sum of order $\nu > 0$ is given by

$${}_h\Delta_a^{-\nu} g(t) = \frac{h}{\Gamma(\nu)} \sum_{s=\frac{a}{h}}^{\frac{t}{h}-\nu} (t - \sigma(sh))_h^{(\nu-1)} \Delta g(sh), \quad a \in \mathbb{R}, \quad t \in (h\mathbb{N})_{a+\nu h}, \quad (1.5.1)$$

where $\sigma(sh) = (s+1)h$.

Definition 1.5.5. [34] The Caputo h -difference operator ${}_h^C\Delta_a^\nu$ of a function $g(t)$ is defined as:

$${}_h^C\Delta_a^\nu g(t) = {}_h\Delta_a^{-(n-\nu)} \Delta_h^n g(t), \quad t \in (h\mathbb{N})_{a+(\nu-1)h}. \quad (1.5.2)$$

For $\nu \notin \mathbb{N}$ is the fractional order and $n = \lceil \nu \rceil + 1$.

Lemma 1.5.6. [11] For any discrete time $t \in (h\mathbb{N})_{a+(\nu-1)h}$, the following inequality holds

$${}_h^C\Delta_a^\nu g^2(t) \leq 2g(t + \nu h) {}_h^C\Delta_a^\nu g(t).$$

Theorem 1.5.7. [67] Consider the discrete fractional initial value problem:

$$\begin{cases} {}_h^C\Delta_a^\nu X(t) = g(t + \nu h, X(t + \nu h)) \\ \Delta^k X(t) = X_k, \quad n = \lceil \nu \rceil + 1, \quad k = 0, 1, \dots, n - 1.. \end{cases} \quad (1.5.3)$$

The equivalent discrete fractional equation for discrete fractional problem (1.5.3) is given by:

$$X(n+1) = X_0 + \frac{h^\nu}{\Gamma(\nu)} \sum_{j=0}^n \frac{\Gamma(n-j+\nu)}{\Gamma(n-j+1)} g(j+1, X(j+1)), \quad t \in \mathbb{N}_{a+h}, \quad (1.5.4)$$

where

$$X_0 = \sum_{k=0}^{n-1} \frac{(t-a)^{(k)}}{\Gamma(k+1)} \Delta_h^k X(k).$$

1.6 Stability of difference systems

The study of discrete fractional systems's asymptotic stability is crucial because it advances our understanding of chaos and provides evidence for the convergence of a system's states to zero (or different equilibrium points) as infinity approaches. When discussing the stabilization and discrete fractional dynamical systems, this is especially crucial. This section will begin with a brief definition of stability, followed by a discussion of stability theorems for both linear and nonlinear difference equations in both fractional and integer orders. Comments and examples are given.

1.6.1 Stability types

Consider the following vector difference equation

$$\begin{cases} x(n+1) = g(n, x(n)) \\ x(0) = x_0 \end{cases} . \quad (1.6.1)$$

where $x(n) \in \mathbb{R}^n$ and $g : \mathbb{R}^{n+1} \rightarrow \mathbb{R}^{n+1}$. Suppose that $g(n, x(n))$ is continuous.

Definition 1.6.1. A point x_e is called equilibrium point of (1.6.1) if it satisfies:

$$g(x_e) = x_e. \quad (1.6.2)$$

A system is said to be stable around an equilibrium point if when weak disturbances are applied, it remains in the vicinity of this point.

Definition 1.6.2. An equilibrium point x_e of a discret system is stable in the sense of Lyapunov if and only if

$$\forall \varepsilon > 0, \exists \delta > 0 : \|x_0 - x_e\| \leq \delta \Rightarrow \|x(k) - x_e\| \leq \varepsilon.$$

Otherwise the equilibrium point is unstable.

Definition 1.6.3. An equilibrium point x_e of a discret system is attractive if

$$\lim_{k \rightarrow \infty} \|x(k) - x_e\| = 0.$$

Definition 1.6.4. An equilibrium point x_e of a discrete system is asymptotically stable if it is stable and attractive i.e.,

$$\forall \varepsilon > 0 \exists \delta > 0 : \|x_0 - x_e\| \leq \delta \Rightarrow \lim_{k \rightarrow \infty} \|x(k) - x_e\| = 0.$$

Asymptotic stability means that not only is the point of equilibrium stable, but that we is also able to determine a domain close to the point of equilibrium such that any trajectory, resulting from an initial state x_0 belonging to this domain, tends to x_e when k lead to infinity.

1.6.2 Stability of integer order difference systems

Stability of linear difference system

Consider the integer order difference system:

$$\begin{cases} \Delta x(k) = Ax(k), & k \in \mathbb{N} \\ x(0) = x_0, & x_0 \in \mathbb{R}, \end{cases} \quad (1.6.3)$$

Where $x(k) = (x_1(k), x_2(k), \dots, x_n(k))^T \in \mathbb{R}^n$, A is $n \times n$ constant matrix.

Theorem 1.6.5. [30] If all the eigenvalues λ_i of A satisfies $|\lambda_i + 1| < 1$, $1 \leq i \leq n$, then the trivial solution of the system (1.6.3) is asymptotically stable on \mathbb{N} . Furthermore, if there is an eigenvalue λ of A with $|\lambda + 1| > 1$, then the trivial solution of the system (1.6.3) is unstable on \mathbb{N} .

Example 1.6.6. Consider the following linear system :

$$\Delta x(k) = \begin{pmatrix} a & a \\ a & a \end{pmatrix} x(k), \quad k \in \mathbb{N}, \quad \forall a \in \mathbb{R}. \quad (1.6.4)$$

The characteristic equation for A is given by: $\lambda^2 - 2a\lambda = 0$. The eigenvalue of A are: $\lambda_1 = 0, \lambda_2 = 2a$, by Theorem 1.6.5 the trivial solution of (1.6.4) is asymptotically stable on \mathbb{N} if and only if $|a| < \frac{1}{2}$.

Example 1.6.7. Consider the following linear system:

$$\Delta x(k) = \begin{pmatrix} 1 & 6 \\ 0 & -2 \end{pmatrix} x(k), \quad k \in \mathbb{N}. \quad (1.6.5)$$

The characteristic equation for A given by: $\lambda^2 + \lambda - 2 = 0$. The eigenvalue of A are: $\lambda_1 = -2, \lambda_2 = 1$. Since $|\lambda_1| = 2 > 1$, by Theorem 1.6.5 the trivial solution of (1.6.5) is unstable on \mathbb{N} .

Remark 1.6.8. Let λ_i be eigenvalues of A . Assume $|\lambda_i + 1| \leq 1$, $1 \leq i \leq n$. If whenever $|\lambda_i + 1| = 1$ and λ_i is a simple eigenvalue of A . Then the trivial solution of (1.6.3) is stable on \mathbb{N} . If there is a non simple eigenvalue λ of A satisfying $|\lambda + 1| = 1$, then we can't conclude.

Example 1.6.9. Consider the following system:

$$\Delta x(k) = \begin{pmatrix} -1 + \cos \theta & \sin \theta \\ -\sin \theta & -1 + \cos \theta \end{pmatrix} x(k), \quad k \in \mathbb{N}. \quad (1.6.6)$$

Where θ is a real constant. For each θ the eigenvalues of the coefficient matrix in (1.6.6) are:

$\lambda_1 = e^{+i\theta} - 1$, $\lambda_2 = e^{-i\theta} - 1$. Since $|\lambda_1 + 1| = |\lambda_2 + 1| = 1$ and both eigenvalues are simple, we have by Remark 1.6.8 that the trivial solution of (1.6.6) is stable on \mathbb{N} .

Stability of non linear systems

Consider the following non-linear system:

$$\begin{cases} \Delta x(k) = f(x(k)), \quad k \in \mathbb{N} \\ x(0) = x_0, \quad x_0 \in \mathbb{R}. \end{cases} \quad (1.6.7)$$

Where $f : \mathbb{R}^n \rightarrow \mathbb{R}^n$, a continuously differentiable non linear function, suppose that $x = 0$ is an equilibrium point for the system (1.6.7).

•Linearisation method (Lyapunov indirect method):

Theorem 1.6.10. [30] Let J be the Jacobian matrix of f at 0:

If all the eigenvalues λ_i of J satisfies $|\lambda_i + 1| < 1$, $1 \leq i \leq n$, then the trivial solution of the (1.6.7) is globally asymptotically stable on \mathbb{N} . Furthermore, if there is an eigenvalue λ of J with $|\lambda + 1| > 1$, then the trivial solution of the system (1.6.7) is unstable on \mathbb{N} .

Example 1.6.11. Consider the following non-linear system:

$$\begin{cases} \Delta x(k) = \frac{2y(k)}{1+x^2(k)} \\ \Delta y(k) = \frac{x(k)}{1+y^2(k)} \end{cases}. \quad (1.6.8)$$

The jacobian matrix at the origine given is by:

$$J = \begin{pmatrix} 0 & 2 \\ 1 & 0 \end{pmatrix}$$

The characteristic equation for J is : $\lambda^2 - 2$, hence the eigenvalues are $\lambda_1 = \sqrt{2}$, $\lambda_2 = -\sqrt{2}$, it is clear that $|\lambda_i + 1| = 1 + \sqrt{2} > 1$, where $i = 1, 2$. Then, by theorem 1.6.10 the trivial solution of (1.6.8) is unstable on \mathbb{N} .

Remark 1.6.12. If some eigenvalues of the Jacobian matrix J are 1, we cannot conclude about the local stability of the equilibrium point.

• **Lyapunov direct method:** For the study of the nonlinear stability, the most traditional method is based on the linearization and the use of the eigenvalues of the linearized system, Lyapunov proposed a second method, inspired by the idea of mechanical energy of Lagrange who formulated the principle of stability of mechanical systems. This method, called Lyapunov's direct method, is based on the search for a scalar function of definite sign with real values.

Theorem 1.6.13. [30] If there exists a function $V : \mathbb{R}^n \rightarrow \mathbb{R}_+$, which is continuous and differentiable such that:

- $V(0) = 0$,
- $V(x(k)) > 0, \forall x \in \mathbb{R}^n \setminus \{0\}, \forall k \in \mathbb{N}$,
- $\Delta V(x(k)) = V(x(k+1)) - V(x(k)) \leq 0, \forall x \in \mathbb{R}^n \setminus \{0\}, \forall k \in \mathbb{N}$.

Then the trivial solution of (1.6.7) is asymptotically stable, Moreover if:

$$\Delta V(k) = V(x(k+1)) - V(x(k)) < 0, \forall x \in \mathbb{R}^n \setminus \{0\}, \forall k \in \mathbb{N}.$$

Then the trivial solution of (1.6.7) is asymptotically stable.

Example 1.6.14. Consider the following non-linear system [99]:

$$\begin{cases} \Delta x(k) = \frac{y(k)}{1 + y^2(k)} - x(k) \\ \Delta y(k) = \frac{x(k)}{1 + y^2(k)} - y(k) \end{cases}. \quad (1.6.9)$$

It has an equilibrium point at the origin. which has the origin as only the equilibrium point. First, we will select the following Lyapunov function: $V(x(k), y(k)) = x^2(k) + y^2(k)$, this is clearly continuous and positive definite on \mathbb{R} . Therefore, we find out

$$\Delta V(x(k), y(k)) = V(x(k), y(k)) \left(\frac{1}{(1 + y^2(k))^2} - 1 \right) < 0. \quad (1.6.10)$$

Then, by Theorem 1.6.13 the trivial solution of the system (1.6.9) is asymptotically stable.

1.6.3 Stability of fractional order difference systems

Stability of linear systems

Now, we investigate the stability of the equilibrium point $x = 0$ of the ν -th order linear system of difference equation

$${}^C\Delta_a^\nu x(t) = Ax(t + \nu - 1). \quad (1.6.11)$$

Where $0 < \nu < 1$, $a \in \mathbb{R}$ is a starting point, A is a an $n \times n$ constant matrix. concerning the stability and existence of asymptotic results. The most common theorems used are Lyapunov stability and the stabilization of the origin equilibrium point. They are respectively announced in the following theorems.

Theorem 1.6.15. [19] *The zero equilibrium of the linear system (1.6.11) is asymptotically stable if:*

$$\lambda \in \{z \in \mathbb{C} : |z| < \left(2 \cos \frac{|\arg z| - \pi}{2 - \nu}\right)^\nu, \text{ and } |\arg z| > \frac{\nu\pi}{2}\},$$

for all the eigenvalues λ of A .

Example 1.6.16. Consider the following linear fractional discrete system:

$$\begin{cases} {}^C\Delta_a^\nu x(t) = -x(t + \nu - 1) \\ {}^C\Delta_a^\nu y(t) = 0.5x(t + \nu - 1) - y(t + \nu - 1) \end{cases}, \quad (1.6.12)$$

where $0 < \nu < 1$, $t \in \mathbb{N}_{a-\nu+1}$ and the matrix A is given by

$$A = \begin{pmatrix} -1 & 0 \\ 0.5 & -1 \end{pmatrix}$$

The eigenvalues of the matrix A are $\lambda_1 = -1$, $\lambda_2 = -1$. Hence

$$|\lambda_j| = 1 < \left(2 \cos \frac{|\arg z| - \pi}{2 - \nu}\right)^\nu \text{ and } |\arg \lambda_j| = \pi > \frac{\nu\pi}{2}, \quad j = 1, 2.$$

According to Theorem 1.6.15, the trivial solution of the system (1.6.12) is asymptotically stable. The time evolution of the states of the system (1.6.12) is shown in Figure 1.1.

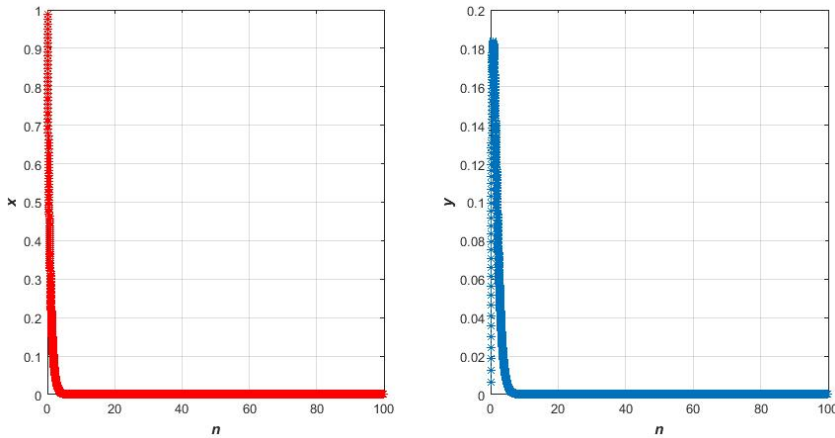


Figure 1.1: Time evolution of states of the system (1.6.12) for $\nu = 0.95$.

Stability of non linear systems

Concerning the stability and existence of asymptotic results. Most common theorems used are Lyapunov stability, and the stabilization of origin equilibrium point. They are respectively announced in the following theorems.

Theorem 1.6.17. [11] *The fractional nonlinear discrete system*

$${}_h^C \Delta_a^\nu X(t) = f(t + h\nu, X(t + h\nu)), \quad t \in (h\mathbb{N})_{a+(1-\nu)h}. \quad (1.6.13)$$

is asymptotically stable if there exists a positive definite and decreasing scalar function $V(t, X(t))$ for the equilibrium point $x = 0$, such that ${}_h^C \Delta_a^\nu V(t, X(t)) \leq 0$.

Example 1.6.18. Consider the following non-linear fractional h -difference system

$$\begin{cases} {}_h^C \Delta_a^\nu x(t) = -x(t + h\nu) - y(t + h\nu)x(t + h\nu), \\ {}_h^C \Delta_a^\nu y(t) = x^2(t + h\nu) - y(t + h\nu), \end{cases} \quad (1.6.14)$$

where $0 < \nu < 1$, $t \in \mathbb{N}_{a+(1-\nu)h}$.

By using the Lyapunov function $V(z_1, z_2) = \frac{1}{2}x^2 + \frac{1}{2}y^2$ and according to Lemma 1.5.6, we obtain

$$\begin{aligned}
{}_h^C \Delta_a^\nu V &\leq x(t + h\nu) {}_h^C \Delta_a^\nu x(t) + y(t + h\nu) {}_h^C \Delta_a^\nu y^2(t) \\
&\leq -x^2(t + h\nu) - y(t + h\nu)x^2(t + h\nu) \\
&\quad + y(t + h\nu)x^2(t + h\nu) - y^2(t + h\nu) \\
&= -x^2(t + h\nu) - y^2(t + h\nu) < 0.
\end{aligned}$$

Hence, according to Theorem 1.6.17 the system (1.6.14) is asymptotically stable. The time evolution of the states of the system (1.6.14) is shown in Figure 1.2.

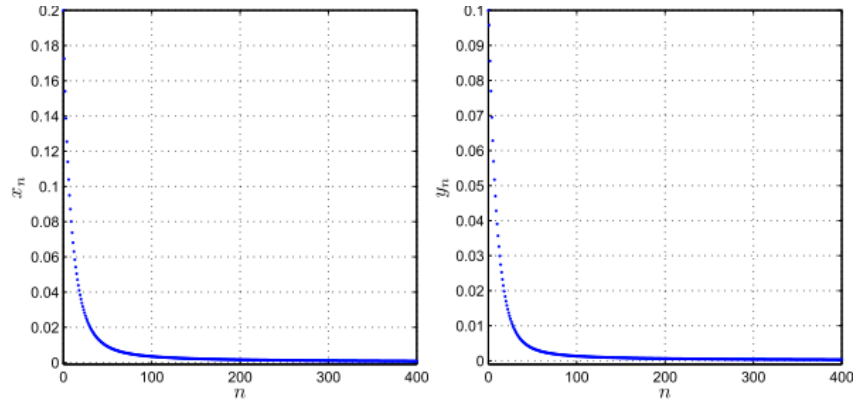


Figure 1.2: Time evolution of states of the system (1.6.14) for $\nu = 0.9$.

1.7 Conclusion

We provide a few definitions, theorems, and fundamental properties in this chapter that will be helpful in our future research. We will first go over a few fundamental functions before reviewing some terminology and discrete fractional calculus-related characteristics. Subsequently, the operators for fractional addition and fractional difference are defined. Additionally, the fundamental ideas behind the fractional h-difference operator are presented. An overview of current stability results for discrete systems with fractional and integer orders, both linear and non-linear, are given in the final part.

CHAPTER 2

CHAOS IN FRACTIONAL ORDER MAPS

2.1 Introduction

Chaos in discrete fractional dynamical systems is a fascinating and complex area of study that intersects mathematics, physics, and engineering. Although the field of chaos in fractional orders is new, there are many studies that have been published [50][84]. These systems are characterized by their discrete nature and the use of fractional calculus, an extension of traditional calculus that deals with derivatives and integrals of non-integer orders. This approach allows for a more nuanced understanding of systems that display memory and hereditary properties, which are common in many real-world scenarios. In the context of chaos theory, these discrete fractional dynamical systems exhibit behavior that is highly sensitive to initial conditions, leading to unpredictable and seemingly random outcomes despite being governed by deterministic rules. This chaotic behavior is not just a theoretical curiosity but has practical implications in various fields, such as signal processing, control theory, and biological modelling. In this chapter, we will explore the mathematical theory of chaos in more detail, starting with giving some of the basics concerning discrete dynamical systems, and then giving definitions and characteristics of

chaotic systems. The concept of Lyapunov exponents will be discussed for integer and fractional discrete-time systems. finally, different ways to evolve from a regular dynamic system toward chaos will be represented.

2.2 Basics of discrete dynamical systems

Chaos does not have a universally accepted mathematical definition, a popularly used definition was originally given by **Devaney** in 1989 [37]. Before we can provide a definition of chaos, we first need to define some necessary notions. We define the discrete dynamical system can be given as

$$u_{k+1} = G(u(k), \mu), \quad k = 1, 2, \dots \quad (2.2.1)$$

Where, G is a matrix function, $u(k) \in U \subseteq \mathbb{R}^n$ is the state vector and $\mu \in V \subseteq \mathbb{R}^n$ is the parameters vector.

Definition 2.2.1. *Let u be a point and let G be a map. The **orbit** of u under G is the set of points $\{u, G(u), G^2(u), \dots\}$. The starting point u for the orbit is called the initial value of the orbit.*

Definition 2.2.2. *Let G be a map on \mathbb{R}^n . We designate u^* a **periodic point** of period k if $G^k(u^*, \mu) = u^*$ where k is the smallest positive integer satisfying this condition. The orbit with initial point u^* (which consists of k points) is termed a periodic orbit of period k . We frequently employ the abbreviated terms **period- k point** and **period- k orbit**.*

Definition 2.2.3. *A **trajectory** represents the sequence of states traversed by a dynamical system over time, depicting the evolution of the system's state based on its governing maps and initial conditions. This sequence of states can be envisioned as a trajectory through the system's state space.*

Definition 2.2.4. *The collection of all potential states of a dynamic system is called its **phase space**. It can also be defined as an abstract space in which each variable represents a dimension n necessary for the description of the system at a given moment, the degree of freedom characterizing the phase space. It represents the order which is equal to the dimension of the state space.*

Definition 2.2.5. We call a **phase portrait** a graph which gives the appearance of Trajectories in phase space.

2.3 Concept of chaos theory

The concept of chaos was initially introduced in the examination of discrete dynamical systems by Li and Yorke in 1975 [64]. Various other definitions followed. Until the late 1980, the exploration of chaotic dynamics was predominantly confined to research literature. Devaney's book, "An Introduction to Chaotic Dynamical Systems," published in 1986 [37], served as a milestone, popularizing chaos as a mathematical concept and integrating it into university textbooks, including Holmgren's [44].

A dynamical system is described simply as a pair (X, F) , where $F : X \rightarrow X$ represents a map from a topological or metric space X to itself. So, let us get an eye on this property before citing the definition of chaos.

2.3.1 Mathematical definitions of chaotic attractors

Definition 2.3.1. Let (X, d) be a metric space and G a continuous map on X . We say that the topological dynamical system (X, G) has the property of **sensitive dependence on initial conditions** if there exists $\delta > 0$ such that, for any $x \in X$ and any neighborhood U of x , there exists $y \in U$ and $k \geq 0$ such that $|G^k(x) - G^k(y)| > \delta$.

Definition 2.3.2. Let X be a metric space. The function $G : X \rightarrow X$ is said to be **topologically transitive** if for any pair of non-empty open sets $U, W \subset X$, there exists $k \in \mathbb{N}$ such that $G^k(U) \cap W \neq \emptyset$.

Definition 2.3.3. A subset $I \subset X$ is said to be **dense** in X if for every $z \in X$ there a exists sequence $(z_n)_{n \in \mathbb{N}} \in I$ such that $\lim_{n \rightarrow \infty} z_n = z$.

In the following, we present the definition of chaos

Definition 2.3.4. Let G be an application. Suppose the corresponding dynamical system has an attractor A . This system is said to be **chaotic** on its attractor if

- 1- G possesses sensitive dependence on initial values.
- 2- $G : A \rightarrow A$ is topologically transitive.
- 3- The set of periodic points of G is dense in A .

2.3.2 Characteristics of chaotic maps

- **Sensitivity to initial conditions**

Sensitivity to initial conditions also known as the **butterfly effect**, refers to the rapid and unpredictable divergence in a system's behavior due to small variations in the initial conditions. This concept, a key finding of the 20th century, reveals that even deterministic systems can exhibit inherent unpredictability. In the 1960, meteorologist Edward Lorenz [59] discovered that in his computer-based weather model, which used twelve variables, Small differences in initial conditions could lead to significantly different weather outcomes. He noted that two states, initially almost identical, could evolve into markedly distinct states over time. Lorenz pointed out that since any real system would have some level of observational error, making precise predictions for a distant future state is impossible. This observation, particularly relevant to weather forecasting, highlights the limitations in achieving highly accurate long-term forecasts due to the natural inaccuracy and incompleteness of weather observations.

- **Positive Lyapunov exponent**

It requires nonlinear systems to separate or mutually approximate motion paths and then assess the total effect of this. When the Lyapunov exponent is positive, it means that the distance between neighboring orbits is growing exponentially and that there is information loss between those places. We will talk about chaotic degrees later on, but a bigger Lyapunov exponent indicates a more substantial loss of information.

- **Strange attractor**

The term 'Strange Attractor' is used to describe an attractor (a region or shape to which points are 'pulled' as the result of a certain process) that displays sensitive dependence on initial conditions (that is, points which are initially close on the attractor become exponentially separated with time).

Definition 2.3.5. *A bounded subset A of the phase space is a strange attractor for a trans-*

formation T of the space if there exists a neighborhood U of A , i.e. for every point in A , there exists a ball containing this point and contained in \mathbb{R} satisfying the following properties:

1. **Attractor:** U is an absorbing zone, which means that every orbit by T whose initial point is in U is entirely contained in U . Additionally, every orbit of this type becomes and remains as close to A as desired.
2. **Sensitivity:** The orbits whose initial point is in \mathbb{R} are extremely sensitive to initial conditions.
3. **Mixing property:** For any point in A , there exist orbits starting in \mathbb{R} that pass as close as desired to this point.

Definition 2.3.6. Suppose $A \subset \mathbb{R}^n$ is an attractor. Then, we say that A is a **strange attractor** if it is chaotic.

We give below some examples of strange attractors:

2.4 Examples of strange attractors

2.4.1 Fractional Lozi map

The fractional version of the Lozi map [50] is given as follows

$$\begin{cases} {}^C\Delta_a^\nu x(t) = -a|x(t + \nu - 1)| + y(t + \nu - 1) - x(t + \nu - 1) + 1 \\ {}^C\Delta_a^\nu y(t) = bx(t + \nu - 1) - y(t + \nu - 1) \end{cases}, \quad (2.4.1)$$

where $0 < \nu < 1$, $t \in \mathbb{N}_{a+1-\nu}$.

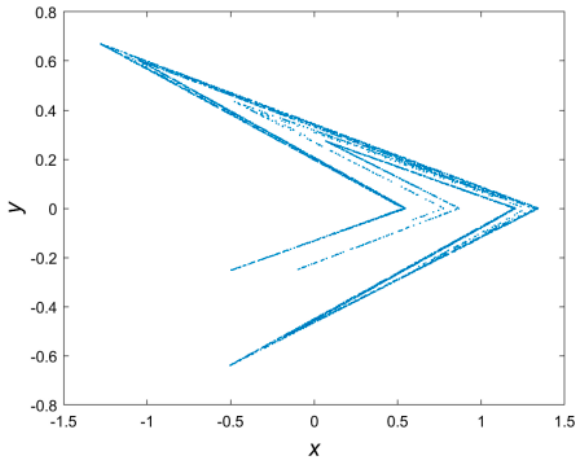


Figure 2.1: The Lozi attractor for $(x_0, y_0) = (0, 0)$, $\nu = 0.98$, $a = 1.7$ and $b = 0.5$.

2.4.2 Fractional Rössler map

The fractional version of the Lozi map [49] is given as follows

$$\begin{cases} {}^C\Delta_a^\nu x(t) = b_1 x(t + \nu - 1)(1 - x(t + \nu - 1)) \\ \quad - b_2(z(t + \nu - 1) + b_3)(1 - 2y(t + \nu - 1)) - x(t + \nu - 1) \\ {}^C\Delta_a^\nu y(t) = b_4 y(t + \nu - 1)(1 - y(t + \nu - 1)) + b_5 z(t + \nu - 1) - y(t + \nu - 1) \\ {}^C\Delta_a^\nu z(t) = b_6(1 - b_7 x(t + \nu - 1))((z(t + \nu - 1) + b_3)(1 - 2y(t + \nu - 1)) - 1) - z(t + \nu - 1) \end{cases}, \quad (2.4.2)$$

where $0 < \nu < 1$, $t \in \mathbb{N}_{a+1-\nu}$ and $(b_1, b_2, b_3, b_4, b_5, b_6, b_7) = (3.8, 0.05, 0.35, 3.78, 0.2, 0.1, 1.9)$

2.5 Lyapunov exponent

The average multiplicative separation rate between a derivative product explains the separation rate between any point x and the closest fixed point x^* . This measure indicates whether two orbits will remain near or will be infinitely distant. The term Lyapunov number has been used to express this rate. Then, the Lyapunov exponent can be defined as the natural logarithm of the Lyapunov number. The LEs give a tool to measure the sensitive dependence on the initial conditions. In particular, one positive value of LEs

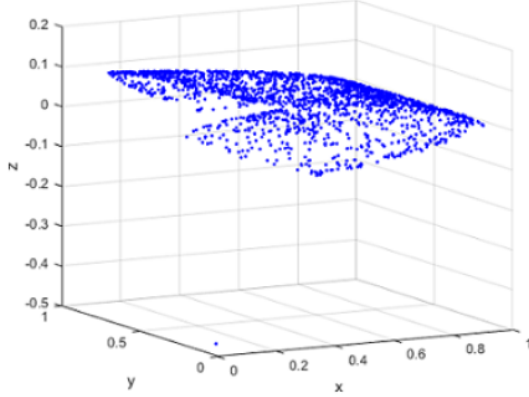


Figure 2.2: The Rössler attractor for $(x_0, y_0, z_0) = (0.1, 0.2, -0.5)$, $\nu = 0.903$.

means that the system is in chaos.

2.5.1 Definition of Lyapunov exponents in integer-order maps

Considering the following difference equations define the discrete dynamical system.

$$x(n+1) = f(x(n)), \quad (2.5.1)$$

f is a nonlinear continuous differentiable function, and x is the phase space vector. To clarify what LE is, we begin with an initial condition that belongs to the discrete dynamical system's trajectory x , and a neighborhood point of the trajectory x' , where the initial distance (δx_0) is extremely small. Let (δx_n) be the distance after n iteration. The sensitivity to initial conditions can be quantified as

$$\|\delta x_n\| \approx \|\delta x_0\| e^{n\lambda}, \quad (2.5.2)$$

where λ is the maximum Lyapunov exponent (MLE), which describes the rate at which two close initial points of a dynamical system diverge or converge. The MLE can be estimated for long iterations as follows:

$$\lambda = \lim_{n \rightarrow \infty} \frac{1}{n} \ln \frac{\|\delta x_n\|}{\|\delta x_0\|}. \quad (2.5.3)$$

The maximum LE alone does not fully characterize the instability of a m -dimensional dynamical system. There are m exponents (equal to the dimension of the phase space)

which are customarily ranked from largest to smallest, as

$$\lambda_1 \geq \lambda_2 \geq \dots \geq \lambda_m.$$

By taking into account a small m -dimensional sphere of initial conditions in the phase space of the discrete dynamical system (2.5.1), rather than just one nearby initial condition, we can go beyond equation (2.5.3) to determine all m -Lyapunov exponents. This is reflected by the **tangent space** given by the Jacobian matrix of the system (2.5.1), the corresponding matrix partial derivatives are given by the chain rule

$$D_x f^n(x(0)) = J(f^{n-1}(x(0))) \times J(f^{n-2}(x(0))) \times \dots \times J(f(x(0))) \times J((x(0))), \quad (2.5.4)$$

Consequently, the separation of two initial points $x(0)$ and $x'(0)$ after discrete-time n is then become

$$\delta x_n \simeq D_{x_0} f^n(x(0)) \delta x_0. \quad (2.5.5)$$

Oseledec (1968) then states in [69] that we can characterise the average rate of growth as

$$\lambda_1 = \lim_{n \rightarrow \infty} \frac{1}{n} \ln \|J^n(x(0))u\|. \quad (2.5.6)$$

The limit exists for almost all $x(0)$ and for almost all tangent vectors u it is equal to the maximum Lyapunov exponent λ_1 . Additionally, if we indicate by $a_i(n, x)$ the i^{th} eigenvalue of J^n arranged in a way that $a_1(n, x) \geq a_2(n, x) \geq \dots \geq a_m(n, x)$. The i^{th} Lyapunov exponent, $\lambda_i(x)$, is then defined as

$$\lambda_k = \lim_{n \rightarrow \infty} \frac{1}{n} \ln |\lambda_k^{(n)}|, \quad k = 1, \dots, m. \quad (2.5.7)$$

Because we are unable to compute the matrix J^n , which necessitates the calculation of the product (2.5.5), it is exceedingly challenging to determine the Lyapunov exponents analytically. For chaotic attractors, the components of matrix J^n grow very large even after just a few iterations, while for periodic attractors, they remain null. As a result, numerical computation becomes crucial to avoiding this problem [27]. Numerous techniques have been proposed for calculating LEs, such as the Wolf method [109] and the QR decomposition method [100] (where Q is an orthogonal matrix and R is an upper triangular matrix). In situations where the vectors are frequently renormalized via the

GramShmidt process, the Wolf algorithm is most frequently employed. However, because fractional-order discrete systems take into account all of the previous variable values, the Wolf method does not apply to them, in contrast to integer-order dynamical systems. This led to the creation of a more practical new algorithm for estimating fractional discrete systems' Lyapunov exponents. Recently, in [110] Wu and Balaneau explored applying the Jacobian matrix algorithm to discrete fractional maps. In the remaining portion of this section, we go into further detail about the algorithm and numerical computation.

2.5.2 Lyapunov exponents in fractional-order maps

The fractional order difference equations with the ν -Caputo operator are given by

$$\begin{cases} {}^C\Delta_a^\nu x(t) = g(x(t + \nu - 1)) \\ \Delta^k(a) = x_k, \quad m = \lceil \nu \rceil + 1 \quad k = 0, 1, \dots, m - 1. \end{cases} \quad (2.5.8)$$

Where $g(t) = (g_1(t), \dots, g_m(t))^T$ is a vector-valued nonlinear function, $x(t) = (x_1(t), \dots, x_m(t))^T$ the state vector and the fractional order value $m - 1 < \nu \leq m$. To set up the tangent map corresponding to the above system, we would need at first the Jacobian matrix of the right side which is given by

$$G(n) = \begin{pmatrix} \frac{\partial g_1}{\partial x_1}(n) & \frac{\partial g_1}{\partial x_2}(n) & \dots & \frac{\partial g_1}{\partial x_m}(n) \\ \vdots & \vdots & \vdots & \vdots \\ \frac{\partial g_m}{\partial x_1}(n) & \frac{\partial g_m}{\partial x_2}(n) & \dots & \frac{\partial g_m}{\partial x_m}(n) \end{pmatrix}. \quad (2.5.9)$$

Then, the Jacobian matrix $J(n)$ is defined by

$$J(n) = \begin{pmatrix} a_{11}(n) & a_{12}(n) & \dots & a_{1m}(n) \\ \vdots & \vdots & \vdots & \vdots \\ a_{m1}(n) & a_{m2}(n) & \dots & a_{mm}(n) \end{pmatrix}. \quad (2.5.10)$$

where $J(0) = I$ is the identity matrix. Each element of the matrix J can be calculated by multiplying the matrix $G(n)$ with the matrix $J(n)$, ie:

$$J = \begin{pmatrix} \frac{\partial g_1}{\partial x_1}(n) & \frac{\partial g_1}{\partial x_2}(n) & \dots & \frac{\partial g_1}{\partial x_m}(n) \\ \vdots & \vdots & \vdots & \vdots \\ \frac{\partial g_m}{\partial x_1}(n) & \frac{\partial g_m}{\partial x_2}(n) & \dots & \frac{\partial g_m}{\partial x_m}(n) \end{pmatrix} \times \begin{pmatrix} a_{11}(n) & a_{12}(n) & \dots & a_{1m}(n) \\ \vdots & \vdots & \vdots & \vdots \\ a_{m1}(n) & a_{m2}(n) & \dots & a_{mm}(n) \end{pmatrix}. \quad (2.5.11)$$

Then, The tangent map system is given as follows

$$\begin{cases} a_{11}(n+1) = a_{11}(0) + \frac{1}{\Gamma(\nu)} \sum_{j=0}^n \frac{\Gamma(n-j+\nu)}{\Gamma(n-j+1)} a_{11}(j) \frac{\partial g_1}{\partial x_1}(j) + a_{12}(j) \frac{\partial g_1}{\partial x_2}(j) + \dots + a_{1m}(j) \frac{\partial g_1}{\partial x_m}(j), \\ \vdots \quad \vdots \quad \vdots \\ a_{mm}(n+1) = a_{m1}(0) + \frac{1}{\Gamma(\nu)} \sum_{j=0}^n \frac{\Gamma(n-j+\nu)}{\Gamma(n-j+1)} a_{m1}(j) \frac{\partial g_m}{\partial x_1}(j) + a_{m2}(j) \frac{\partial g_m}{\partial x_2}(j) + \dots + a_{mm}(j) \frac{\partial g_m}{\partial x_m}(j). \end{cases} \quad (2.5.12)$$

According to the discrete equation (2.5.12), the tangent map holds a discrete memory effect. Therefore, the LEs of the fractional order discrete-time system can be derived from the following equation

$$\lambda_k = \lim_{i \rightarrow \infty} \frac{1}{i} \ln |\lambda_k^{(i)}|, \quad k = 1, \dots, m. \quad (2.5.13)$$

By using the spectrum's sign to determine the stability of the FODTSs, we can effectively carry out this method going forward, the next theorem illustrates this objective.

Theorem 2.5.1. [61] *When the average Lyapunov exponent is positive, it indicates a chaotic system, when it is negative, it indicates a periodic orbit; and when it is zero, it indicates a bifurcation, which means the orbits are moving periodically.*

2.6 Bifurcation diagrams

A system's dynamic behaviour varies along with its parameter changes. Small quantitative changes in the system's states are usually produced by small changes in the parameter. A bifurcation is a specific change in the map's behavior. Thus, the fundamental change in the dynamics of nonlinear systems under parameter variation is described by the bifurcation phenomenon. It is regarded as a tool that aids in understanding equilibrium loss and the effects it has on complex behavior because of this. Bifurcation diagrams facilitate the swift identification of qualitative shifts in the asymptotic solution by portraying specific properties of a dynamical system's solution about a control parameter. Bifurcations encompass various types, such as Hopf, Pitchfork, Transcritical, Saddle-node, Period doubling, and Neimark–Sacker. Typically, A **bifurcation diagram** is a portion of the parameter space on which all bifurcation points are represented (see Figure 2.3).

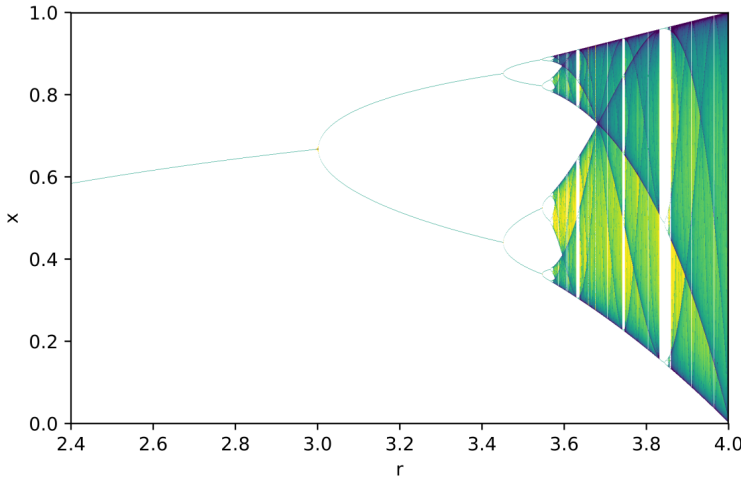


Figure 2.3: The bifurcation diagram of the logistic map.

2.7 Routes of chaos

What triggers a system to devolve into chaos remains a mystery. Regular dynamic systems may progress toward chaos in a variety of ways. Let us pretend for a second that the control parameter does influence the investigated dynamics. By adjusting this parameter, the system may go from a steady state to a periodic one; thereafter, it can follow a transition scenario and become chaotic after reaching a particular threshold. Various examples show how a fixed point may devolve into chaos. Rather than being a gradual process, the bifurcation is the hallmark of a fixed point's move to chaos. When two dynamic regimes abruptly diverge in terms of quality, this is called a bifurcation. Theory predicted all of these possibilities, and many tests have verified them. An early physics model for studying chaos was the Rayleigh-Benard thermal convection, which involves a fluid layer being subjected to a vertical temperature differential between two horizontal plates. Since then, chaos theory has been validated in other domains. We will quickly go over a few distinct kinds of evolution.

2.7.1 By period doubling

The most well-known example of this transition scenario is when, as the control parameter of the experiment is increased, the frequency of the periodic regime doubles, then is multiplied by 4, 8, 16,...etc. As the doublings get closer together, we move closer to a point of accumulation where we might theoretically obtain an infinite frequency; at this point, the system deviates into chaos. At this point, the system degenerates into chaos. Robert May has specifically studied it in population dynamics using the logistic map, $X_{n+1} = rX_n(1 - X_n)$. The sequence either converges to a fixed point or diverges, where r is a parameter that affects. As soon as r exceeds 3, the system bifurcates, which causes it to alternate between two values near the fixed point. This is referred to as a period 2 attractor cycle. These two attractors continue to move away from the fixed point and are increased until a new bifurcation happens. Each point splits, giving us a period 4 attractor cycle.

2.7.2 By intermittency

Through intermittency, this scenario is distinguished by the irregular appearance of chaotic bursts in a regularly oscillating system. After a certain amount of time, or "regularity," the system maintains a periodic or nearly periodic regime before abruptly destabilizing and erupting into chaos. After that, it stabilizes once more before later igniting another burst. It has been noted that as one moves further away from the critical value of the constraint, the frequency and duration of the chaotic phases tend to increase. Intermittency, in particular, presupposes that there is no attractor nearby and that the limit cycle, which corresponds to the periodic state from which this transition phenomenon arises, bifurcates sub-critically. In the Rossler system, this is what is seen.

2.7.3 By quasi-periodicity

The Lorenz model (1963) was used as an example in Ruelle and Takens' (1971) theoretical work to highlight the scenario via quasi-periodicity. Numerous experiments have supported this theory, including the well-known Rayleigh-Bénard in a small box experiment

in thermo-hydrodynamic convection and the Belousov-Zhabotinsky reaction in chemistry, among others. The "competition" of different frequencies in the dynamical system leads to this path to chaos. If we alter a parameter in a system that exhibits periodic behavior at a single frequency, a second frequency emerges. The behavior is periodic if the ratio between the two frequencies is logical. However, if the ratio is irrational, the behavior is quasi-periodic, and the trajectories in this situation cover a torus' surface. A third frequency then appears when we alter the parameter once more, and so on until chaos. Additionally, there are systems that go straight from two frequencies to chaos.

2.8 Conclusion

This chapter aims to provide a concise overview of key concepts in chaos theory within nonlinear discrete dynamical systems of fractional order ν . It introduces fundamental mathematical concepts and numerical tools essential for analyzing these irregular geometrical entities, laying the groundwork for the analysis and numerical simulations presented in our thesis. To clarify the findings, examples are given.

CHAPTER 3

THE FRACTIONAL DISCRETE USHIO SYSTEM: CHAOS AND STABILIZATION

3.1 Introduction

Developing control strategies for achieving stabilization is critical to chaotic systems research. The primary objective is to derive a one-dimensional control law that asymptotically brings both map trajectories to zero, thereby stabilizing chaotic systems. Fractional discrete chaotic systems have recently attracted more attention than ever before. There has been a lot of focus on studying control mechanisms that can successfully stabilize the chaotic dynamics at the origin. [79], [78], [47], [51], [114]. In this chapter, we provide a novel Ushio map of fractional order, extending the integer-order Ushio system proposed by T. Ushio in 1995 [97] as a contraction map. We first study the presence of chaotic behaviors in the fractional Ushio system, and then we stabilize the chaotic fractional discrete-time Ushio system by introducing a one-dimensional linear control law.

3.2 The fractional Ushio system

According to [97], the Ushio map was first suggested in the following way:

$$\begin{cases} x(k+1) = dx(k) - x^3(k) + y(k) \\ y(k+1) = 0.5x(k) \end{cases}, \quad (3.2.1)$$

where d is a bifurcation parameter. Due to its properties, the Ushio map finds applications in various fields [112], [33] beyond mathematics, including engineering, physics, and computer science. Researchers have used it to explore complex behaviors in systems and to develop methods for controlling or harnessing chaos in practical scenarios. Studying the dynamical behaviors of the fractional version was motivated by this.

Herein, by exploiting the Caputo h -difference operator in (3.2.1), the fractional Ushio map given as follows:

$$\begin{cases} {}_h^C \Delta_a^\gamma x(t) = -x^3(t + h\gamma) + (d - 1)x(t + h\gamma) + y(t + h\gamma) \\ {}_h^C \Delta_a^\gamma y(t) = -y(t + h\gamma) + 0.5x(t + h\gamma) \end{cases}, \quad (3.2.2)$$

Using phase portrait, bifurcation diagram, and the greatest Lyapunov exponents, we demonstrate that the fractional Ushio map is chaotic in the section that follows.

3.3 Chaotic behavior of fractional-order Ushio map

3.3.1 Phase portrait

According to Theorem 1.5.7, the equivalent implicit discrete formula corresponding the fractional-order Ushio map (3.2.2) can be written in the form:

$$\begin{cases} x(n+1) = x(0) + \frac{h^\gamma}{\Gamma(\gamma)} \sum_{j=0}^n \frac{\Gamma(n-j+\gamma)}{\Gamma(n-j+1)} ((d-1)x(j+1) - x^3(j+1) + y(j+1)) \\ y(n+1) = y(0) + \frac{h^\gamma}{\Gamma(\gamma)} \sum_{j=0}^n \frac{\Gamma(n-j+\gamma)}{\Gamma(n-j+1)} (0.5x(j+1) - y(j+1)) \end{cases}, \quad (3.3.1)$$

with $x(0)$ and $y(0)$ serving as the initial conditions. In this context, the Ushio system's chaotic behavior is investigated using the implicit system in equation (3.3.1) with the initial conditions $(x(0), y(0)) = (0.1, -0.3)$ and $d = 1.9$, as seen in Figure 3.1.

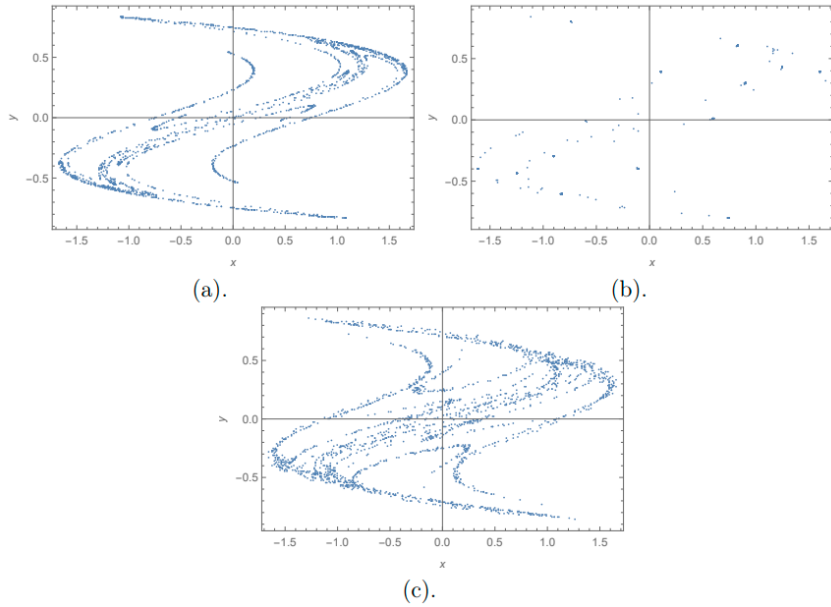


Figure 3.1: Phase portrait of the FO Ushio map (3.2.2) for (a) $\gamma = 1$, (b) $\gamma = 0.95$, (c) $\gamma = 0.82$.

3.3.2 Bifurcation diagram and largest Lyapunov exponent

While phase portraits are valuable for examining the characteristics of solutions, but are not adequate to achieve a thorough understanding. At this stage, the proposed fractional-order Ushio map (3.2.2) is reported using a bifurcation diagram and Lyapunov exponents. To check and ensure the chaos and to compare the results to guarantee the dynamical behaviors of the novel fractional map, we vary the bifurcation parameter d in the range $[0, 2]$ and keep the same initial conditions $(x(0), y(0)) = (0.1, -0.3)$. The bifurcation diagram and largest Lyapunov exponents are established in Figures 3.2 and Figures 3.3 respectively. For the value $\gamma = 1$, it is observed that chaotic behavior emerges when d exceeds 1.61. With γ set at 0.95, as depicted in Figure 3.2(b), the threshold for chaos shifts, beginning at $d \geq 1.66$. Conversely, for $\gamma = 0.82$, Figure 3.2(c) indicates that chaos begins to manifest at $d \geq 1.6$, and the states proceed towards infinity when d surpasses 2. From these observations, it is inferred that a decrease in d leads to a transition from chaotic to stable behavior. However, the largest Lyapunov exponent changed its sign twice to the negative, indicating that he briefly displayed chaotic behavior toward periodic cycles and

the opposite as shown in Figures 3.3. Additionally, it is noted that the fractional order map exhibits similar functioning and behavior patterns as its integer-order counterpart.

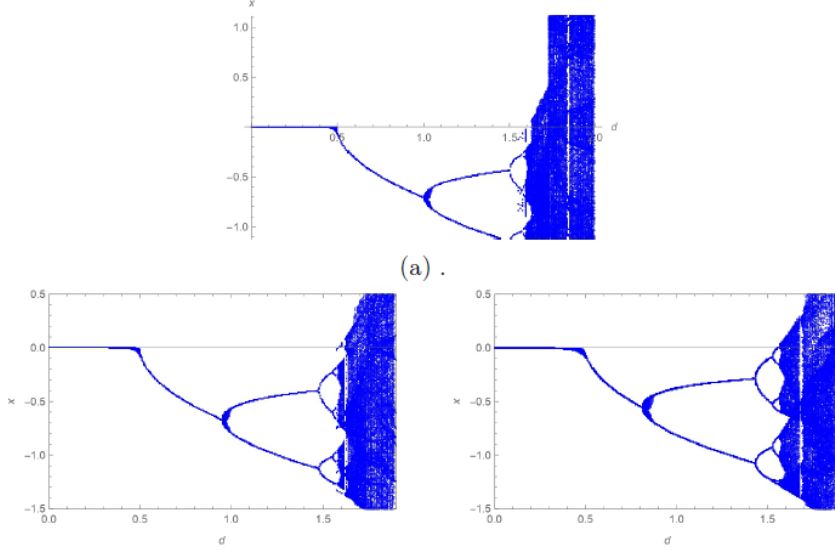


Figure 3.2: Bifurcation diagram of the FO Ushio map (3.2.2) for (a) $\gamma = 1$, (b) $\gamma = 0.95$, (c) $\gamma = 0.82$.

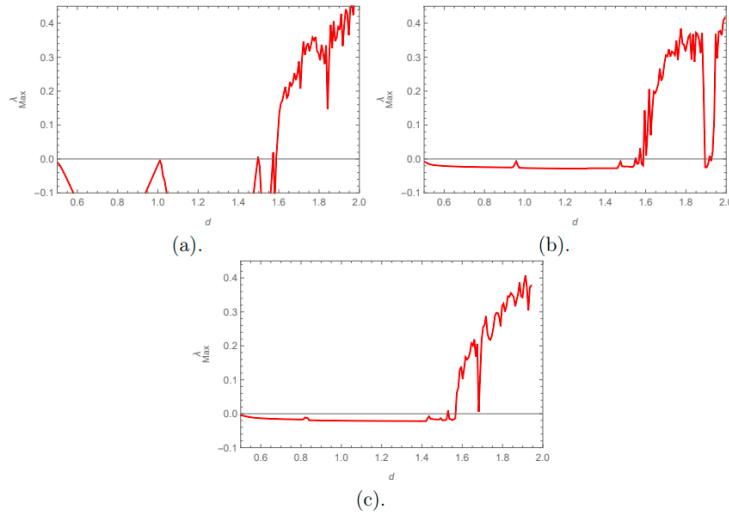


Figure 3.3: Largest Lyapunov exponent of the FO Ushio map (3.2.2) for (a) $\gamma = 1$, (b) $\gamma = 0.95$, (c) $\gamma = 0.82$.

3.4 Chaos stabilization scheme

To demonstrate a discovery on the stabilization of the dynamics of the fractional Ushio system (3.2.2) at zero, this section aims to create a linear control law. By adding a new time-varying parameter $\mathbf{L}(t)$, the goal of "stabilization" is to reduce one of the system's states to zero in a reasonable amount of time.

Theorem 3.4.1. [113] *The one-dimensional control law (3.4.1) can stabilize the two-dimensional fractional Ushio system (3.2.2).*

$$\mathbf{L}(t) = -1.5y(t) - dx(t), \quad t \in (h\mathbb{N})_{a+(1-\gamma)h}. \quad (3.4.1)$$

Proof. The controlled fractional Ushio system involves the time-varying control parameter $\mathbf{L}(t)$ and is given by

$$\begin{cases} {}_h^C \Delta_a^\gamma x(t) = -x^3(t + h\gamma) + (d - 1)x(t + h\gamma) + y(t + h\gamma) + \mathbf{L}(t + h\gamma) \\ {}_h^C \Delta_a^\gamma y(t) = -y(t + h\gamma) + 0.5x(t + h\gamma) \end{cases}, \quad (3.4.2)$$

where $t \in (h\mathbb{N})_{a+(1-\gamma)h}$. Substituting the proposed control law (3.4.1) into (3.4.2) yields the simplified dynamics

$$\begin{cases} {}_h^C \Delta_a^\gamma x(t) = -x(t + h\gamma) - x^3(t + h\gamma) - 0.5y(t + h\gamma) \\ {}_h^C \Delta_a^\gamma y(t) = -y(t + h\gamma) + 0.5x(t + h\gamma) \end{cases}. \quad (3.4.3)$$

Now, we need to demonstrate that (3.4.3) has a trivial solution that is globally asymptotically stable. If this is the case, we can determine that the controlled system described in equation (3.4.2) is certain to converge to zero in all of its states. The Lyapunov approach, which was previously summarized by Theorem 1.6.17, which is can be applied to this issue. To observe this, one must take into consideration the next Lyapunov function:

$$V(x(t), y(t)) = \frac{1}{2}(x^2(t) + y^2(t)). \quad (3.4.4)$$

So, we can deduce the following statement by using the fractional Caputo h -difference operator on (3.4.4).

$${}_h^C \Delta_a^\gamma V(x(t), y(t)) = \frac{1}{2}({}_h^C \Delta_a^\gamma x^2(t) + {}_h^C \Delta_a^\gamma y^2(t)), \quad t \in (h\mathbb{N})_{a+(1-\gamma)h}. \quad (3.4.5)$$

By using Lemma 1.5.6, we get

$$\begin{aligned}
{}_h^C \Delta_a^\gamma V(x(t), y(t)) &\leq x(t + h\gamma) {}_h^C \Delta_a^\gamma x(t) + y(t + h\gamma) {}_h^C \Delta_a^\gamma y(t) \\
&= -x^2(t + h\gamma) - x^4(t + h\gamma) - 0.5x(t + h\gamma)y(t + h\gamma) \\
&\quad + 0.5x(t + h\gamma)y(t + h\gamma) - y^2(t + h\gamma) \\
&= -(x^2(t + h\gamma) + x^4(t + h\gamma) + y^2(t + h\gamma)) < 0.
\end{aligned}$$

This suggests that the linear control law (3.4.1) efficiently stabilizes all states of the system (3.2.2) at the origin. As illustrated in Figure 3.4, the phase space and the evolution of all states of the controlled system (3.4.2) are plotted to verify the efficacy of the established controller. All chaotic dynamics of the fractional Ushio system described in (3.4.2) stabilize at zero under the linear control law given in (3.4.1), as shown by such diagrams. \square

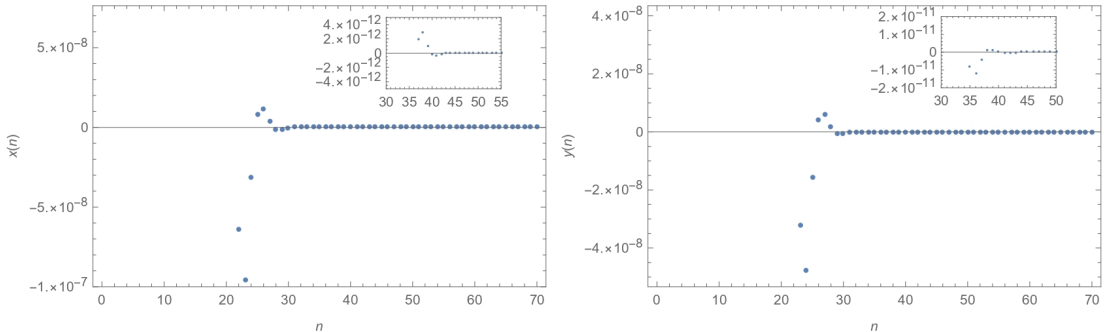


Figure 3.4: Time evolution the system (3.4.2) by using the control law (3.4.1) with $\gamma = 0.95$ and $d = 1$.

3.5 Conclusion

This chapter has advanced the field of research by introducing accurate linear control strategies to stabilize the behavior of certain fractional maps defined using the Caputo h -difference operator. The main accomplishment has been demonstrated through the validation of a novel theorem, which relies on the use of appropriate Lyapunov functions. As the control law developed in this study is both one-dimensional and linear, it offers

a cost-effective and simple implementation. To conclude, The efficacy of each of the suggested control strategies has been shown using the simulation results.

Part II

FRACTIONAL DIFFERENTIAL SYSTEMS

CHAPTER 4

OVERVIEW OF FRACTIONAL-ORDER DIFFERENTIAL OPERATORS

4.1 Introduction

Gottfried Wilhelm Leibniz's work on calculus indeed laid foundational aspects for differential calculus, and his interaction with l'Hôpital brought to light intriguing questions about the nature of calculus that would provoke thought and further development in the field for centuries. Leibniz's notation and conceptual framework for calculus were revolutionary, introducing a formal way to talk about infinitesimals and the change between quantities. The discussion between Leibniz and l'Hôpital about fractional derivatives, where l'Hôpital asked about the case when the derivative is $\frac{1}{2}$, touches on what we now refer to as fractional calculus. Leibniz's response, acknowledging the potential paradox while also foreseeing "useful consequences" emerging from it, underscores his profound insight. He seemed to understand that while the concept challenged the mathematical understanding of the time, it held the potential for significant advancements. Many areas of mathematics and the hard sciences have found use for fractional calculus, which investigates the possibility of taking real or complex number powers of the differentiation operator. It allows

for the generalization of classical calculus, providing new methods to solve differential equations, model complex systems, and describe phenomena in physics, engineering, and beyond, where traditional models are insufficient. This chapter covers various types of fractional integrals and derivatives, presenting definitions and fundamental properties of the most significant and commonly utilized types. Additionally, stability theorems for fractional-order dynamical systems are discussed. The chapter concludes with an introduction to the Adomian decomposition method, supplemented by an illustrative example to elucidate the method's application.

4.2 Riemann-Liouville fractional integral

Cauchy is frequently credited with the famous formula that reduces the calculation of the n -fold integral of a function $f(t)$ to a single integral of convolution type. Based on the Riemann-Liouville method, this eventually results in the concept of the fractional integral of order ν ($\nu > 0$). We begin by reviewing the assumption that the n -fold integral of a function f is continuous over the interval $[a, b]$, where $b > 0$. Remembering that $F(y, t)$ is jointly continuous allows us to begin by saying that

$$\int_a^y dy_1 \int_a^{y_1} F(y_1, t) dt = \int_a^y dt \int_t^y F(y_1, t) dy_1. \quad (4.2.1)$$

Specifically, only in cases where $F(y, t)$ is a function of a variable t can (4.2.1) be expressed as

$$\int_a^y dy_1 \int_a^{y_1} f(t) dt = \int_a^y f(t) dt \int_t^y dy_1 = \int_a^t (y - t) f(t) dt, \quad (4.2.2)$$

This is the two-fold integral simplified to one integral formula. The following formula for the 3-fold integral reduced to a single integral is obtained through a similar approach.

$$\int_a^y dy_1 \int_a^{y_1} dy_2 \int_a^{y_2} f(t) dt = \int_a^t \frac{(y - t)^2}{2} f(t) dt. \quad (4.2.3)$$

We can deduce the Cauchy formula of n -fold integral for $x > a$, $n \in \mathbb{N}^*$

$$J_a^n f(y) =_a D_y^{-n} f(y) = \int_a^y dy_1 \int_a^{y_1} dy_2 \dots \int_a^{y_{n-1}} f(t) dt = \frac{1}{(n-1)!} \int_a^t (y - t)^{n-1} f(t) dt. \quad (4.2.4)$$

Utilizing the Gamma function, this formula can be expressed as

$$J_a^n f(y) = {}_a D_y^{-n} f(y) = \frac{1}{\Gamma(n)} \int_a^y (y-t)^{n-1} f(t) dt. \quad (4.2.5)$$

Changing n to a positive real number ν in equation (4.2.5) is possible since the gamma function gives an analytical extension of the factorial to all positive real values. Therefore, the fractional integral of Riemann-Liouville of order $\nu > 0$ may be defined in the following way:

$$J_a^\nu f(y) = {}_a^{RL} D_y^{-\nu} f(y) = \frac{1}{\Gamma(\nu)} \int_a^y (y-t)^{\nu-1} f(t) dt, \quad y > a, \quad \nu > 0. \quad (4.2.6)$$

Remark 4.2.1. If $f \in L^1[a, b]$ with $\nu > 0$, then the integral $J_a^\nu f(y)$ exists for almost every $y \in [a, b]$. Furthermore, the function $J_a^\nu f$ itself is also belongs to $L^1[a, b]$.

Some basic properties

- $\forall \lambda_1, \lambda_2 \in \mathbb{R}$

$$J_a^\nu (\lambda_1 f(t) + \lambda_2 g(t)) = \lambda_1 J_a^\nu f(t) + \lambda_2 J_a^\nu g(t). \quad (4.2.7)$$

- h is a continuous function for $x \geq a$ then

$$\lim_{\nu \rightarrow 0} J_a^\nu h(x) = h(x). \quad (4.2.8)$$

and

$$J_a^q (J_a^\nu h(x)) = J_a^\nu (J_a^q h(x)) = J_a^{q+\nu} h(x). \quad (4.2.9)$$

-

$$J_a^\nu C = \frac{C}{\Gamma(\nu+1)} (t-a)^\nu, \quad (4.2.10)$$

where C is constant.

-

$$J_a^\nu (s-a)^\alpha = \frac{\Gamma(\alpha+1)}{\Gamma(\alpha+\nu+1)} (s-a)^{\nu+\alpha}. \quad (4.2.11)$$

4.3 Riemann-Liouville fractional derivatives

We next go on to the corresponding differential operators. The following identity is first reviewed, which is relevant to a function ϕ with a continuous n^{th} derivative on the interval $[a, b]$:

$$D^n \phi = D^m D^{m-n} \phi, \quad (4.3.1)$$

where $n, m \in \mathbb{N}$, such that $m > n$.

Let's now assume that n is not an integer. Given the preceding sections, the right-hand portion of (4.3.1) holds significance. As a result, the Riemann-Liouville fractional differential operator is defined as follows.

Definition 4.3.1. Let $\nu \in \mathbb{R}_+$ and $m = \lceil \nu \rceil$. The Riemann-Liouville fractional differential operator of order ν is defined by

$${}_a^{RL} D_t^\nu \phi = D^m J_a^{m-\nu} \phi. \quad (4.3.2)$$

Equivalently, we have

$${}_a^{RL} D_t^\nu \phi(t) = \begin{cases} \frac{1}{\Gamma(m-\nu)} \frac{d^m}{dt^m} \int_a^t (t-s)^{m-\nu-1} \phi(s) ds, & m-1 < \nu < m \\ \frac{d^m}{dt^m} \phi(t), & \nu = m \end{cases} \quad (4.3.3)$$

Some basic properties

- Composition with integer-order derivatives.

$$D^n ({}_a^{RL} D_t^\nu \phi(t)) = {}_a^{RL} D_t^{\nu+n} \phi(t). \quad (4.3.4)$$

$${}_a^{RL} D_t^\nu (\phi^{(n)}(t)) = {}_a^{RL} D_t^{\nu+n} \phi(t) - \sum_{j=0}^{n-1} \frac{\phi^j(a)(t-a)^{j-n-\nu}}{\Gamma(j-n-\nu+1)}. \quad (4.3.5)$$

- Composition using fractional-order Derivatives. Take the two fractional Riemann-Liouville operators ${}_a^{RL} D_t^\nu$ and ${}_a^{RL} D_t^\alpha$ with $m = \lceil \nu \rceil$ and $n = \lceil \alpha \rceil$ then

$${}_a^{RL} D_t^\alpha ({}_a^{RL} D_t^\nu \phi(t)) = {}_a^{RL} D_t^{\nu+\alpha} \phi(t) - \frac{(t-a)^{-\alpha-j}}{\Gamma(-\alpha-j+1)} \sum_{j=1}^m [{}_a^{RL} D_t^{\nu-j} \phi(t)]_{t=a} \quad (4.3.6)$$

$${}_a^{RL} D_t^\nu ({}_a^{RL} D_t^\alpha \phi(t)) = {}_a^{RL} D_t^{\nu+\alpha} \phi(t) - \frac{(t-a)^{-\nu-j}}{\Gamma(-\nu-j+1)} \sum_{j=1}^n [{}_a^{RL} D_t^{\alpha-j} \phi(t)]_{t=a} \quad (4.3.7)$$

Remark 4.3.2. In overall, the Riemann-Liouville fractional operators ${}_a^{RL}D_t^\alpha$ and ${}_a^{RL}D_t^\nu$ do not commute, except when $\nu = \alpha$. For $\alpha \neq \nu$, we have

$${}_a^{RL}D_t^\alpha({}_a^{RL}D_t^\nu\phi(t)) = {}_a^{RL}D_t^\nu({}_a^{RL}D_t^\alpha\phi(t)) = {}_a^{RL}D_t^{\nu+\alpha}\phi(t), \quad (4.3.8)$$

only if both sums in the right-hand sides of (4.3.6) and (4.3.7) vanish. For this, we have to require the conditions

$$[{}_a^{RL}D_t^{\nu-j}\phi(t)]_{t=a} = 0, \quad j = 1, 2, \dots, m, \quad (4.3.9)$$

and

$$[{}_a^{RL}D_t^{\alpha-j}\phi(t)]_{t=a} = 0, \quad j = 1, 2, \dots, n. \quad (4.3.10)$$

If $\phi(t)$ has a sufficient number of continuous derivatives, then the conditions (4.3.9) and (4.3.10) are equivalent to

$$\phi^{(j)}(a) = 0, \quad j = 0, 2, \dots, n - 1, \quad (4.3.11)$$

$$\phi^{(j)}(a) = 0, \quad j = 0, 2, \dots, m - 1. \quad (4.3.12)$$

As conclusion the ν -th and α -th Riemann-Liouville fractional derivatives commute if

$$\phi^{(j)}(a) = 0, \quad j = 0, 2, \dots, r - 1. \quad (4.3.13)$$

Where $r = \max(n, m)$.

4.4 Caputo's fractional derivative

The theory and practice of integrals and derivatives with fractions, as well as their uses in pure mathematics (e.g., solving differential equations of integer order, defining new function classes, and summing series), has been significantly shaped by the definition 4.3.1 of fractional differentiation of the Riemann-Liouville type. However, to align with the requirements of modern technology, the well-established pure mathematical approach needs to undergo key modifications. Fractional derivatives find extensive application in numerous publications, notably within the theory of viscoelasticity and hereditary solid

mechanics, where they offer a more precise depiction of material properties. The development of beginning conditions for fractional-order differential equations is a natural consequence of mathematical modeling's advancement with improved rheological models. Definitions of fractional derivatives are necessary for applied issues to use physically comprehensible initial conditions, such as $f(a), f'(a)$, etc. The Riemann-Liouville approach produces undesirable beginning conditions at the lower terminal $t = a$, where they include things like the limit values of the Riemann-Liouville fractional derivatives. For example

$$\lim_{t \rightarrow a} ({}^{RL}_a D_t^{\nu-1} f(t)) = b_1,$$

$$\lim_{t \rightarrow a} ({}^{RL}_a D_t^{\nu-2} f(t)) = b_2,$$

...

$$\lim_{t \rightarrow a} ({}^{RL}_a D_t^{\nu-m} f(t)) = b_m.$$

b_k , $k = 1, 2, \dots, m$, are constants given. Even though these types of initial value may be handled theoretically, initial value difficulties still arise.

Even though initial value problems with these kinds of initial conditions can be mathematically solved (see, for instance, the solutions provided in [91]) and this book, their solutions are piratically and pointless since such initial conditions have no known physical interpretation. Here, we see a disagreement between the demands of practical application and the refined and well-established mathematical theory. In 1967, M. Caputo first proposed a specific solution to this conflict in his paper [16], followed by his book [17] two years later. More recently, El-Sayed [29] proposed a similar solution in Banach spaces.

Definition 4.4.1. Let $\nu \in \mathbb{R}_+$ and $m-1 < \nu < m$. Caputo's fractional differential operator of order ν is defined as

$${}_a^C D_t^\nu f(t) = J_a^{m-\nu} \frac{d^m}{dt^m} f(t) = \frac{1}{\Gamma(m-\nu)} \int_a^t \frac{f^{(m)}(\tau) d\tau}{(t-\tau)^{\nu+1-m}}, \quad (m-1 < \nu < m). \quad (4.4.1)$$

Remark 4.4.2. In a natural setting, the Caputo derivative of the function $f(t)$ becomes the conventional m -th derivative of the function $f(t)$ as ν approaches m . In particular, if $m-1 \leq \nu < m$ and $f(t)$ is a function with $m+1$ continuous bounded derivatives in $[a, T]$ for all $T > a$, then

$$\lim_{\nu \rightarrow m} ({}^C_a D_t^\nu f(t)) = \lim_{\nu \rightarrow m} \left(\frac{f^{(m)}(a)(t-a)^{m-\nu}}{\Gamma(m-\nu+1)} + \frac{1}{\Gamma(m-\nu+1)} \int_a^t (t-\tau)^{m-\nu} f^{(m+1)}(\tau) d\tau \right)$$

$$= f^{(m)}(a) + \int_a^t f^{(n+1)}(\tau) d\tau = f^{(m)}(t), \quad m = 1, 2, \dots$$

Caputo's method offers a significant advantage: the initial condition for a fractional differential equation involving Caputo derivatives retains the same form as differential equations of integer order. Specifically, it encompasses the limit values of the derivatives of integer-order unknown functions at the lower terminal $t = a$.

properties of Caputo derivative

- Let $\lambda, \gamma \in \mathbb{R}$

$${}_a^C D_t^\nu (\lambda f(t) + \gamma h(t)) = \lambda {}_a^C D_t^\nu f(t) + \gamma {}_a^C D_t^\nu h(t).$$

- **Interpolation**

If $m = \nu$ then the definition (4.4.1) implies that

$${}_a^C D_t^\nu f(t) = J_a^0 \frac{d^m}{dt^m} f(t) = \frac{d^m}{dt^m} f(t).$$

- **Composition**

Let $n \in \mathbb{N}$ and $m = \lceil \nu \rceil$, we have

$${}_a^C D_t^\nu ({}_a^C D_t^n f(t)) = {}_a^C D_t^{\nu+n}.$$

- if F continuous on $[a, b]$, then

$${}_a^C D_t^\nu J_a^\nu F(t) = F(t).$$

- if $F \in C^m[a, b]$, then

$$J_a^\nu {}_a^C D_t^\nu F(t) = F(t) - \sum_{i=0}^{m-1} \frac{F(a)^{(i)}}{i!} (t-a)^i.$$

4.5 Stability of fractional order differential systems

Fractional-order systems introduce a new dimension to control theory, enabling the analysis and control of systems with dynamics described by fractional (non-integer) order differential equations [10]. These systems offer a more accurate representation of real-world

processes by incorporating memory and hereditary features. A cornerstone of control theory, stability analysis checks that, given certain circumstances, a system stays within its bounds and converges to its target state. Methods such as Lyapunov stability theory and frequency-domain analysis are employed to analyze the stability of fractional-order systems, which exhibit various types of stability including asymptotic and exponential stability. Overall, stability analysis in fractional-order systems is crucial for understanding the behavior of complex dynamical systems and designing robust control strategies.

4.5.1 Stability of fractional order linear systems

We consider the following fractional differential linear system

$${}_a^C D_t^\nu x_i(t) = A(x_i(t)), \quad i = 1, \dots, n. \quad (4.5.1)$$

Where ${}_a^C D_t^\nu$ refers to the Caputo operator of order ν , $m = \lceil \nu \rceil$, $(x_1(t), x_2(t), \dots, x_n(t))$ is the state vector, and A is a constant matrix.

Theorem 4.5.1. [66] *The fractional-order linear system described by (4.5.1) is asymptotically stable if and only if*

$$|\arg \lambda_i| > \frac{\nu\pi}{2}, \quad i = 1, 2, \dots, n. \quad (4.5.2)$$

λ_i , $i = 1, 2, \dots, n$, are the eigenvalues of the matrix A .

Example 4.5.2. Consider the following linear system

$$\begin{cases} {}_0^C D_t^{0.5} z_1(t) = -z_1(t), \\ {}_0^C D_t^{0.5} z_2(t) = \frac{1}{3} z_2(t). \end{cases} \quad (4.5.3)$$

The matrix A given by

$$A = \begin{pmatrix} -1 & 0 \\ 0 & \frac{1}{3} \end{pmatrix}$$

The eigenvalues of the matrix A are:

$$\lambda_1 = \cos(\pi) + i \sin(\pi), \quad \lambda_2 = \frac{1}{3}(\cos(\pi) + i \sin(\pi)).$$

It is clear that $|\arg \lambda_1| = |\arg \lambda_2| = \pi > \frac{0.5\pi}{2} = \frac{\pi}{4}$.

According to Theorem 4.5.1, the trivial solution of the system (4.5.3) is asymptotically stable.

4.5.2 Stability of fractional order nonlinear systems

Direct method(Linearization)

Now consider a nonlinear fractional system given by

$${}_a^C D_t^\nu x_i(t) = h_i(x_i(t)), \quad i = 1, \dots, n. \quad (4.5.4)$$

${}_a^C D_t^\nu$ is the Caputo operator of order ν , $m - 1 < \nu < m$, $(x_i(t))_{i=1,\dots,n} \in \mathbb{R}^n$ is the state vector and the function $h_i : \mathbb{R}^n \rightarrow \mathbb{R}$ has second continuous partial derivatives at an equilibrium point x^* .

Theorem 4.5.3. [6] The fractional order nonlinear system described by (4.5.4) is asymptotically stable if only if

$$|\arg(eig(J|_{x^*}^*))| > \frac{\nu\pi}{2}, \quad i = 1, 2, \dots, n. \quad (4.5.5)$$

Where $J|_{x^*}^*$ is the Jacobian matrix of a system (4.5.4) at the equilibrium point x^* and $eig(J|_{x^*}^*)$ are the eigenvalues of the Jacobian matrix at the origin.

Example 4.5.4. Consider the following fractional nonlinear system

$$\begin{cases} {}_0^C D_t^{\frac{1}{2}} y_1(t) = -y_2(t) + y_1(y_1^2(t) + y_2^2(t) - 1), \\ {}_0^C D_t^{\frac{1}{2}} y_2(t) = y_1(t) + y_2(y_1^2(t) + y_2^2(t) - 1), \end{cases} \quad (4.5.6)$$

the system (4.5.6) have only equilibrium point $(y_1^*, y_2^*) = (0, 0)$. The Jacobian matrix at the origin is given by

$$J|_{x^*=0} = \begin{pmatrix} -1 & -1 \\ 1 & -1 \end{pmatrix}$$

The eigenvalues of the Jacobian matrix are:

$$\lambda_1 = -1 + i, \quad \lambda_2 = -1 - i.$$

One might easily conclude that $|\arg \lambda_1| = |\arg \lambda_2| = \frac{3}{4}\pi > \frac{\pi}{4}$. Based on Theorem 4.5.3, This means that the system's (4.5.6) trivial solution is asymptotically stable.

Lyapunov method

The fundamental theorem of Lyapunov's method for stability, when extended to fractional systems, remains conceptually similar to that for integer-order systems but with adaptations to account for the fractional derivatives. The core idea is to demonstrate the stability of an equilibrium point of the system by finding a suitable Lyapunov function associated with the system that helps in assessing its stability. Here's a generalized form of Lyapunov's stability theorem for fractional-order systems:

Take the following equation that represents a fractional-order dynamical system:

$${}_a^C D_t^\nu x(t) = f(x(t)), \quad i = 1, \dots, n. \quad (4.5.7)$$

$f : \mathbb{R}^n \rightarrow \mathbb{R}^n$ is a vector field assumed to be locally Lipschitz continuous. Let $x = 0$ be an equilibrium point of the system (4.5.7).

Theorem 4.5.5. [21] If there exists a positive definite function $V(x(t))$ such that ${}_a^C D_t^\nu V(x(t)) < 0, \forall t > 0$, the trivial solution of the fractional order system (4.5.7) is asymptotically stable.

Theorem 4.5.6. [5] $\forall t > 0$ we have

$$\frac{1}{2} {}_a^C D_t^\nu (x^T(t)x(t)) \leq x^T(t) {}_a^C D_t^\nu x(t). \quad (4.5.8)$$

Example 4.5.7. Consider the following fractional-order system:

$${}_a^C D_t^\nu x(t) = -x^3(t), \quad (4.5.9)$$

with $0 < \nu \leq 1$. We consider the Lyapunov function

$$V(x) = \frac{1}{2}x^2.$$

This function is positive definite and by using the Theorem 4.5.6 we get

$${}_a^C D_t^\nu V(x(t)) \leq x_a^C D_t^\nu x(t) = x(-x^3(t)) = -x^4(t) < 0.$$

by Theorem 4.5.5 for fractional-order systems (4.5.9), we can conclude that the equilibrium point $x = 0$ is asymptotically stable.

4.6 Adomian decomposition method

The inverse operator method (ADM), also called the Adomian decomposition method (ADM), was developed for solving both linear and nonlinear differential equations by American physicist Adomian in the 1980s [2]. First, the equation must be divided into constant, linear, and nonlinear components. Next, the solution must be divided into infinite parts. It has been used recently for fractional-order chaotic systems [40], with developments like the fractional-order chaotic fast iterative algorithm and Lyapunov exponent spectrum algorithms, among others [101]. High-precision approximate solutions are provided by ADM [15], which has been successfully applied to fractional-order chaotic systems because it preserves the system nonlinearities. This method has several advantages over other conventional numerical methods in many areas. On the other hand, in comparison to other techniques, ADM produces chaos at much lower orders. For example, the lowest recorded order in the literature for chaos utilizing ADM in the Chen system is 0.24. Conversely, for the same system, the Adams-Bashforth-Moulton method requires a minimum order of 0.64 [96].

4.6.1 Algorithm description

The fractional-order chaotic system is described as:

$${}^C D_{t_0}^q \Phi(t) = L\Phi + N\Phi + g(t), \quad (4.6.1)$$

where $\Phi^{(k)}(a) = a_k$, $k = 0, \dots, n - 1$, represents the initial condition of the system, $\Phi(t) = [\Phi_1(t), \Phi_2(t), \dots, \Phi_n(t)]^T$ is the state vector, $g(t) = [g_1(t), g_2(t), \dots, g_n(t)]^T$ is constant vector, $L\Phi$ and $N\Phi$ represent the linear and the nonlinear terms respectively.

We apply the integral operator, to both sides of equation (4.6.1) we obtain

$$\Phi = J_{t_0}^q L\Phi + J_{t_0}^q N\Phi + J_{t_0}^q g(t) + \psi, \quad (4.6.2)$$

where

$$\psi = \sum_{k=0}^{n-1} \frac{a_k (t - t_0)^k}{k!}.$$

The solution of the system (4.6.1) given as

$$\Phi(t) = \sum_{i=0}^{\infty} \Phi^i.$$

The nonlinear term is given as [25]

$$\begin{cases} \Lambda_j^i = \frac{1}{i!} \left[\frac{d^i}{d\tau^i} N(\nu_i^j(\tau)) \right]_{\tau=0} \\ \nu_i^j(\tau) = \sum_{k=0}^i (\tau)^k \Phi_j^k, \quad i = 0, 1, 2, \dots, \infty, \quad j = 1, 2, \dots, n. \end{cases} \quad (4.6.3)$$

Then, the nonlinear term can be expressed as

$$N\Phi(t) = \sum_{i=0}^{\infty} \Lambda^i(\Phi^1(t), \Phi^2(t), \dots, \Phi^i(t)).$$

The numerical solution of system (4.6.2) can be expressed as follows

$$\Phi(t) = \sum_{i=0}^{\infty} \Phi^i = J_{t_0}^q L \sum_{i=0}^{\infty} \Phi^i + J_{t_0}^q N \sum_{i=0}^{\infty} \Lambda_j^i + J_{t_0}^q g(t) + \psi.$$

where Φ^i is calculated by

$$\begin{cases} \Phi^0 = J_{t_0}^q g(t) + \psi \\ \Phi^1 = J_{t_0}^q L \Phi^0 + J_{t_0}^q N \Lambda^0(\Phi^0) \\ \dots \\ \Phi^i = J_{t_0}^q L \Phi^{i-1} + J_{t_0}^q N \Lambda^{i-1}(\Phi^0, \Phi^1, \dots, \Phi^{i-1}) \\ \dots \end{cases}, \quad (4.6.4)$$

4.6.2 Algorithm example

Consider fractional-order memristor laser chaotic system

$$\begin{cases} {}^C D_t^q x_1 = -ax_1 + bx_1x_2 - |x_3|A \sin(2\pi f x_4) \\ {}^C D_t^q x_2 = -(1 + c + (x_1)^2)x_2 + c - 1 \\ {}^C D_t^q x_3 = A \sin(2\pi f x_4) \\ {}^C D_t^q x_4 = 1 \end{cases}. \quad (4.6.5)$$

where a, b, c, A, f , are the bifurcation parameters, and $q \in (0, 1)$. The ADM is used to parse this new autonomous FO memristive laser chaotic system, the linear and nonlinear terms in this system can be broken down and expressed as

$$\begin{bmatrix} L_{x_1} \\ L_{x_2} \\ L_{x_3} \\ L_{x_4} \end{bmatrix} = \begin{bmatrix} -ax_1 \\ -x_2 - cx_2 \\ 0 \\ 0 \end{bmatrix}, \quad \begin{bmatrix} N_{x_1} \\ N_{x_2} \\ N_{x_3} \\ N_{x_4} \end{bmatrix} = \begin{bmatrix} bx_1x_2 - |x_3|A \sin(2\pi f x_4) \\ -(x_1)^2 x_2 \\ A \sin(2\pi f x_4) \\ 0 \end{bmatrix}, \quad \begin{bmatrix} g_{x_1} \\ g_{x_2} \\ g_{x_3} \\ g_{x_4} \end{bmatrix} = \begin{bmatrix} 0 \\ c - 1 \\ 0 \\ 1 \end{bmatrix}. \quad (4.6.6)$$

According to equation (4.6.3), the nonlinear term can be expressed as

$$\begin{cases} A_{1-1}^0 = bx_1^0 x_2^0 \\ A_{1-1}^1 = b(x_1^1 x_2^0 + x_1^0 x_2^1) \\ A_{1-1}^2 = b(x_1^2 x_2^0 + 2x_1^1 x_2^1 + x_1^0 x_2^2) \end{cases} \quad (4.6.7)$$

$$\begin{cases} A_{1-2}^0 = A|x_3^0| \sin(2\pi f x_4^0) \\ A_{1-2}^1 = A(2\pi f x_4^1 \cos(2\pi f x_4^0)|x_3^0| + x_3^1 \sin(2\pi f x_4^0) \operatorname{sgn}(x_3^0)) \\ A_{1-2}^2 = A(2\pi f x_4^2 \cos(2\pi f x_4^0)|x_3^0| - 2\pi^2 f^2 \sin(2\pi f x_4^0)|x_3^0| \\ \quad + 0.5(x_3^1)^2 \sin(2\pi f x_4^0) \operatorname{sgn}(x_3^0) + x_3^2 \sin(2\pi f x_4^0) \operatorname{sgn}(x_3^0)) \\ \quad + x_3^1 x_4^1 \pi f \cos(2\pi f x_4^0) \operatorname{sgn}(x_3^0) \end{cases} \quad (4.6.8)$$

$$\begin{cases} A_2^0 = -(x_1^0)^2 x_2^0 \\ A_2^1 = -x_2^1 (x_1^0)^2 - 2x_2^0 x_1^1 x_1^0 \\ A_2^2 = -x_2^2 (x_1^0)^2 - x_2^1 x_1^1 x_1^0 - 2x_2^0 x_1^2 x_1^0 - x_2^0 (x_1^1)^2 \end{cases} \quad (4.6.9)$$

$$\begin{cases} A_3^0 = A \sin(2\pi f x_4^0) \\ A_3^1 = 2A\pi f x_4^1 \cos(2\pi f x_4^0) \\ A_3^2 = 2A(\pi f x_4^2 \cos(2\pi f x_4^0) - \pi^2 f^2 (x_4^1)^2 \sin(2\pi f x_4^0)) \end{cases} . \quad (4.6.10)$$

According to the initial conditions of this system, the state variables are expressed as

$$\begin{cases} x_1^0 = x_1(t_0) \\ x_2^0 = x_2(t_0) \\ x_3^0 = x_3(t_0) \\ x_4^0 = x_4(t_0) \end{cases} . \quad (4.6.11)$$

Let $c_1^0 = x_1^0, c_2^0 = x_2^0, c_3^0 = x_3^0, c_4^0 = x_4^0$, that is, $c^0 = [c_1^0, c_2^0, c_3^0, c_4^0]$. According to equation (4.6.5) and the properties of R-L integral operator, the following formula is obtained:

$$\begin{cases} x_1^1 = (-ac_1^0 + bc_1^0c_2^0 - A|c_3^0| \sin(2\pi f c_4^0)) \frac{(t-t_0)^q}{\Gamma(q+1)} \\ x_2^1 = (-c_2^0 - cc_2^0 - (c_1^0)^2 c_2^0 + c - 1) \frac{(t-t_0)^q}{\Gamma(q+1)} \\ x_3^1 = (A \sin(2\pi f c_4^0)) \frac{(t-t_0)^q}{\Gamma(q+1)} \\ x_4^1 = \frac{(t-t_0)^q}{\Gamma(q+1)} \end{cases} . \quad (4.6.12)$$

Let the system parameters be assigned to the corresponding variables.

When $c_1^1 = -ac_1^0 + bc_1^0c_2^0 - A|c_3^0| \sin(2\pi f c_4^0)$, $c_2^1 = -c_2^0 - cc_2^0 - (c_1^0)^2 c_2^0 + c - 1$, $c_3^1 = A \sin(2\pi f c_4^0)$, $x_4^1 = 1$ then $x^1 = c^1 \frac{(t-t_0)^q}{\Gamma(q+1)}$ can be obtained. According to equation (4.6.5), the coefficients of the last two terms of the derived system are expressed as

$$\begin{cases} c_1^2 = -ac_1^1 + b(c_1^1c_2^0 + c_1^0c_2^1) - A(2\pi f c_4^1 \cos(2\pi f c_4^0)|c_3^0| + c_3^1 \sin(2\pi f c_4^0) \operatorname{sgn}(c_3^0)) \\ c_2^2 = (-c_2^1 - cc_2^1 - c_1^1(c_1^0)^2 - 2c_1^0c_1^1c_2^0 + c - 1) \\ c_3^2 = 2A\pi f c_4^1 \cos(2\pi f c_4^0) \\ c_4^2 = 1 \end{cases} \quad (4.6.13)$$

$$\begin{cases} c_1^3 = -ac_1^2 + b(c_1^2c_2^0 + c_1^1c_2^1\frac{\Gamma(2q+1)}{\Gamma^2(q+1)} + c_1^0c_2^2) - A(2\pi f c_4^2 \cos(2\pi f c_4^0)|c_3^0| \\ \quad - 2\pi^2 f^2(c_4^1)^2 \sin(2\pi f c_4^0)|c_3^0| + 0.5(c_3^1)^2 \sin(2\pi f c_4^0) sgn(c_3^0) \\ \quad + c_3^2 \sin(2\pi f c_4^0) sgn(c_3^0) + c_3^1 c_4^1 \pi f \cos(2\pi f c_4^0) sgn(c_3^0) \frac{\Gamma(2q+1)}{\Gamma^2(q+1)}) \\ c_2^3 = -c_2^2 - cc_2^2 - c_2^2(c_1^0)^2 - c_2^1 c_1^1 c_1^0 \frac{\Gamma(2q+1)}{\Gamma^2(q+1)} - 2c_2^0 c_1^2 c_1^0 - c_2^0(c_1^1)^2 + c - 1 \\ c_3^3 = 2A(\pi f c_4^2 \cos(2\pi f c_4^0) - \pi^2 f^2(c_4^1)^2 \sin(2\pi f c_4^0)) \\ c_4^3 = 1 \end{cases}. \quad (4.6.14)$$

Therefore, the solution of the fractional-order memristor laser chaotic system (4.6.5) is obtained as

$$\tilde{x}_j(t) = c_j^0 + c_j^1 \frac{(t-t_0)^q}{\Gamma(q+1)} + c_j^2 \frac{(t-t_0)^{2q}}{\Gamma(2q+1)} + c_j^3 \frac{(t-t_0)^{3q}}{\Gamma(3q+1)}, \quad j = 1, 2, 3. \quad (4.6.15)$$

4.7 Conclusion

This chapter briefly introduces fractional-order differential operators, covering essential concepts, theorems, definitions, and examples.

CHAPTER 5

COMPLEXITY ANALYSIS OF FRACTIONAL-ORDER CHAOTIC SYSTEMS

5.1 Introduction

Since its introduction in the 1980s, the idea of complexity has gained significant attention in modern scientific research. Many definitions and understandings of complexity exist today as a result of the varied viewpoints that researchers with different academic backgrounds have used to examine the concept. There are currently at least 45 different definitions of complexity, which represent the varied perspectives of many researchers. Examples of these definitions include Kolmogorov complexity, temporal complexity, space complexity, and semantic complexity. Entropy is a valuable tool for characterizing complexity since it measures a system's degree of disorder or chaos. Entropy is the foundation of many contemporary definitions of complexity. In 1865, Clausius was the first to apply the notion of entropy to the field of physics. This first definition was created to quantify the chaos in a thermodynamic system and is referred to as thermodynamic entropy. In conclusion, complexity is a complex idea that is defined and addressed differently by different scholars. Entropy plays a significant role in many modern definitions of complexity,

especially in its use in quantifying disorder in systems. In this chapter, we give some important definitions and notions about FO continuous dynamical systems, and then we will discuss the chaos and Complexity measure algorithms. In the end, fractional continuous chaotic systems will be presented along with their applications.

5.2 Fractional order continues-time dynamical systems

FO continuous-time systems represent a modern and versatile approach to modeling dynamical systems that exhibit complex behaviors beyond what traditional integer-order systems can capture. In these systems, Non-integer orders of differentiation or integration are used in fractional calculus to explain the change of a system's state over time. Different branches of science and engineering may now more accurately and fluidly model real-world events because of this break from conventional integer-order calculus. We need to establish a few key principles before we can define complexity analysis. The following form is provided for the FO continuous dynamical system, which will be defined first.

$${}_a^C D_t^\nu u = F(t, u), \quad (5.2.1)$$

where $u \in \mathbb{R}^n$, F is defined on a suitable subset $V \subset \mathbb{R}^{n+1}$ and $\nu = [\nu_1, \nu_2, \dots, \nu_n]^T$ are the FO, $0 < \nu_i \leq 1$, ($i = 1, 2, \dots, n$) (we adopt this restriction of FO ν because fractional equations in this range require only one initial condition to guarantee the uniqueness of the solution). When $\nu_1 = \nu_2 = \dots = \nu_n$, the system (5.2.1) is called a commensurate order system, otherwise, it is an incommensurate order system. If the function F depends explicitly on it, then (5.2.1) is called a non-autonomous system; otherwise, it is called an autonomous system.

For any $t > 0$, we say that u^* is an equilibrium point of the Caputo fractional dynamical system (5.2.1) if and only if $F(t, u^*) = 0$.

5.3 Brief overview of chaos

One of the most important subfields of nonlinear research is chaos theory, which deals with the complex, apparently chaotic, external motion of deterministic systems caused by

internal nonlinearity. In contrast to regular motion, which is scale-dependent, nonlinear systems often exhibit chaos in their natural motion. As research into chaotic systems has progressed, the field of chaos science has acquired theoretical frameworks and mathematical implications that are both deep and rich. Furthermore, it has been increasingly used in engineering and has grown to be a crucial aspect of contemporary science. The swift advancement of computer technology has accelerated the development of chaos theory and its applied research, encouraging its intersection and application with other subjects. In chemistry, physics, electronics, medicine, biology, engineering, economics, and other technological and scientific domains, chaos, for instance, has a significant theoretical and applied status. Thus, it has made a substantial contribution to several scientific domains. The famous scientist Ford [38] asserted at the inaugural International Chaos conference that the three major scientific revolutions of the 20th century were quantum physics, chaos, and relativity. The following were his main arguments: Quantum mechanics shattered Newton's dream of controlled measuring methods, chaos shattered Laplace's predictable illusion, and Einstein's theory of relativity shattered the illusion of absolute space and time. Understanding and describing the dynamic behaviors of chaotic systems may lead to a better understanding of the complex and multidimensional human condition.

Remark 5.3.1. *All the notions, tools, and characteristics of chaos in the FOD maps in part one are similar in the FOC systems.*

5.4 Fractional-order chaotic systems

5.4.1 Fractional-order Lorenz chaotic system

The Fractional-order Lorenz chaotic system is a standard chaotic system, described by the following equation:

$$\begin{cases} {}_a^C D_t^\nu x_1 = 40(x_2 - x_1) \\ {}_a^C D_t^\nu x_2 = x_1(10 - x_3) + 25x_3, \\ {}_a^C D_t^\nu x_3 = x_1x_2 - 3x_3 \end{cases} \quad (5.4.1)$$

Recently, Jia et al. [45] analyzed the dynamics of fractional-order Lorenz chaotic systems with the FO $q = 0.9$, the phase diagrams of the FO Lorenz chaotic attractor on different planes are shown in Figure 5.1.

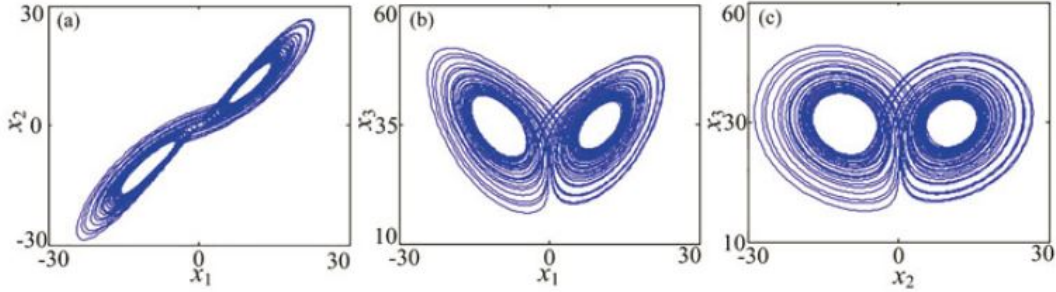


Figure 5.1: FO Lorenz chaotic attractors: (a) $x_1 - x_2$ plane, (b) $x_1 - x_3$ plane, and (c) $x_2 - x_3$ plane.

5.4.2 Fractional-order Rössler chaotic system

Rössler system proposed by Rössler OE in 1976, As one of the classic continuous chaotic systems, the system has been extensively investigated, specifically, the integer-order chaotic was examined in [90]. The corresponding FO Rössler system is written as

$$\begin{cases} {}_a^C D_t^\nu x = -y - z \\ {}_a^C D_t^\nu y = x + 0.55y, \\ {}_a^C D_t^\nu z = 2 + z(x - 4) \end{cases} \quad (5.4.2)$$

Taking the order $q = 0.8$, the attractor of the FO Rössler system is obtained as shown in Figure 5.2.

5.4.3 Fractional-order Lorenz-Stenflo chaotic system

Stenflo proposed the Lorenz-Stenflo system in 1996 [93], which consists of four nonlinear ordinary differential equations. In a revolving environment, it simulates the propagation of waves with limited amplitude and gravity. The FO Lorenz-Stenflo system is represented

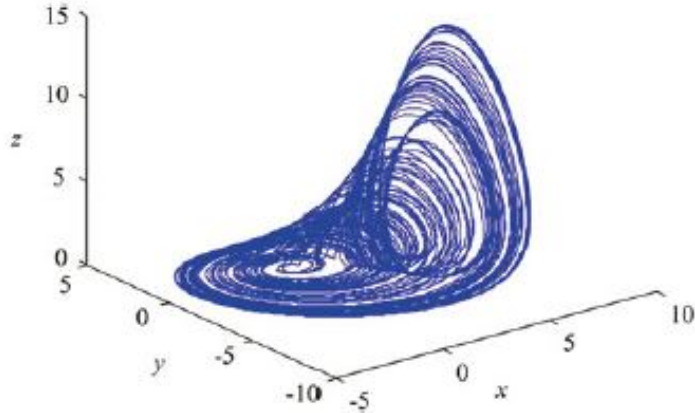


Figure 5.2: Attractor of the FO Rössler system (5.4.2).

by the following equations:

$$\begin{cases} {}_a^C D_t^\nu x = y - x + v \\ {}_a^C D_t^\nu y = 0.7x - xz - y \\ {}_a^C D_t^\nu z = xy - 26z \\ {}_a^C D_t^\nu v = -x - v \end{cases}, \quad (5.4.3)$$

The attractor of the FO Lorenz-Stenflo system is obtained as shown in Figure 5.3 with the order $q = 0.7$.

5.5 Complexity measure algorithms

The complexity of a chaotic system is defined by how close a chaotic sequence is to a random sequence when correlation methods are used. Indicative of growing complexity, closeness enhances the associated application system's security. The inherent complexity of chaotic systems embodies chaotic dynamics. Both structural and behavioral complexity may be shown via chaotic sequences, with the latter being quantifiable. Examining the size of the probability of new patterns within very short periods is one approach to estimating the likelihood of generating a new pattern. Various computational complexity techniques exist for chaotic pseudo-random sequences, many of which, such as the approximate entropy (ApEn) algorithm [88], are grounded in the Kolmogorov method, Shannon

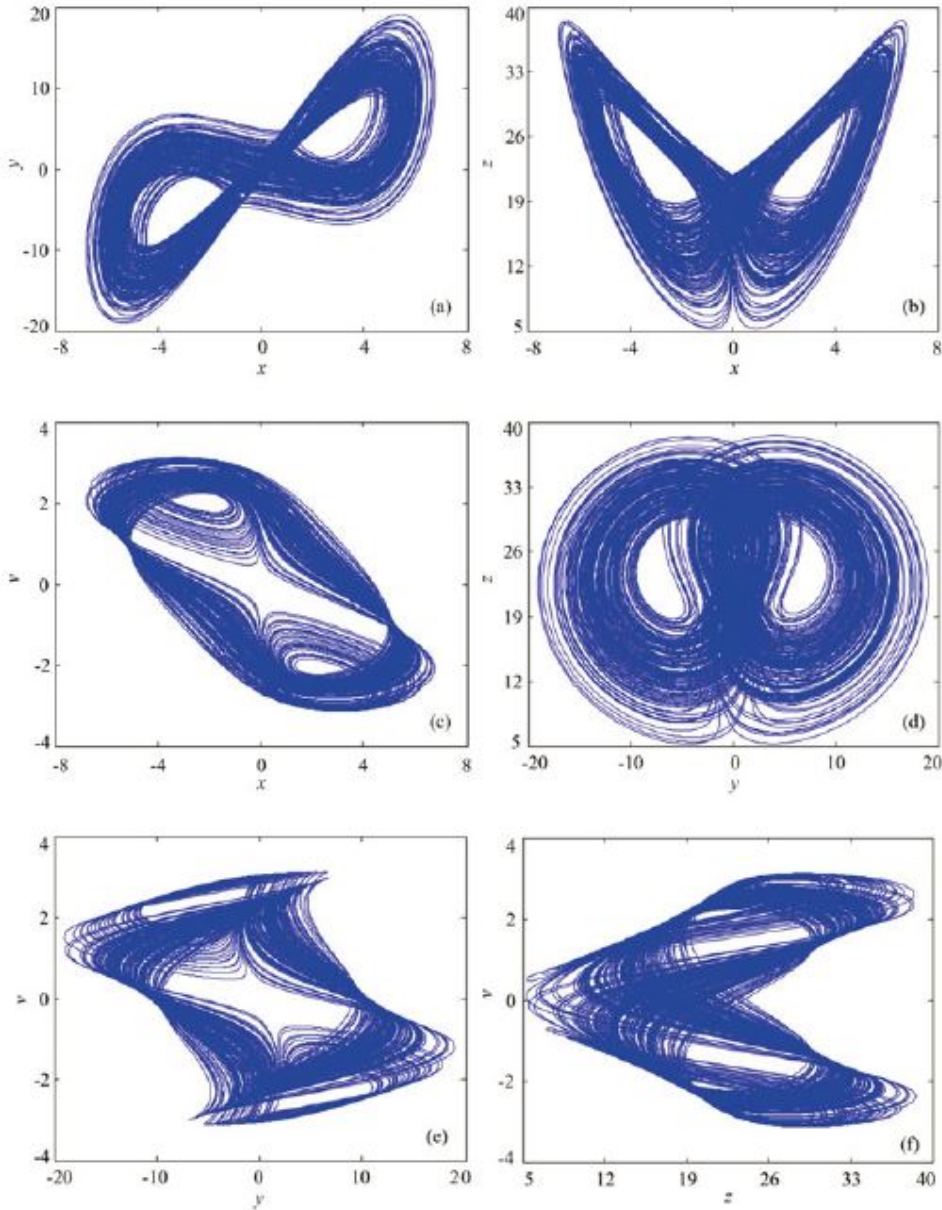


Figure 5.3: Attractors of the FO Lorenz-Stenflo system (5.4.3): (a) $x - y$ plane, (b) $x - z$ plane, (c) $x - v$ plane, (d) $y - z$ plane, (e) $y - v$ plane and (f) $z - v$ plane.

entropy, and fuzzy entropy (FuzzyEn) algorithm [24]. Describing the dynamics of chaotic systems often involves assessing their complexity. The phase diagram, bifurcation diagram, and Lyapunov exponent have effects comparable to those of this approach. In this context, the C_0 method and the spectral entropy (SE) algorithm are introduced.

5.5.1 Spectral entropy complexity algorithm

According to [95], the spectral entropy complex method can be described as follows: it may use the Fourier transform to create an energy distribution and then use the Shannon entropy to get the corresponding SE.

Step 1: Continuous Fourier transformation (CFT)

$$X(f) = \int_{-\infty}^{+\infty} x(t)e^{-2j\pi ft}dt, \quad (5.5.1)$$

Where $x(t)$ is the state of the system $X(f)$ is the Fourier Transform of $x(t)$.

Step 2: Power Spectral Density (PSD)

$$S(f) = |X(f)|^2, \quad (5.5.2)$$

The PSD $S(f)$ represents the distribution of power across different frequencies f .

Step 3: Normalization of PSD

Normalize the PSD values $S(f)$ to ensure they are comparable across different systems or observations.

Step 4: Entropy Calculation

The entropy H of the normalized PSD values $S(f)$ can be computed using Shannon entropy or other entropy measures:

$$H = - \int_{-\infty}^{+\infty} p(f) \log(p(f)). \quad (5.5.3)$$

Where $p(f)$ represents the normalized PSD values.

Step 5: Complexity Calculation

Derive complexity measures from the entropy values. For example, taking the exponential function of the entropy:

$$SEC = \exp(H). \quad (5.5.4)$$

These formulas provide the mathematical framework for computing SEC for a continuous dynamical system. However, practical implementations may involve numerical methods for computing integrals and handling continuous data. Additionally, interpretations of complexity in continuous systems may require additional analysis and consideration of the system's dynamics.

5.5.2 C_0 complexity algorithm

It is possible to determine the complexity of a sequence (C_0) by separating it into its regular and irregular parts and then measuring the proportion of the sequence's irregular parts. This is the algorithm that uses this technique for computing [94].

Step 1: Fourier transforms on discrete sets $y^N, n = 1, \dots, N$.

$$Y(k) = \sum_{n=0}^{N-1} y(n)e^{-j\frac{2\pi}{N}nk} = \sum_{n=0}^{N-1} y(n)W_N^{nk}, \quad k = 0, 1, 2, \dots, N-1. \quad (5.5.5)$$

Step 2: eliminate of irregular parts. The definition of the mean square value of the amplitude spectrum $Y(k), k = 1, \dots, N-1$ is

$$G_N = \frac{1}{N} \sum_{k=0}^{N-1} |Y(k)|^2. \quad (5.5.6)$$

Add a control parameter r . If the square value spectrum components are more than rG_N , then replace them with zero. The elements whose square values are less than or equal to rG_N , known as the irregular parts, should be modified as follows:

$$\bar{Y}(k) = \begin{cases} Y(k) & \text{if } |Y(k)|^2 > rG_N \\ 0 & \text{otherwise.} \end{cases}. \quad (5.5.7)$$

Step 3: Fourier inverse transformation for the sequence $\bar{Y}(k)$

$$\bar{y}(n) = \frac{1}{N} \sum_{k=0}^{N-1} \bar{Y}(k)e^{j\frac{2\pi}{N}nk} = \frac{1}{N} \sum_{n=0}^{N-1} \bar{Y}(k)W_N^{-nk}, \quad k = 0, 1, 2, \dots, N-1. \quad (5.5.8)$$

Step 4: Define C_0 complexity as

$$C_0(r, N) = \sum_{n=0}^{N-1} |y(n) - \bar{y}(n)|^2 / \sum_{n=0}^{N-1} |y(n)|^2. \quad (5.5.9)$$

Remark 5.5.1. For any time series, the C_0 complexity ranges between 0 and 1. Hence, C_0 complexity can be used as a randomness finding complexity of a time series.

5.6 Chaos synchronization

Several researchers from many domains have been intrigued by the phenomena of synchronization because of its potential applications in the realm of nonlinear sciences [73][70].

It stems from the concept of "synchronous", meaning sharing a common time, and involves the coordination of dynamics between two or more systems. In other words, when a master system's time-dependent variables are time-matched with those of a dynamical slave system, the process is called synchronization. There are few literature that has taken into account the dynamics synchronization problems in the field of chaotic systems with integer order, in the discrete time chaotic systems [71][76][83], in continuous time chaotic systems [14][36][74]. Similar to in chaotic systems with fractional order including the discrete time chaotic systems [13][48][47], and in the continuous time chaotic systems [26][75][81]. Recently, synchronization schemes between integer order and fractional order chaotic systems inspired a great deal of motivation [85][77][80]. A real-life example of synchronization is synchronization of satellites. Satellites in a constellation often need to operate in synchrony to achieve various objectives such as global coverage, accurate positioning, communication, and remote sensing. For instance, in a GPS (Global Positioning System) satellite constellation, each satellite needs to be synchronized precisely with the others to ensure accurate positioning information for users on Earth. These satellites orbit the Earth at high speeds and altitudes, and precise timing synchronization is essential for the signals they transmit to be received and processed correctly by GPS receivers on the ground. In this section, we present different synchronization types between fractional-order chaotic systems.

The general form of the master-slave is given as follows

$$\begin{cases} {}_a^C D_t^\nu U(t) = F_1(U(t)), \\ {}_a^C D_t^\nu V(t) = F_2(V(t)) + C(t), \end{cases} \quad (5.6.1)$$

where $U(t) = (U_1(t), U_2(t), \dots, U_n(t))^T \in \mathbb{R}^n$ is the master state vector and $V(t) = (V_1(t), V_2(t), \dots, V_m(t))^T \in \mathbb{R}^m$ is the slave state vector. $F_1 : \mathbb{R}^n \rightarrow \mathbb{R}^n$, $F_2 : \mathbb{R}^m \rightarrow \mathbb{R}^m$ are non-linear functions and $C(t)$ is the control vector to be determined.

Definition 5.6.1. *Synchronization is used to understand the sensitivity based on the initial conditions. It has been proven that synchronizing two or more chaotic systems proves the ability to follow closely the same movement of these dual systems together.*

5.6.1 Different synchronization types

Full (Complete) synchronization

Complete synchronization (CS) [86] occurs when there is a complete coincidence between the state variables of the two systems that are synchronized.

Definition 5.6.2. *We consider the master-slave pair (5.6.1), the complete synchronization error is defined by*

$$e(t) = V(t) - U(t). \quad (5.6.2)$$

In this case the control $C(t)$ is chosen so that

$$\lim_{t \rightarrow \infty} \|e(t)\| = 0, \quad (5.6.3)$$

where $\|\cdot\|$ is the euclidean norm.

Remark 5.6.3. *If $F_1 = F_2$, then the synchronization is called identical complete synchronization. Otherwise, it is called non-identical complete synchronization.*

Anti-synchronization

In synchronization, two or more dynamical systems adjust their states over time so that they behave in a coordinated manner. However, in anti-synchronization [35], the systems adjust their states in such a way that they become exactly opposite or out of phase with each other.

Definition 5.6.4. *We consider the master-slave pair (5.6.1), The error system can be defined as follows*

$$e(t) = V(t) + U(t), \quad (5.6.4)$$

and verifies

$$\lim_{t \rightarrow \infty} \|e(t)\| = 0, \quad (5.6.5)$$

Projective synchronization

In projective synchronization [72], the state variables of the two systems are not identical, but there exists a linear transformation (projection) between them, such that the

trajectories of the systems are synchronized up to this transformation. This implies that the overall behavior or shape of the trajectories in phase space remains the same, even though the states themselves may differ.

Definition 5.6.5. *The master-slave pair (5.6.1) are said to be projective synchronized, if there exists non zero vector $\alpha = (\alpha_i)_{1 \leq i \leq n}$ such that*

$$\lim_{t \rightarrow \infty} \|V_i(t) - \alpha_i U_i(t)\| = 0, \quad (5.6.6)$$

Generalized synchronization

This type of synchronization is a generalization of many types of synchronization [26]. In this case, if there exists a controller $C(t)$, and a continuous function $\Psi : \mathbb{R}^n \rightarrow \mathbb{R}^n$ such the error system

$$e(t) = V(t) - \Psi U(t), \quad (5.6.7)$$

goes towards zero. Then, the master-slave system is synchronized under the generalized synchronization.

Q-S synchronization

We say that the Q-S synchronization [82] is achieved between the master-slave pair (5.6.1), if ther exists a control $C(t)$ and tow functions, $Q : \mathbb{R}^n \rightarrow \mathbb{R}^d$ and $S : \mathbb{R}^m \rightarrow \mathbb{R}^d$, such that the error system satisfies

$$\lim_{t \rightarrow \infty} \|e(t)\| = \lim_{t \rightarrow \infty} \|Q(U(t)) - S(V(t))\| = 0. \quad (5.6.8)$$

5.7 Application of fractional chaotic systems in image encryption

The possibility that image encryption based on FO chaotic systems might provide very high levels of security for both transmission and storage has attracted a lot of interest. There has been extensive usage of traditional chaotic systems in encryption techniques due to their sensitivity to beginning circumstances and unpredictability. Nevertheless, FO

chaotic systems are already well-suited for cryptography applications, but the inclusion of non-integer orders makes them considerably more complicated and unpredictable. It is common practice to use the chaotic dynamics produced by FO chaotic systems to encrypt images by first converting them into a scrambled or encrypted version of the original. The encryption technique uses the FO system's chaotic trajectories to randomly alter the picture data or scramble the pixel values. Unauthorized users without the correct decryption keys will see the encrypted picture as random noise, thanks to this mechanism. For high-entropy encryption key generation, FO chaotic systems are a good fit because of their benefits, such as being very sensitive to system settings and beginning circumstances. Their bigger key space, made possible by their continuous dynamics, further fortifies them against cryptanalytic assaults of all kinds. In conclusion, FO chaotic system based image encryption offers a potential method for protecting picture data in several contexts, such as communication, cloud storage, and multimedia systems. These encryption algorithms provide strong security against unwanted access and guarantee the secrecy and integrity of critical picture data by making use of the intrinsic complexity and unpredictability of FO chaotic systems.

5.8 Conclusion

We started by discussing chaos in fractional-order continuous-time dynamical systems, providing examples of such systems. Then, we introduced complexity measures like the spectral entropy (SE) algorithm and C_0 algorithm and synchronization concept was presented. Application of fractional chaotic systems in image encryption were treated recently.

CHAPTER 6

THE FRACTIONAL-ORDER HALVORSEN CIRCULANT SYSTEM AND ITS APPLICATION ON IMAGE ENCRYPTION

6.1 Introduction

In recent years, there has been a surge of interest in utilizing fractional calculus [22] to analyze chaotic systems, sparking investigations into their behavior and applications featuring non-integer order characteristics. Numerous chaotic models in three dimensions have been extensively studied in the literature, including the Tigan, Chen, Cai, Chen-Lee, Lorenz, Rössler, Lu, and Liu systems. This exploration holds significant implications for science and engineering, particularly in control systems and chaos theory, with notable applications such as memristors [87], encryption [53], and information protection [32]. This chapter delves into the FO Caputo derivative and its application to the Halvorsen circulant system (FO-HCS), offering a numerical solution via the Adomian decomposition method (ADM). Dynamics analysis techniques such as phase diagrams, bifurcation diagrams, complexity assessments, and Lyapunov exponents are employed to understand

FO-HCS behavior. Additionally, synchronization and stabilization of FO-HCS are explored, showcasing the application of stability theory in synchronization and adaptive control. Furthermore, we leverage extended fractional sequences to enhance image encryption methods, capitalizing on the unique properties of fractional-order systems. Our proposed method employs a keystream generator based on the improved FO-HCS chaotic behavior, ensuring maximum security for image data. Simulation results demonstrate the safety and reliability of this approach for handling image data.

6.2 The Fractional-order Halvorsen circulant system

The FOHCS is suggested using the Caputo differential operator as follows:

$$\begin{cases} {}_0^C D_t^q x = -ax - by - bz - y^2 \\ {}_0^C D_t^q y = -ay - bz - bx - z^2 \\ {}_0^C D_t^q z = -az - bx - by - x^2 \end{cases}, \quad (6.2.1)$$

where $0 < q \leq 1, a, b \in \mathbb{R}$ are the system parameters.

6.2.1 Solution of the fractional-order Halvorsen circulant system

The numerical solution of the FOHCS (6.2.1) obtained by using ADM is indicated by

$$\begin{cases} x_{n+1} = \sum_{j=0}^5 \frac{k_1^j h^{jq}}{\Gamma(jq + 1)} \\ y_{n+1} = \sum_{j=0}^5 \frac{k_2^j h^{jq}}{\Gamma(jq + 1)} \\ z_{n+1} = \sum_{j=0}^5 \frac{k_3^j h^{jq}}{\Gamma(jq + 1)} \end{cases}, \quad (6.2.2)$$

where h , Γ represent the integration step size and the Gamma function, and $k_i^j(\cdot)$ are defined as

$$k_1^0 = x(n), \quad k_2^0 = y(n), \quad k_3^0 = z(n).$$

$$\begin{cases} k_1^1 = -ak_1^0 - bk_2^0 - bk_3^0 - (k_2^0)^2 \\ k_2^1 = -ak_2^0 - bk_1^0 - bk_3^0 - (k_3^0)^2 \\ k_3^1 = -ak_3^0 - bk_2^0 - bk_1^0 - (k_1^0)^2 \end{cases}, \quad (6.2.3)$$

$$\begin{cases} k_1^2 = -ak_1^1 - bk_2^1 - bk_3^1 - \frac{\Gamma(2q+1)}{\Gamma^2(q+1)} k_2^1 k_2^0 \\ k_2^2 = -ak_2^1 - bk_1^1 - bk_3^1 - \frac{\Gamma(2q+1)}{\Gamma^2(q+1)} k_3^1 k_3^0 \\ k_3^2 = -ak_3^1 - bk_2^1 - bk_1^1 - \frac{\Gamma(2q+1)}{\Gamma^2(q+1)} k_1^1 k_1^0 \end{cases}, \quad (6.2.4)$$

$$\begin{cases} k_1^3 = -ak_1^2 - bk_2^2 - bk_3^2 - \left[\frac{\Gamma(2q+1)}{\Gamma^2(q+1)} \right] k_2^2 k_2^0 - \left[\frac{\Gamma(2q+1)}{\Gamma^2(q+1)} \right] (k_2^1)^2 \\ k_2^3 = -ak_2^2 - bk_1^2 - bk_3^2 - \left[\frac{\Gamma(2q+1)}{\Gamma^2(q+1)} \right] k_3^2 k_3^0 - \left[\frac{\Gamma(2q+1)}{\Gamma^2(q+1)} \right] (k_3^1)^2 \\ k_3^3 = -ak_3^2 - bk_2^2 - bk_1^2 - \left[\frac{\Gamma(2q+1)}{\Gamma^2(q+1)} \right] k_1^2 k_1^0 - \left[\frac{\Gamma(2q+1)}{\Gamma^2(q+1)} \right] (k_1^1)^2 \end{cases}, \quad (6.2.5)$$

$$\begin{cases} k_1^4 = -ak_1^3 - bk_2^3 - bk_3^3 - \frac{\Gamma(2q+1)}{\Gamma^2(q+1)} k_2^3 k_2^0 - \frac{\Gamma(3q+1)}{\Gamma(q+1)\Gamma(2q+1)} k_2^2 k_2^1 \\ k_2^4 = -ak_2^3 - bk_1^3 - bk_3^3 - \frac{\Gamma(2q+1)}{\Gamma^2(q+1)} k_3^3 k_3^0 - \frac{\Gamma(3q+1)}{\Gamma(q+1)\Gamma(2q+1)} k_3^2 k_3^1 \\ k_3^4 = -ak_3^3 - bk_2^3 - bk_1^3 - \frac{\Gamma(2q+1)}{\Gamma^2(q+1)} k_1^3 k_1^0 - \frac{\Gamma(3q+1)}{\Gamma(q+1)\Gamma(2q+1)} k_1^2 k_1^1 \end{cases}, \quad (6.2.6)$$

$$\begin{cases} k_1^5 = -ak_1^4 - bk_2^4 - bk_3^4 - \frac{\Gamma(4q+1)}{\Gamma^2(q+1)} (k_2^4 k_2^0 + k_2^3 k_2^1) - \frac{\Gamma(4q+1)}{\Gamma(q+1)\Gamma(3q+1)} (k_2^3 k_2^1 + (k_2^2)^2) \\ k_2^5 = -ak_2^4 - bk_1^4 - bk_3^4 - \frac{\Gamma(4q+1)}{\Gamma^2(q+1)} (k_3^4 k_3^0 + k_3^3 k_3^1) - \frac{\Gamma(4q+1)}{\Gamma(q+1)\Gamma(3q+1)} (k_3^3 k_3^1 + (k_3^2)^2) \\ k_3^5 = -ak_3^4 - bk_2^4 - bk_1^4 - \frac{\Gamma(4q+1)}{\Gamma^2(q+1)} (k_1^4 k_1^0 + k_1^3 k_1^1) - \frac{\Gamma(4q+1)}{\Gamma(q+1)\Gamma(3q+1)} (k_1^3 k_1^1 + (k_1^2)^2) \end{cases}. \quad (6.2.7)$$

6.2.2 Dynamics analysis of FOHCS

Change the value of q in the FOHCS (6.2.1) in this section. Given that this parameter may be changed, we would preferably analyze its dynamical properties in this component. The FO q is assumed to be changed between 0.55 and 1.0 with a 0.05 step size. The parameters will also be held constant, and we will assume that the initial conditions are 0.2, 0.6, and 0.2. In 6.1(b), you can see a depiction of the relevant bifurcation diagram.

It is seen that the system is mostly chaotic when $0.65 \leq q < 1$. The complexity of the system may be partially described by using the largest Lyapunov exponent, and Figure 6.1(a) displays a range of LEs. At $q = 0.65$, a positive LE is realized in the FOHCS, resulting in the system's chaotic behavior. As demonstrated in Figure 6.1(c), the positive LE causes the chaotic behavior, as indicated by taking $q = 0.65$. In addition, Figure 6.2 displays the attractor with a clear FO. The attractor displays strange behavior and its chaotic nature becomes apparent when $q \geq 0.65$.

6.2.3 Complexity of FOHCS

Simultaneously, change q from 0.55 to 1 using a step size of 0.01 and a from 1 to 5. Based on the SE and C_0 complexity, Figures 6.3 show the chaos diagram in this $q - a$ parameter plane. There is With an increase in order q , the FOHCS complexity exhibits a decreasing trend. Practical applications benefit from the more noticeable trend of decreasing complexity C_0 and SE , as well as the high complexity region that is seen. As a result, the FOHCS system is an appropriate model for real-world applications. It shows how the chaos diagram may be used in practical settings to choose parameters for FOHCS systems.

6.2.4 Complexity with variation a and q

One could think of a system's nonlinear dynamic behavior as an investigation into the system's complexity. Examining if a chaotic sequence is near a random sequence is a complex task. If it approaches a random sequence more closely, the system's complexity is probably quite high. Figure 6.4 displays the C_0 complexity and SE complexity of the system concerning FO q when the system's parameters match those studied in Figure 6.1. Large complexity is correlated with smaller order and vice versa, as seen in Figure 6.1, where the FO q , the LLE describes the dynamic properties. Next, we discovered that the C_0 and SE complexity algorithms were used in the research of Figure 6.4. A comparative study of the two algorithms revealed that while they can both reflect the same dynamical behavior, the C_0 complexity can better characterize the dynamic phenomenon.

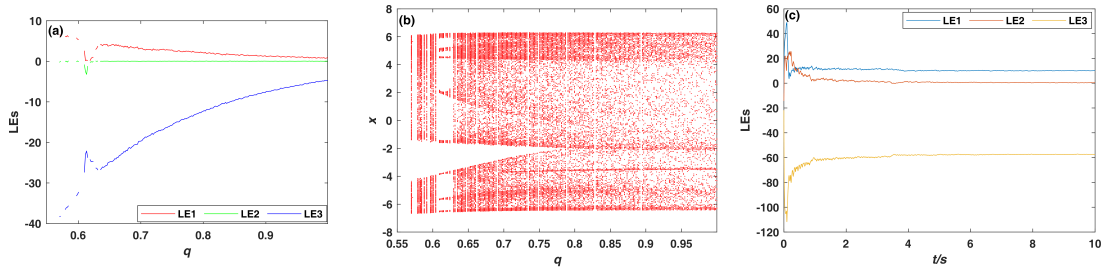


Figure 6.1: dynamics of FOHCS: (a) LEs (b) bifurcation diagram, and (c) LEs with $q = 0.65$.

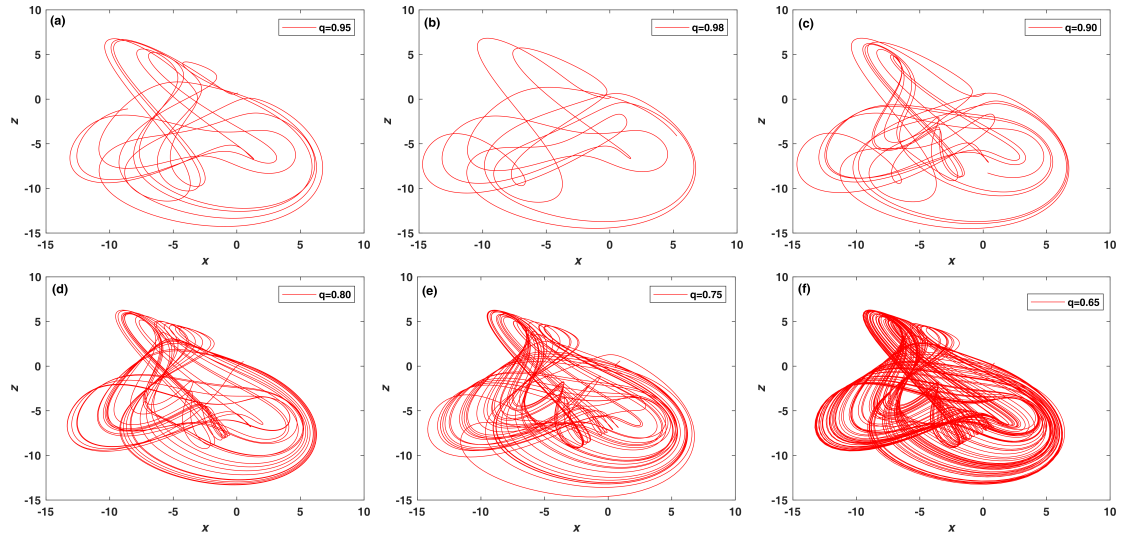


Figure 6.2: FOHCS attractor with different value of q .

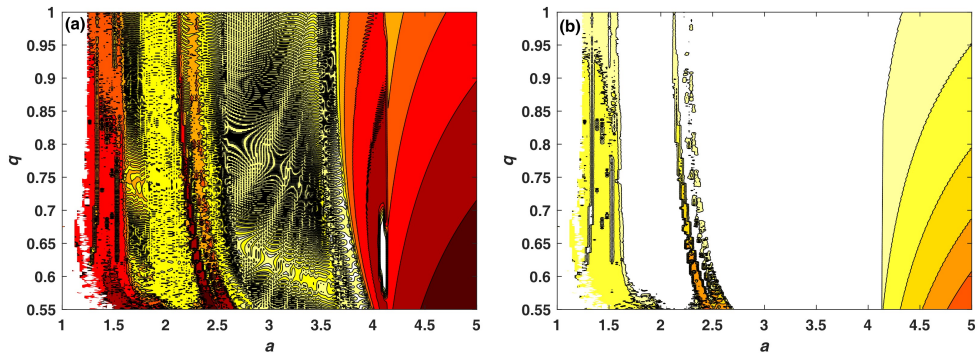


Figure 6.3: Chaos diagram of FOHCS on q - a plan: (a) SE complexity, (b) C_0 complexity.

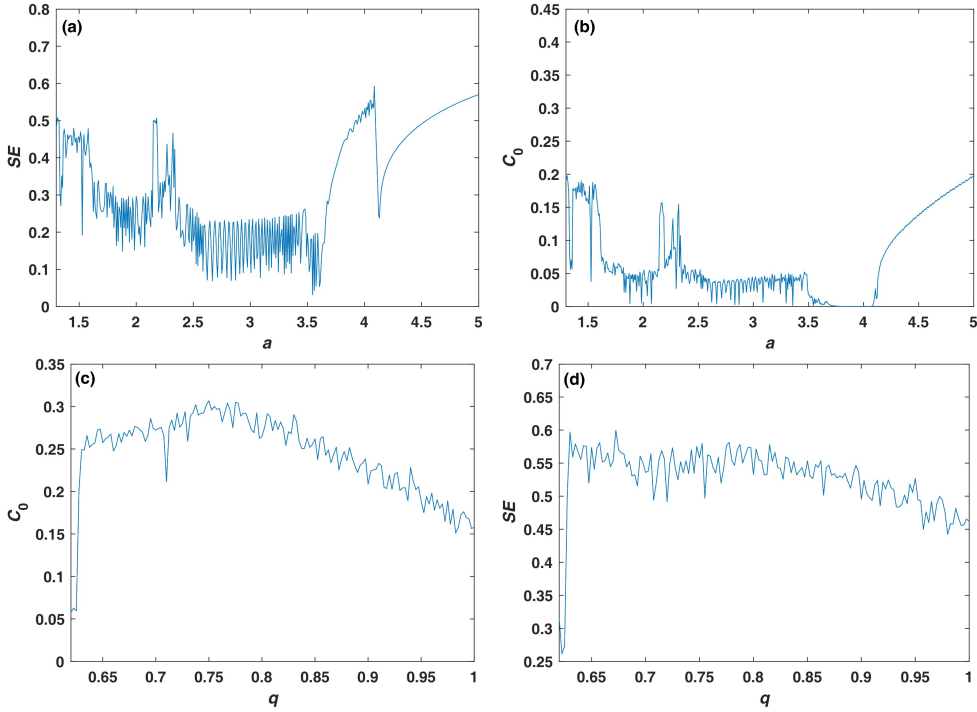


Figure 6.4: FOHCS complexity: (a) SE complexity with $q = 0.65$, (b) C_0 complexity with $q = 0.65$, (c) C_0 complexity with $a = 1.27$, and (d) SE complexity with $a = 1.27$.

6.2.5 Chaos control

This section presents two strategies for controlling the FOHCS. The primary objective of the first strategy is to stabilize the system by ensuring that all of its states converge to zero in due time. A master and a slave FOHCS are made to asymptotically follow the same trajectory using the second controller, whose objective is complete synchronization.

Stabilization law.

In this subsection, we're diving into the world of FOHCS stabilization. Now, in control theory and dynamical systems, stabilization is like keeping a system on track making sure its behavior stays close to zero as time goes on. To achieve this with the FOHCS (6.2.1), we're proposing a three-dimensional control law.

Theorem 6.2.1. [39] The following 3D control law can stabilize the FOHCS (6.2.1).

$$\begin{cases} L_1 = bz + by + y^2 \\ L_2 = bz + z^2 \\ L_3 = x^2 \end{cases}, \quad (6.2.8)$$

Proof. The controlled FOHCS is given by

$$\begin{cases} {}_0^C D_t^q x = -ax - by - bz - y^2 + L_1 \\ {}_0^C D_t^q y = -ay - bx - bz - z^2 + L_2 \\ {}_0^C D_t^q z = -az - by - bx - x^2 + L_3 \end{cases}, \quad (6.2.9)$$

Replacing (6.2.8) by (6.2.9) we obtain

$$\begin{cases} {}_0^C D_t^q x = -ax \\ {}_0^C D_t^q y = -ay - bx \\ {}_0^C D_t^q z = -az - by - bx \end{cases}, \quad (6.2.10)$$

we have to show that the trivial solution in equation (6.2.10) is globally asymptotically stable. After this is proven, we will conclude that all of the states in the controlled system, which is represented by equation (6.2.10), will eventually converge to zero. We can achieve this task by using the assumptions that were previously presented in Theorem 4.5.1. We can write equation (6.2.10) as follows:

$${}_0^C D_t^q (x(t), y(t), z(t))^T = A(x(t), y(t), z(t))^T.$$

Where

$$A = \begin{pmatrix} -a & 0 & 0 \\ -b & -a & 0 \\ -b & -b & -a \end{pmatrix}$$

For matrix A , the eigenvalues are as follows: $\lambda_1 = -a$, $\lambda_2 = -a$, $\lambda_3 = -a$. The

requirements of theorem 4.5.1 are met by the eigenvalues of the matrix A. It is then shown that the trivial solution is stable. As such, the states given by equation (6.2.1) are stabilized effectively. This suggests that the application of the proper control law given in equation (6.2.8) at the origin results in an effective stabilization of all states within the system represented by equation (6.2.10). As we can see, the states in Figure 6.5 are moving towards zero.

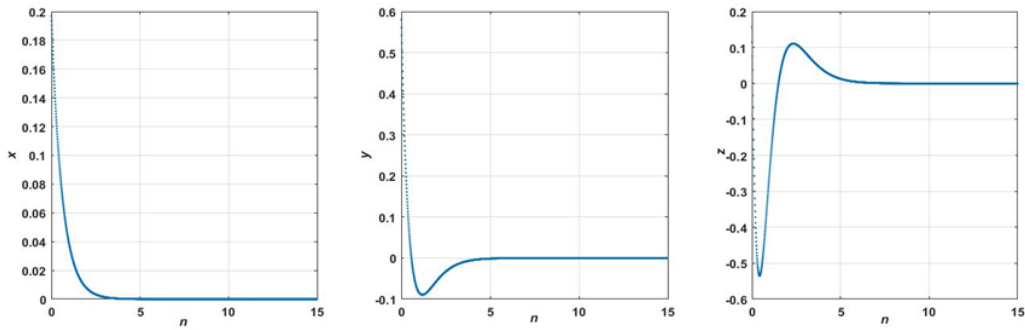


Figure 6.5: Time evolution of the system of the FOHCS (6.2.1) using the control law (6.2.8).

Synchronization of fractional HCS.

The synchronization of chaotic systems is another crucial component. This notion is based on the idea of adding one or more appropriate controllers to the so-called "slave system". A distinct chaotic system known as the "master system" is used to coerce the slave system into mimicking its behavior as the clock ticks toward infinity. Under these conditions, we think about two fractional Halvorsen circulant chaotic systems. We will look at the possibility of using a three-dimensional controller to bring these two fractional systems into harmony. The two systems of master-slave relationships are outlined below:

$$\begin{cases} {}_0^C D_t^q x_m = -ax_m - by_m - bz_m - y_m^2 \\ {}_0^C D_t^q y_m = -ay_m - bx_m - bz_m - z_m^2 \\ {}_0^C D_t^q z_m = -az_m - by_m - bx_m - x_m^2 \end{cases}, \quad (6.2.11)$$

and

$$\begin{cases} {}_0^C D_t^q x_s = -ax_s - by_s - bz_s - y_s^2 + U_1 \\ {}_0^C D_t^q y_s = -ay_s - bx_s - bz_s - z_s^2 + U_2 \\ {}_0^C D_t^q z_s = -az_s - by_s - bx_s - x_s^2 + U_3 \end{cases}, \quad (6.2.12)$$

$(U_1, U_2, U_3) \in \mathbb{R}^3$ is a control vector to be determined. The error that occurs between the slave and master systems is

$$(e_1(t), e_2(t), e_3(t))^T = (x_s(t), y_s(t), z_s(t))^T - (x_m(t), y_m(t), z_m(t))^T$$

Theorem 6.2.2. [39] According to the three-dimensional control law described by (6.2.13), the pair of master-slave fractional Halvorsen circulant chaotic systems are synchronized.

$$\begin{cases} U_1 = y_s^2 - y_m^2 + be_2 + be_3 \\ U_2 = z_s^2 - z_m^2 + be_1 + be_3 \\ U_3 = x_s^2 - x_m^2 + be_1 + be_2 \end{cases}, \quad (6.2.13)$$

Proof. The error system can be derived as follows

$$\begin{cases} {}_0^C D_t^q e_1(t) = -ae_1 - be_2 - e_2(y_m + y_s) - be_3 + U_1 \\ {}_0^C D_t^q e_2(t) = -ae_2 - be_1 - e_3(z_m + z_s) + U_2 \\ {}_0^C D_t^q e_3(t) = -ae_3 - be_2 - e_1(x_m + x_s) + U_3 \end{cases}, \quad (6.2.14)$$

substituting the control law (6.2.13) into the system (6.2.14), we get

$$\begin{cases} {}_0^C D_t^q e_1(t) = -ae_1 \\ {}_0^C D_t^q e_2(t) = -ae_2 \\ {}_0^C D_t^q e_3(t) = -ae_3 \end{cases}, \quad (6.2.15)$$

the system (6.2.15) can be written as follow:

$${}_0^C D_t^q (e_1(t), e_2(t), e_3(t))^T = M(e_1(t), e_2(t), e_3(t))^T$$

where

$$M = \begin{pmatrix} -a & 0 & 0 \\ 0 & -a & 0 \\ 0 & 0 & -a \end{pmatrix}$$

The matrix M has three equal eigenvalues $-a$. According to Theorem 4.5.1, We were able to demonstrate that the error system (6.2.15) moves in the direction of the origin. In conclusion, it is shown that the master (6.2.11) system and slave (6.2.12) system can accomplish the desired synchronization with the proposed control rules in the form (6.2.13). Figure 6.6 shows up the simulation results.

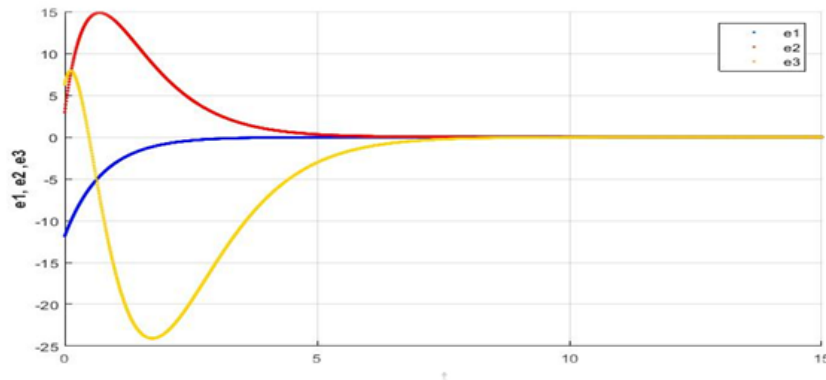


Figure 6.6: Error synchronization of the FOHCS (6.2.1).

6.3 The technique of encryption and decryption

6.3.1 Chaotic sequence generator

Floating point numbers represent state values in chaotic systems; therefore, sequences constructed from these values are unsuitable for direct image cryptography applications. Normalize the chaotic state value of an image with grey level L to an integer between 0 and $L - 1$. The outcome of the transformation is a chaotic pseudorandom sequence that can be implemented in an image cryptosystem. This study employs two distinct equations to convert the chaotic state's values to integers:

$$p_i = \text{floor}(x_i \times 10^r) \bmod L,$$

$$p_i = \text{floor}(x_i \times 2^c) \bmod L.$$

6.3.2 RSA Algorithm

Two keys are utilized by the RSA, a widely recognized asymmetric encryption algorithm: a public key for encryption and a private key for decryption. The inverse also holds: data encrypted with the public key cannot be decrypted without the corresponding private key. Due to its dual-key architecture, RSA is classified as asymmetric. It is based on the Euler theorem of number theory, and its security is contingent on the difficulty of factoring enormous numbers. Digital signatures and data encryption are two of the applications of RSA. The RSA process entails the encryption of plaintext using the recipient's public key. Once the ciphertext is received, it is decrypted by the receiver using their private key. This mechanism guarantees secure communication as access to the private key is restricted to the receiver alone. By decreasing the amount of key transmission in the communication channel, this mechanism improves security.

Algorithm: RSA Algorithm

Input Select two different prime numbers p and q

1. Calculate Euler function, $\phi(n) = (p - 1)(q - 1)$
2. $n = p \times q$
3. Randomly select public key e , $1 < e < \phi(n)$, and $\text{gcd}(\phi(n), e) = 1$
4. Calculate the private key $d \cdot e \equiv 1 \pmod{\phi(n)}$, $d = e^{-1} \pmod{\phi(n)}$
 $d \cdot e \equiv 1 \pmod{\phi(n)}$, $d = e^{-1} \pmod{\phi(n)}$

Encryption method

5. for each plaintext m , calculate $c = m^e \pmod{n}$

Decryption method.

6. for each ciphertext c , calculate $m = c^d \pmod{n}$

Output: The public key, which consists of n and e and the private key, which is d .

6.3.3 Encryption and decryption process

Image Encryption Process

Step 1: Select the prime numbers p and q in order to compute $c = p \times q$ and $\phi(c) = (p - 1)(q - 1)$.

Step 2: The RSA algorithm is utilised to produce the keys (d, c) and (e, c) .

Step 3: Integers (r_1, r_2, r_3) that are selected at random are regarded as confidential information. Subsequently, these values are employed in conjunction with a key (e, c) to compute $C_i = r_i^e \bmod c$, where $i = 1, 2, 3$. Subsequently, the values that ensue are transmitted to the receiver.

Step 4: :The equation (6.3.1) is utilised to calculate the parameter values x_0 , y_0 , and z_0 for the fractional chaotic HCS.

$$\begin{cases} x_0 = \sqrt{\log(C_1 + r_1)} \\ y_0 = \sqrt{\log(C_2 + r_2)} \\ z_0 = \sqrt{\log(C_3 + r_3)} \end{cases}, \quad (6.3.1)$$

To generate pseudorandom sequences S , X , and R , substitute parameters x_0 , y_0 , and z_0 into equations (6.2.1) and convert the values generated into the range of 0 to 255:

$$\begin{cases} S = \text{mod } (\text{floor}((s + 100) \times 10^{10}), 256) \\ X = \text{mod } (\text{floor}((s + 100) \times 10^{14}), 256) \\ R = \text{mod } (\text{floor}((s + 100) \times 10^{16}), 256) \end{cases}, \quad (6.3.2)$$

Step 5: To acquire image B, nonrepetitive permutations are executed on image A using the key stream X . Run a permutation using plaintext.

Step 6: Finding an encrypted image matrix E using transformed C is the last step.

Image Decryption Process

The decryption of an image is the inverse operation of encryption; it operates as follows:

Step 1: The receiver decrypts the original image using a private $key(d, c)$ and the ciphertext information C_i , $r_i = C_i^d \bmod c$, $i = 1, 2, 3$. The parameters x_0 , y_0 , and z_0 of the

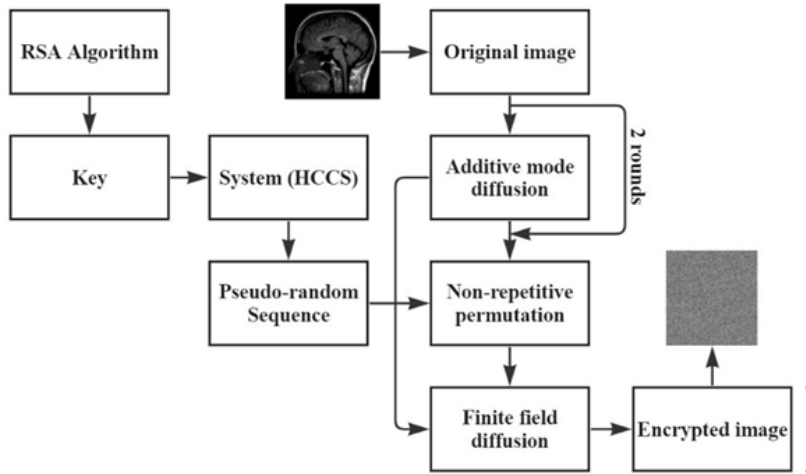


Figure 6.7: Encryption flowchart.

Halvorsen circulant system are subsequently computed utilizing equation (6.3.1)

Step 2: By replacing the parameters x_0 , y_0 , and z_0 in equations (6.2.1) and (6.3.1), pseudorandom sequences S' , X' , and R' are produced. The range of values that are generated is 0 to 255.

$$\begin{cases} S' = \text{mod } (\text{floor}((s' + 100) \times 10^{10}), 256), \\ X' = \text{mod } (\text{floor}((s' + 100) \times 10^{14}), 256), \\ R' = \text{mod } (\text{floor}((s' + 100) \times 10^{16}), 256), \end{cases}, \quad (6.3.3)$$

Step 3: To produce picture B' , nonrepetitive permutations are applied to image C' using the key stream X' . Make a permutation with plaintext.

Step 4: Get the original picture matrix P' by transforming A' .

6.4 Simulations

To ensure the security and effectiveness of the proposed image cryptosystem. It is assumed that several pictures, including standard experimental images, have been subjected to thorough examination. The results of the tests are then compared to the results obtained using the standard methods and approaches. A range of grayscale pictures, including medical images, are chosen as examples of plaintext images to demonstrate the visual

effect of encryption. No personally identifiable information about the matching plaintext photographs is revealed by the encryption results, as demonstrated in Figure 6.8, and the encrypted images are fully compatible with the originals. The results show that both the encrypted and original images work flawlessly. According to the results of the research, the proposed algorithm-based image cryptography system provides accurate picture decryption and efficient image encryption.

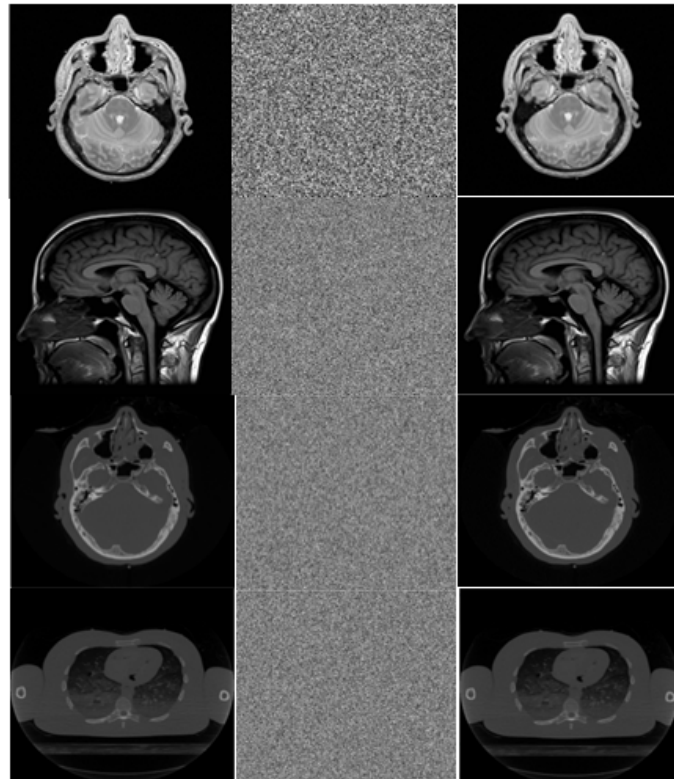


Figure 6.8: Image Encryption and Decryption process

6.4.1 Histogram

The distribution of an image's different grayscale values is shown by its histogram. A histogram may help understand how the image's intensity is distributed. An evenly distributed range of intensities is unusual in important photographs. To withstand various statistical assaults, the encrypted picture must have a uniform distribution. This research offers a comparative analysis of the histograms to evaluate the effectiveness of the proposed

technique. The results and related histograms of the encryption approach are shown in Figure 6.9. The recommended method's encrypted picture features a histogram with three channels because of the dimension modification stage. The histogram demonstrates that the three encrypted picture channels have very similar intensity distributions. All sorts of statistical attacks can't break the proposed picture encryption method, as shown in the study and comparison.

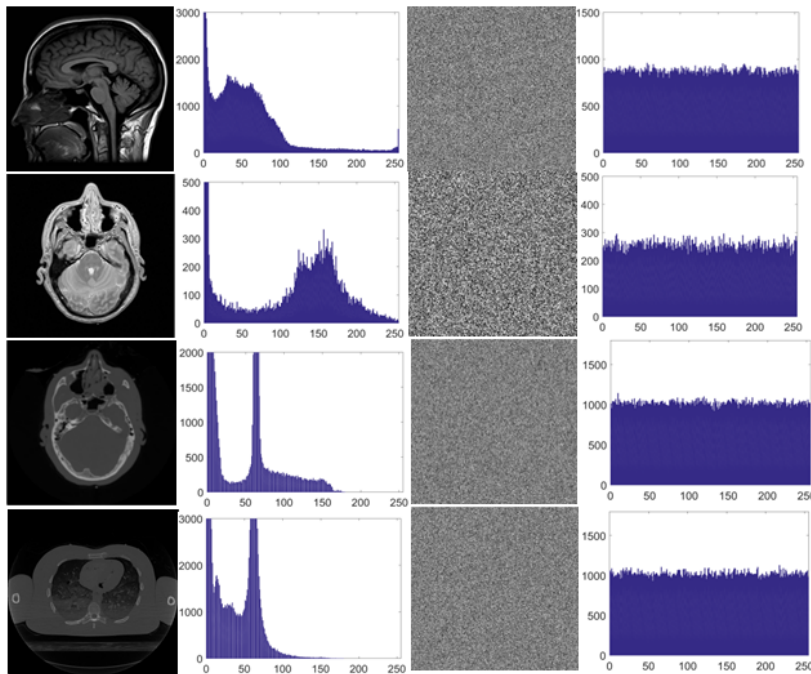


Figure 6.9: Histogram of correlation and coefficient

6.4.2 Adjacent pixel correlation

There is usually a strong correlation between the values of nearby pixels in plaintext pictures that successfully communicate information. To ensure that the encryption process does not allow for the recovery of both the plaintext and the cipher text, it is necessary to disrupt this substantial connection. Using the original and encrypted pictures, we randomly picked 10^4 surrounding pixels to determine the correlation strength in the x , y , and z axes. The correlation coefficient is calculated using the following formula:

$$\begin{cases} r_{xy} = \frac{\text{cov}(x, y)}{\sqrt{D(x)D(y)}} \\ E(x) = \frac{1}{N} \sum_{i=1}^N (x_i) \\ D(x) = \frac{1}{N-1} \sum_{i=1}^N ((x_i) - E(x))^2 \\ \text{cov}(x, y) = \frac{1}{N} \sum_{i=1}^N ((x_i) - E(x))((y_i) - E(y)) \end{cases}, \quad (6.4.1)$$

The variables x and y stand for two neighboring pixel values. In Figure 6.10, we can see the outcomes of the correlation test. Along the x, y , and z axes, the pixels of the plaintext picture are scattered equally. Hence, there is a close connection between the plaintext picture and the image proper. The ciphertext picture seems to have randomly distributed pixels after encryption as if all links between them had been obliterated. Simultaneously, the process is the same for all the photographs in the standard collection, irrespective of their size. All the data about the correlation coefficients are shown in Figure 6.10. These coefficient values are rather low for the encrypted text pictures.

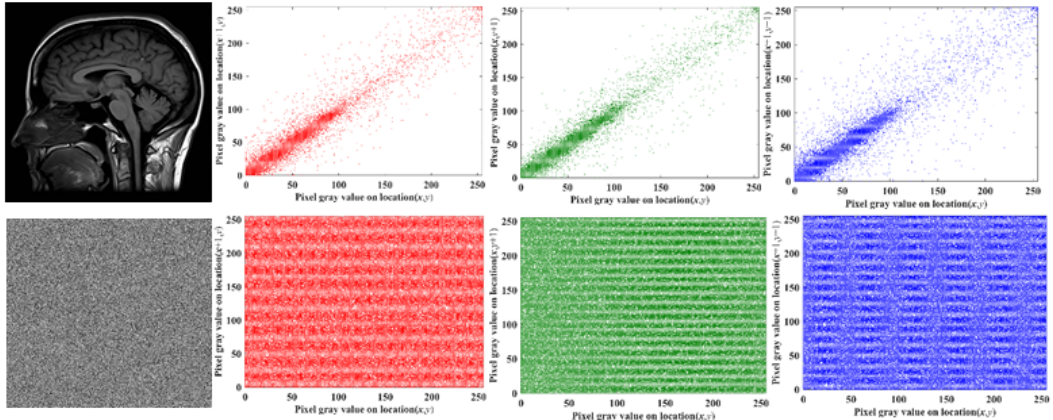


Figure 6.10: Correlation adjacent pixels in the original and encrypted images.

6.4.3 Key analysis

The proposed image cryptosystem's security features, including its key space size and key variation sensitivity, will be investigated. The fundamental components of the proposed

image cryptosystem are the system parameters and starting settings. The key space of the proposed system is around 2^{697} , which is much larger than the 2^{100} required by theory, as shown in Table 6.1, which is approximately $10^{210} = (10^{10})^{21} \approx 2^{697}$. If this is not the

Table 6.1: Key space comparison.

Proposed	[41]	[107]	[57]	[89]	[111]	[63]
Keyspace	2^{697}	2^{425}	2^{256}	2^{256}	2^{312}	2^{154}

case, the method is very vulnerable to brute force assaults. Additionally, to determine how sensitive the decryption key is in picture encryption, the mean square error MSE between the original and decrypted pictures is computed. The MSE value is zero when the correct decryption keys are used, as shown in Figure 6.11. Additionally, when one key is changed, all keys are updated simultaneously. That the original and encrypted images are different and that the decoded picture does not include any discernible information is supported by this. The sensitivity of each key is further shown by this.

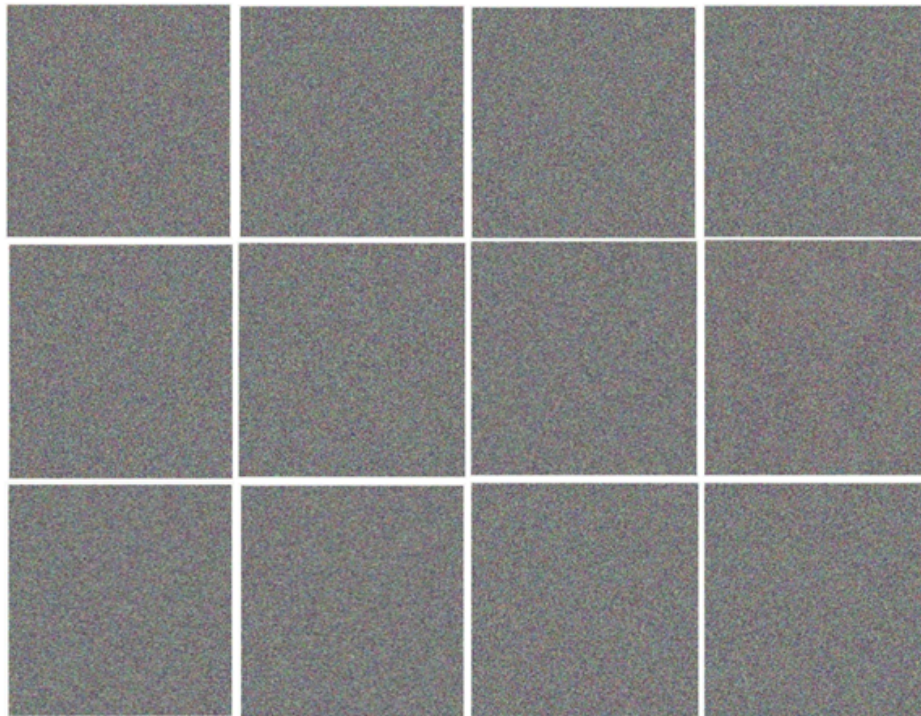


Figure 6.11: Key sensitivity analysis with using correct key

6.4.4 Entropy analysis

With increasing information entropy, an image's visual information communication capabilities deteriorate. More viewable information means less information entropy in an encrypted picture. Compared to a clear image, an encrypted one should have a much higher information entropy. The theoretical value, which is calculated as 8,

$$E = - \sum_{j=1}^k p(y_j) \log_2 p(y_j), \quad (6.4.1)$$

the probability of the gray value y_j is denoted as $p(y_j)$. The experiment determines the information entropy by first creating unique 3D cubes from test images and then encrypting each one separately. To summarize, the information entropy of the ciphertext image cube is much greater than that of the plaintext cube, reaching a maximum of 7.9998 and being quite near to the theoretical value, as shown in Table 6.2. This data suggests that the proposed encryption method outperforms competing methods in terms of security.

Table 6.2: Image correlation coefficient

Image	Original			Encrypted			Entropy
	H	V	D	H	V	D	
MRI-1.00	0.9955	0.9951	0.9912	-0.0075	0.0017	0.0124	7.9996
MRI-1.00	0.8300	0.8376	0.8040	-0.0186	0.0241	0.0151	7.9987
MRI-1.10	0.9963	0.9960	0.9928	-0.0182	-0.0075	-0.0158	7.9998
MRI-1.01	0.9537	0.9721	0.9341	0.0014	-0.0102	0.0007	7.9993
MRI-1.00	0.9755	0.9875	0.9650	-0.0197	0.0214	-0.0308	7.9991
MRI-1.11	0.9756	0.9864	0.9639	0.0001	0.0077	-0.0083	7.9992
MRI-1.01	0.9963	0.9959	0.9927	0.0050	-0.0007	0.0137	7.9997
MRI-1.11	0.7273	0.7239	0.6890	-0.0041	-0.0228	-0.0006	7.9901
MRI-1.01	0.5128	0.6579	0.3391	0.0053	0.0356	0.0142	7.9993
MRI-1.11	0.6031	0.7346	0.4783	-0.0127	-0.0182	0.0197	7.9993
[108]	-	-	-	-0.0125	0.0433	0.0400	7.9970
[106]	-	-	-	-0.0053	-0.0008	0.0084	7.9993

6.4.5 Different attack

By examining the plaintext output of various encryption processes, the differential attack approach leverages this information to target the cryptographic algorithm. This implies that two distinct ciphertext images will be produced from even little modifications to the plaintext image's pixel structure. The Blocked Average Change Intensity (*BACI*), the Uniform Average Change Intensity (*UACI*), and The Number of Pixels Conversion Rate (*NPCR*) are the two metrics used to assess an image's resistance to differential attacks. These are frequently employed to assess the ciphertext image on a qualitative level. The *BACI*, *UACI*, and *NPCR* can be calculated as follows if the ciphertext pictures C_1 and C_2 are produced by encrypting a plaintext image that varies by one bit:

$$NPCR = \frac{\sum_{ij} D(i, j)}{M \times N} \times 100\%. \quad (6.4.2)$$

$$D(i, j) = \begin{cases} 1, & c_1(i, j) \neq c_2(i, j) \\ 0, & \text{otherwise} \end{cases}. \quad (6.4.3)$$

$$UACI = \frac{1}{M \times N} \sum_{ij} \frac{|c_1(i, j) - c_2(i, j)|}{255} \times 100\%. \quad (6.4.4)$$

$$BACI = \frac{m}{(M - 1) \times (N - 1)} \times 100\%. \quad (6.4.5)$$

Where M and N are the width and height of the image, respectively. For each pixel position (i, j) , if the pixel values in the corresponding positions of two ciphertext images, $C_1(i, j)$ and $C_2(i, j)$, are the same, then the value of $d(i, j)$ is 0, otherwise, it's 1. This helps us identify changes in pixel values between the two images. To measure how much the images differ, we use a statistic called the Non-Parametric Change Ratio *NPCR*.

$$\sigma_u^2 = \frac{(Q + 2)(Q^2 + 2Q + 3)}{18(Q + 1)^2 Q(M \times N)}.$$

To determine the *BACI*, *UACI*, and *NPCR* values at the pixel level, we used a significance threshold of $\sigma = 0.05$. In terms of the photographs, their respective critical values are as follows: 26.8129% and 99.6099%, 43.48696% and 30.6439%, and 99.6099% and 33.5530%. The results of the tests for *BACI*, *UACI*, and *NPCR* are shown in Table

6.3. according to several different pictures. Although the currently available encryption algorithms do not completely satisfy the requirements of the *BACI*, *UACI*, and *NPCR* tests, the solution that has been suggested is successful in all three of these tests. In addition to being able to survive a wide range of assaults, the algorithm is capable of meeting the needed image security criteria.

Table 6.3: *BACI*, *UACI*, and *NPCR* results for complete encryption

Plaintext image	1 ROUND			2 ROUND		
	<i>BACI</i> (%)	<i>NPCR</i> (%)	<i>UACI</i> (%)	<i>BACI</i> (%)	<i>NPCR</i> (%)	<i>UACI</i> (%)
MRI-1.00	26.8118	99.6066	33.5531	30.6231	99.6002	43.4858
MRI-1.01	26.7635	99.6022	33.4547	30.6437	99.6090	43.4526
MRI-1.10	26.7473	99.6257	33.4222	30.5874	99.6162	43.5017
MRI-1.11	26.7654	99.6097	33.4541	30.6157	99.5941	43.4776
MRI-1.00	26.7596	99.6047	33.4062	29.2014	99.5992	42.0315
MRI-1.01	26.7896	99.6120	33.4708	29.2136	99.6085	41.9806
MRI-1.10	26.7662	99.6021	33.4834	29.2377	99.5971	42.0222
MRI-1.11	26.7708	99.6146	33.4623	29.2084	99.6119	42.0272
MRI-1.01	26.8028	99.6130	33.4753	30.4372	99.6072	43.2066
MRI-1.10	26.7917	99.6128	33.4503	30.4407	99.6153	43.2679
[116]	26.7701	99.6089	33.4633	-	-	-
[108]	-	-	-	-	99.5565	33.9306

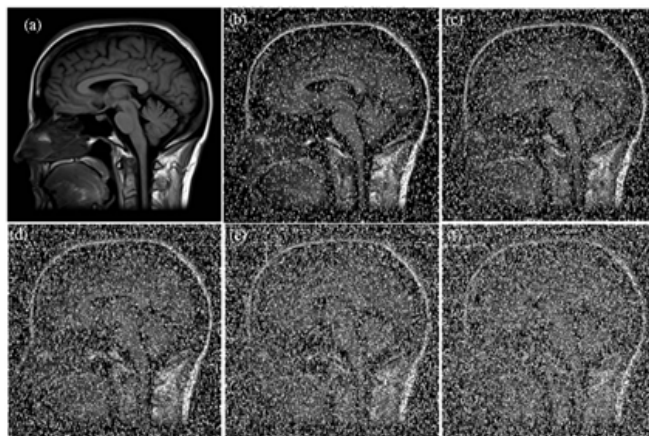


Figure 6.12: The impact of varying ciphertext image intensities on decrypted images.

6.4.6 Robustness analysis

To determine how well our strategy works when there is noise, we do an analysis. Applying Poisson, salt & pepper, and speckle noises to the ciphertext picture yields noise intensities of 0.02 for speckle noise, 0.05 for salt & pepper noise, and 0.1 for Poisson noise. Figure 6.12 shows the results of the tests. Remarkably, even with a noise level of 0.1 for salt & pepper noise, the encrypted picture can still be identified, proving the algorithm's robustness.

6.4.7 Evaluation of known-plaintext and chosen-plaintext attacks

Methods for encrypting images are investigated about known plaintext and selected plain-text assaults. Attackers may utilize both black-and-white and color photos to crack algorithms; these pictures can also gauge how strong a certain cryptosystem is. The changes to the replacement and shift parameters are determined by the image being evaluated. The significance of these pictures in evaluating the resilience of the suggested cryptosystem to various kinds of assaults is shown in Figures 6.10 and 6.13. Like the test cases using black and white photographs, the generated ciphertext pictures have a consistent distribution in their histograms and are readable. According to Table 6.2, the correlation coefficients have decreased significantly, and the entropies of the two images are getting close to 8. Based on these results, it is reasonable to assume that the suggested method can withstand both known and selected plaintext attacks.

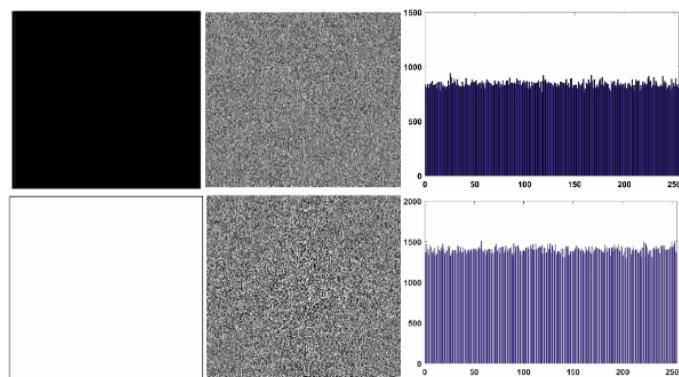


Figure 6.13: Results of encryption for every black and white image.

6.5 Conclusion

In this chapter, we study a novel nonlinear control approach for synchronizing two FO-HCS based on the ADM algorithm. For lower derivative orders q , it is shown that the FOHCS, which shows chaos in its states, has a favorable dynamical feature with increasing complexity. We verify its chaotic behavior by looking at the LEs, bifurcation diagram, and phase space. In addition, we investigated image encryption.

GENERAL CONCLUSION AND PERSPECTIVES

We studied in this thesis some fractional-order dynamical systems in discrete-time and continuous-time and studied some dynamical behaviors. We divided the thesis into two main parts: First, we investigate fractional difference equations, we provide a one-dimensional linear control law for the stabilization of the fractional discrete Ushio system after studying and detecting chaos. Second, in fractional differential equations, we explain the dynamics, where we use phase portrait, bifurcation, Lyapunov exponents, and complexity to confirm the existence of chaos in the FOHCS. Then, two controllers are proposed, the first one is for stabilization and the second is used to achieve complete synchronization between a pair of FOHCS, then goes on to discuss how this system can be used to construct an image encryption method. For future works, we will continue to investigate more interesting systems study fractional discrete systems of high dimensions, and applied in secure communication technology as well as audio and video chaotic encryption.

BIBLIOGRAPHY

- [1] T. Abdeljawad. On riemann and caputo fractional differences. *Computers & Mathematics with Applications*, 62(3):1602–1611, 2011.
- [2] G. Adomian. A new approach to nonlinear partial differential equations. *Journal of Mathematical Analysis and Applications*, 102(2):420–434, 1984.
- [3] V. S. Afraimovich, V. Nekorkin, G. Osipov, and V. D. Shalfeev. *Stability, structures and chaos in nonlinear synchronization networks*, volume 6. World Scientific, 1995.
- [4] R. P. Agarwal, A. M. El-Sayed, and S. M. Salman. Fractional-order chua’s system: discretization, bifurcation and chaos. *Advances in Difference Equations*, 2013:1–13, 2013.
- [5] N. Aguila-Camacho, M. A. Duarte-Mermoud, and J. A. Gallegos. Lyapunov functions for fractional order systems. *Communications in Nonlinear Science and Numerical Simulation*, 19(9):2951–2957, 2014.
- [6] E. Ahmed, A. El-Sayed, and H. A. El-Saka. Equilibrium points, stability and numerical solutions of fractional-order predator–prey and rabies models. *Journal of Mathematical Analysis and Applications*, 325(1):542–553, 2007.
- [7] D. J. Amit and D. J. Amit. *Modeling brain function: The world of attractor neural networks*. Cambridge university press, 1989.

- [8] A. Atangana and S. İğret Araz. Atangana–seda numerical scheme for labyrinth attractor with new differential and integral operators. *Fractals*, 28(08):2040044, 2020.
- [9] F. M. Atici and P. W. Eloe. A transform method in discrete fractional calculus. *International Journal of Difference Equations*, 2(2), 2007.
- [10] A. T. Azar, S. Vaidyanathan, and A. Ouannas. *Fractional order control and synchronization of chaotic systems*, volume 688. Springer, 2017.
- [11] D. Baleanu, G.-C. Wu, Y.-R. Bai, and F.-L. Chen. Stability analysis of caputo–like discrete fractional systems. *Communications in Nonlinear Science and Numerical Simulation*, 48:520–530, 2017.
- [12] N. R. Bastos, R. A. Ferreira, and D. F. Torres. Necessary optimality conditions for fractional difference problems of the calculus of variations. *arXiv preprint arXiv:1007.0594*, 2010.
- [13] S. Bendoukha, A. Ouannas, X. Wang, A.-A. Khennaoui, V.-T. Pham, G. Grassi, and V. V. Huynh. The co-existence of different synchronization types in fractional-order discrete-time chaotic systems with non–identical dimensions and orders. *Entropy*, 20(9):710, 2018.
- [14] S. Boudiar, A. Ouannas, S. Bendoukha, and A. Zara. Coexistence of different types of chaos synchronization between non-identical and different dimensional dynamical systems. *Nonlinear Dyn. Syst. Theory*, 18(3):253–258, 2018.
- [15] D. Cafagna and G. Grassi. Bifurcation and chaos in the fractional-order chen system via a time-domain approach. *International Journal of Bifurcation and Chaos*, 18(07):1845–1863, 2008.
- [16] M. Caputo. Linear models of dissipation whose q is almost frequency independent. *Geophysical Journal International*, 13(5):529–539, 1967.
- [17] M. Caputo and E. Dissipazione. Bologna, 1969.

- [18] T. L. Carroll and L. M. Pecora. Synchronizing chaotic circuits. In *Nonlinear dynamics in circuits*, pages 215–248. World Scientific, 1995.
- [19] J. Čermák, I. Győri, and L. Nechvátal. On explicit stability conditions for a linear fractional difference system. *Fractional Calculus and Applied Analysis*, 18:651–672, 2015.
- [20] A. Chen and Y. Chen. Existence of solutions to anti-periodic boundary value problem for nonlinear fractional differential equations. *Differential Equations and Dynamical Systems*, 19:237–252, 2011.
- [21] D. Chen, R. Zhang, X. Liu, and X. Ma. Fractional order lyapunov stability theorem and its applications in synchronization of complex dynamical networks. *Communications in Nonlinear Science and Numerical Simulation*, 19(12):4105–4121, 2014.
- [22] F. Chen, L. Xia, D. Guo, and Y. Liu. A fractional-order multi-scroll chaotic system. *JOURNAL OF INFORMATION & COMPUTATIONAL SCIENCE*, 10(4):1203–1211, 2013.
- [23] W. Chen, H. Sun, X. Li, et al. *Fractional derivative modeling in mechanics and engineering*. Springer, 2022.
- [24] W. Chen, J. Zhuang, W. Yu, and Z. Wang. Measuring complexity using fuzzyen, apen, and sampen. *Medical engineering & physics*, 31(1):61–68, 2009.
- [25] Y. Cherrault and G. Adomian. Decomposition methods: a new proof of convergence. *Mathematical and Computer Modelling*, 18(12):103–106, 1993.
- [26] Z. Chougui and A. Ouannas. A new generalized synchronization scheme to control fractional chaotic dynamical systems with different dimensions and orders. *Nonlinear Studies*, 27(3), 2020.
- [27] S. L. De Souza and I. L. Caldas. Calculation of lyapunov exponents in systems with impacts. *Chaos, Solitons & Fractals*, 19(3):569–579, 2004.

- [28] Z. Ding and Y. Shen. Projective synchronization of nonidentical fractional-order neural networks based on sliding mode controller. *Neural Networks*, 76:97–105, 2016.
- [29] A. M. El-Sayed. Fractional order evolution equations. *J. of Frac. Calculus*, 7:89–100, 1995.
- [30] S. Eladyi. An introduction to difference equations, 2000.
- [31] K. Fallahi, R. Raoufi, and H. Khoshbin. An application of chen system for secure chaotic communication based on extended kalman filter and multi-shift cipher algorithm. *Communications in Nonlinear Science and Numerical Simulation*, 13(4):763–781, 2008.
- [32] M. Feki. An adaptive chaos synchronization scheme applied to secure communication. *Chaos, Solitons & Fractals*, 18(1):141–148, 2003.
- [33] C.-F. Feng and H.-J. Yang. Projective-lag synchronization scheme between two different discrete-time chaotic systems. *International Journal of Non-Linear Mechanics*, 121:103451, 2020.
- [34] R. A. Ferreira and D. F. Torres. Fractional h-difference equations arising from the calculus of variations. *Applicable Analysis and Discrete Mathematics*, pages 110–121, 2011.
- [35] R. Filali, S. Hammami, M. Benrejeb, and P. Borne. On synchronization, anti-synchronization and hybrid synchronization of 3d discrete generalized hénon map. *Nonlinear Dynamics and Systems Theory*, 12(1):81–95, 2012.
- [36] A. Gasri, A. Ouannas, K. S. Ojo, and V.-T. Pham. Coexistence of generalized synchronization and inverse generalized synchronization between chaotic and hyperchaotic systems. *Nonlinear Analysis: Modelling and Control*, 23(4):583–598, 2018.

- [37] J. Georges, D. Johnson, R. Devaney, and P. D. Straffin. A first course in chaotic dynamical systems: Labs 1-6. *American Mathematical Monthly*, 100(10):961–963, 1993.
- [38] J. Gleick and M. Berry. Chaos-making a new science. *Nature*, 330:293, 1987.
- [39] Y. Hasna, Y. Islam, S. He, G. Ahlem, and M. M. Hassan. Advanced medical image encryption techniques using the fractional-order halvorsen circulant systems: Dynamics, control, synchronization and security applications. *Physica Scripta*, 2024.
- [40] S.-B. He, K.-H. Sun, and H.-H. Wang. Solution of the fractional-order chaotic system based on adomian decomposition algorithm and its complexity analysis. *Acta Physica Sinica*, 63(3):030502, 2014.
- [41] Y. He, Y.-Q. Zhang, X. He, and X.-Y. Wang. A new image encryption algorithm based on the of-lstms and chaotic sequences. *Scientific reports*, 11(1):6398, 2021.
- [42] M. Hénon. A two-dimensional mapping with a strange attractor 94–102, 1976.
- [43] M. Holm. Sum and difference compositions in discrete fractional calculus. *Cubo (Temuco)*, 13(3):153–184, 2011.
- [44] R. Holmgren. *A first course in discrete dynamical systems*. Springer Science & Business Media, 2000.
- [45] H.-Y. Jia, Z.-Q. Chen, and W. Xue. Analysis and circuit implementation for the fractional-order lorenz system. *Acta Physica Sinica*, 62(14):140503, 2013.
- [46] W. G. Kelley and A. C. Peterson. *Difference equations: an introduction with applications*. Academic press, 2001.
- [47] A.-A. Khennaoui, A. Ouannas, S. Bendoukha, G. Grassi, R. P. Lozi, and V.-T. Pham. On fractional-order discrete-time systems: Chaos, stabilization and synchronization. *Chaos, Solitons & Fractals*, 119:150–162, 2019.

- [48] A.-A. Khennaoui, A. Ouannas, S. Bendoukha, G. Grassi, X. Wang, and V.-T. Pham. Generalized and inverse generalized synchronization of fractional-order discrete-time chaotic systems with non-identical dimensions. *Advances in Difference Equations*, 2018:1–14, 2018.
- [49] A.-A. Khennaoui, A. Ouannas, S. Bendoukha, G. Grassi, X. Wang, V.-T. Pham, and F. E. Alsaadi. Chaos, control, and synchronization in some fractional-order difference equations. *Advances in Difference Equations*, 2019(1):1–23, 2019.
- [50] A.-A. Khennaoui, A. Ouannas, S. Bendoukha, X. Wang, and V.-T. Pham. On chaos in the fractional-order discrete-time unified system and its control synchronization. *Entropy*, 20(7):530, 2018.
- [51] A. A. Khennaoui, A. Ouannas, S. Boulaaras, V.-T. Pham, and A. Taher Azar. A fractional map with hidden attractors: chaos and control. *The European Physical Journal Special Topics*, 229:1083–1093, 2020.
- [52] C.-M. Kim, S. Rim, W.-H. Kye, J.-W. Ryu, and Y.-J. Park. Anti-synchronization of chaotic oscillators. *Physics Letters A*, 320(1):39–46, 2003.
- [53] J. Lang. Color image encryption based on color blend and chaos permutation in the reality-preserving multiple-parameter fractional fourier transform domain. *Optics Communications*, 338:181–192, 2015.
- [54] C. Li and W. Deng. Chaos synchronization of fractional-order differential systems. *International Journal of Modern Physics B*, 20(07):791–803, 2006.
- [55] C. Li, X. Liao, and K.-w. Wong. Lag synchronization of hyperchaos with application to secure communications. *Chaos, Solitons & Fractals*, 23(1):183–193, 2005.
- [56] G.-H. Li. Modified projective synchronization of chaotic system. *Chaos, Solitons & Fractals*, 32(5):1786–1790, 2007.
- [57] X. Liu, X. Tong, Z. Wang, and M. Zhang. Uniform non-degeneracy discrete chaotic system and its application in image encryption. *Nonlinear Dynamics*, 108(1):653–682, 2022.

- [58] E. Lorentz. Deterministic non-periodic flow. *J. Atmos. Sci.*, 20:130–141, 1963.
- [59] E. N. Lorenz. Deterministic nonperiodic flow. *Journal of atmospheric sciences*, 20(2):130–141, 1963.
- [60] R. Lozi. Un attracteur étrange (?) du type attracteur de hénon. *Le Journal de Physique Colloques*, 39(C5):C5–9, 1978.
- [61] S. Lynch. *Dynamical systems with applications using MATLAB*. Springer, 2004.
- [62] G. M. Mahmoud and E. E. Mahmoud. Complete synchronization of chaotic complex nonlinear systems with uncertain parameters. *Nonlinear Dynamics*, 62:875–882, 2010.
- [63] N. Mao, X. Tong, M. Zhang, and Z. Wang. A hyperchaotic image encryption algorithm based on lstm neural network and lifting wavelet transform. *Physica Scripta*, 98(7):075215, 2023.
- [64] R. M. May. Biological populations obeying difference equations: stable points, stable cycles, and chaos. *Journal of Theoretical Biology*, 51(2):511–524, 1975.
- [65] K. S. Miller and B. Ross. Fractional difference calculus. In *Proceedings of the international symposium on univalent functions, fractional calculus and their applications*, pages 139–152, 1989.
- [66] C. A. Monje, Y. Chen, B. M. Vinagre, D. Xue, and V. Feliu-Batlle. *Fractional-order systems and controls: fundamentals and applications*. Springer Science & Business Media, 2010.
- [67] D. Mozyrska and E. Girejko. Overview of fractional h-difference operators. In *Advances in harmonic analysis and operator theory: the stefan samko anniversary volume*, pages 253–268. Springer, 2013.
- [68] N. Noroozi, M. Roopaei, P. Karimaghaei, and A. A. Safavi. Simple adaptive variable structure control for unknown chaotic systems. *Communications in Nonlinear Science and Numerical Simulation*, 15(3):707–727, 2010.

- [69] V. I. Oseledec. A multiplicative ergodic theorem, lyapunov characteristic numbers for dynamical systems. *Transactions of the Moscow Mathematical Society*, 19:197–231, 1968.
- [70] A. Ouannas. Chaos synchronization approach based on new criterion of stability. *Nonlinear Dynamics and Systems Theory*, 14(4):395–401, 2014.
- [71] A. Ouannas. Co-existence of various types of synchronization between hyperchaotic maps. *Nonlinear Dyn. Syst. Theory*, 16:312–321, 2016.
- [72] A. Ouannas and R. Abu-Saris. On matrix projective synchronization and inverse matrix projective synchronization for different and identical dimensional discrete-time chaotic systems. *Journal of Chaos*, 2016, 2016.
- [73] A. Ouannas and M. M. Al-Sawalha. A new approach to synchronize different dimensional chaotic maps using two scaling matrices. *Nonlinear Dyn. Syst. Theory*, 15(4):400–408, 2015.
- [74] A. Ouannas, A. T. Azar, and S. Vaidyanathan. New hybrid synchronisation schemes based on coexistence of various types of synchronisation between master-slave hyperchaotic systems. *International Journal of Computer Applications in Technology*, 55(2):112–120, 2017.
- [75] A. Ouannas, S. Bendoukha, A. Karouma, and S. Abdelmalek. A general method to study the co-existence of different hybrid synchronizations in fractional-order chaotic systems. *International Journal of Nonlinear Sciences and Numerical Simulation*, 20(3-4):351–359, 2019.
- [76] A. Ouannas, G. Grassi, A. Karouma, T. Ziar, X. Wang, and V.-T. Pham. New type of chaos synchronization in discrete-time systems: the fm synchronization. *Open Physics*, 16(1):174–182, 2018.
- [77] A. Ouannas and A. Karouma. Different generalized synchronization schemes between integer-order and fractional-order chaotic systems with different dimensions. *Differential Equations and Dynamical Systems*, 26(1):125–137, 2018.

- [78] A. Ouannas, A.-A. Khennaoui, S. Bendoukha, Z. Wang, and V.-T. Pham. The dynamics and control of the fractional forms of some rational chaotic maps. *Journal of Systems Science and Complexity*, 33:584–603, 2020.
- [79] A. Ouannas, A.-A. Khennaoui, S. Momani, G. Grassi, V.-T. Pham, R. El-Khazali, and D. Vo Hoang. A quadratic fractional map without equilibria: Bifurcation, 0–1 test, complexity, entropy, and control. *Electronics*, 9(5):748, 2020.
- [80] A. Ouannas, A.-A. Khennaoui, O. Zehrour, S. Bendoukha, G. Grassi, and V.-T. Pham. Synchronisation of integer-order and fractional-order discrete-time chaotic systems. *Pramana*, 92:1–9, 2019.
- [81] A. Ouannas, Z. Odibat, and T. Hayat. Fractional analysis of co-existence of some types of chaos synchronization. *Chaos, Solitons & Fractals*, 105:215–223, 2017.
- [82] A. Ouannas, Z. Odibat, and N. Shawagfeh. A new q-s synchronization results for discrete chaotic systems. *Differential Equations and Dynamical Systems*, 27(4):413–422, 2019.
- [83] A. Ouannas, Z. Odibat, N. Shawagfeh, A. Alsaedi, and B. Ahmad. Universal chaos synchronization control laws for general quadratic discrete systems. *Applied Mathematical Modelling*, 45:636–641, 2017.
- [84] A. Ouannas, X. Wang, A.-A. Khennaoui, S. Bendoukha, V.-T. Pham, and F. E. Alsaadi. Fractional form of a chaotic map without fixed points: Chaos, entropy and control. *Entropy*, 20(10):720, 2018.
- [85] A. Ouannas, X. Wang, V.-T. Pham, T. Ziar, et al. Dynamic analysis of complex synchronization schemes between integer order and fractional order chaotic systems with different dimensions. *Complexity*, 2017, 2017.
- [86] L. M. Pecora and T. L. Carroll. Synchronization in chaotic systems. *Physical review letters*, 64(8):821, 1990.

- [87] V.-T. Pham, C. K. Volos, S. Vaidyanathan, T. Le, and V. Vu. A memristor-based hyperchaotic system with hidden attractors: Dynamics, synchronization and circuital emulating. *Journal of Engineering Science & Technology Review*, 8(2), 2015.
- [88] S. Pincus. Approximate entropy (apen) as a complexity measure. *Chaos: An Interdisciplinary Journal of Nonlinear Science*, 5(1):110–117, 1995.
- [89] K. Qian, W. Feng, Z. Qin, J. Zhang, X. Luo, and Z. Zhu. A novel image encryption scheme based on memristive chaotic system and combining bidirectional bit-level cyclic shift and dynamic dna-level diffusion. *Frontiers in Physics*, 10:963795, 2022.
- [90] O. E. Rössler. An equation for continuous chaos. *Physics Letters A*, 57(5):397–398, 1976.
- [91] S. G. Samko. Fractional integration and differentiation of variable order. *Analysis Mathematica*, 21(3):213–236, 1995.
- [92] K. Sebastian Sudheer and M. Sabir. Hybrid synchronization of hyperchaotic lu system. *Pramana*, 73:781–786, 2009.
- [93] L. Stenflo. Generalized lorenz equations for acoustic-gravity waves in the atmosphere. *Physica Scripta*, 53(1):83, 1996.
- [94] K. Sun, S. He, C. Zhu, and Y. He. Analysis of chaotic complexity characteristics based on c0 algorithm. *Acta Electronica Sinica*, 41(9):1765–1771, 2013.
- [95] K.-H. Sun, S.-B. He, Y. He, and L.-Z. Yin. Complexity analysis of chaotic pseudo-random sequences based on spectral entropy algorithm. 2013.
- [96] M. Tavazoei and M. Haeri. Unreliability of frequency-domain approximation in recognising chaos in fractional-order systems. *IET Signal Processing*, 1(4):171–181, 2007.
- [97] T. Ushio. Chaotic synchronization and controlling chaos based on contraction mappings. *Physics Letters A*, 198(1):14–22, 1995.

- [98] S. Vaidyanathan, A. T. Azar, K. Rajagopal, and P. Alexander. Design and spice implementation of a 12-term novel hyperchaotic system and its synchronisation via active control. *International Journal of Modelling, Identification and Control*, 23(3):267–277, 2015.
- [99] F. Verhulst. *Nonlinear differential equations and dynamical systems*. Springer Science & Business Media, 2006.
- [100] H. F. von Bremen, F. E. Udwadia, and W. Proskurowski. An efficient qr based method for the computation of lyapunov exponents. *Physica D: Nonlinear Phenomena*, 101(1-2):1–16, 1997.
- [101] H. Wang, K. Sun, and S. He. Characteristic analysis and dsp realization of fractional-order simplified lorenz system based on adomian decomposition method. *International Journal of Bifurcation and Chaos*, 25(06):1550085, 2015.
- [102] S. Wang, Y. Yu, and M. Diao. Hybrid projective synchronization of chaotic fractional order systems with different dimensions. *Physica A: Statistical Mechanics and its Applications*, 389(21):4981–4988, 2010.
- [103] S.-P. Wang, S.-K. Lao, H.-K. Chen, J.-H. Chen, and S.-Y. Chen. Implementation of the fractional-order chen–lee system by electronic circuit. *International Journal of Bifurcation and chaos*, 23(02):1350030, 2013.
- [104] X. Wang and Q. Wang. A novel image encryption algorithm based on dynamic s-boxes constructed by chaos. *Nonlinear Dynamics*, 75:567–576, 2014.
- [105] X. Wang, Q. Wang, and Y. Zhang. A fast image algorithm based on rows and columns switch. *Nonlinear Dynamics*, 79:1141–1149, 2015.
- [106] X. Wang, Y. Wang, S. Unar, M. Wang, and W. Shbing. A privacy encryption algorithm based on an improved chaotic system. *Optics and Lasers in Engineering*, 122:335–346, 2019.

- [107] X. Wang, W. Xue, and J. An. Image encryption algorithm based on tent-dynamics coupled map lattices and diffusion of household. *Chaos, Solitons & Fractals*, 141:110309, 2020.
- [108] X. Wang and H. Zhao. Fast image encryption algorithm based on parallel permutation-and-diffusion strategy. *Multimedia Tools and Applications*, 79(27):19005–19024, 2020.
- [109] A. Wolf, J. B. Swift, H. L. Swinney, and J. A. Vastano. Determining lyapunov exponents from a time series. *Physica D: nonlinear phenomena*, 16(3):285–317, 1985.
- [110] G.-C. Wu and D. Baleanu. Jacobian matrix algorithm for lyapunov exponents of the discrete fractional maps. *Communications in Nonlinear Science and Numerical Simulation*, 22(1-3):95–100, 2015.
- [111] Y. Xian and X. Wang. Fractal sorting matrix and its application on chaotic image encryption. *Information Sciences*, 547:1154–1169, 2021.
- [112] S. Yamamoto, T. Hino, and T. Ushio. Dynamic delayed feedback controllers for chaotic discrete-time systems. *IEEE Transactions on Circuits and Systems I: Fundamental Theory and Applications*, 48(6):785–789, 2001.
- [113] H. Yousfi, A. Gasri, and A. Ouannas. Stabilization of chaotic h-difference systems with fractional order. *Nonlinear Dyn. Syst. Theory*, 468, 2022.
- [114] A. Zarour, A. Ouannas, C. Latrous, and A. Berkane. Linear chaos control of fractional generalized henon map. *Nonlinear Dynamics and Systems Theory*, 21(2):216–224, 2021.
- [115] W. Zhang, S. Zhou, H. Li, and H. Zhu. Chaos in a fractional-order rössler system. *Chaos, Solitons & Fractals*, 42(3):1684–1691, 2009.
- [116] Y. Zhang and Y. Tang. A plaintext-related image encryption algorithm based on chaos. *Multimedia Tools and Applications*, 77(6):6647–6669, 2018.

